TOWARD TRANSITION STATE ANALYSIS OF *O*-GLYCOSIDE HYDROLYSIS BY HUMAN SUCRASE/ISOMALTASE

TOWARD TRANSITION STATE ANALYSIS OF *O*-GLYCOSIDE HYDROLYSIS BY HUMAN SUCRASE/ISOMALTASE

By

RASA BAKHTIARI, B. Sc.

A Thesis

Submitted to the School of Graduate Studies

in Partial Fulfillment of the Requirements

for the Degree

Master of Science

McMaster University

MASTER OF SCIENCE
(Chemistry Graduate Program)

McMaster University
Hamilton, Ontario

TITLE: Toward Transition State Analysis of *O*-Glycoside Hydrolysis by Human Sucrase/Isomaltase

AUTHOR: Rasa Bakhtiari, B. Sc.

SUPERVISOR: Dr. Paul Berti

NUMBER OF PAGES: xii, 110

Abstract

Type 2 diabetes is a major health concern worldwide. One of its complications is postprandial hyperglycemia, i.e., high blood glucose concentrations, caused by glucose fast release from dietary polysaccharides into the bloodstream after meals. α-Glucosidase inhibitor drugs reduce postprandial hyperglycemia by inhibiting maltase/glucoamylase (MGAM) and sucrase/isomaltase (SI). MGAM and SI transform polysaccharides into absorbable monosaccharides, and inhibiting them delays monosaccharide release into the blood. The three commercially available α-glucosidase inhibitors are limited by their absorption abilities, inhibition efficacies, and side effects, which highlights the need for more specific α-glucosidase inhibitors. Because enzymes catalyze their reactions by tightly binding to their cognate transition states (TS), TS analogs can be powerful inhibitors and potential drugs. The measurement and interpretation of kinetic isotope effects (KIEs) is the only method that can directly determine TS structures on large molecules. In this work, methods to prepare radioisotopically labelled maltose were developed, as well as methods to measure KIEs on acid- and enzyme-catalyzed maltose hydrolysis. However, the methods developed did not achieve the required precision for TS analysis. Also, KIEs were calculated computationally for a model reaction of maltose hydrolysis.

Acknowledgements

I would like to take this opportunity to thank Dr. Paul J. Berti for giving me the opportunity to work in his lab and for all his guidance and support during my graduate work. As well, I would like to thank my committee member, Dr. William Leigh for providing feedback and support. Also, I would like to thank Dr. Paul W. Ayers for his help and useful suggestions with computational calculations. In addition, I would like to thank Dr. David Rose for generously providing the Ct-SI enzymes. I also thank my lab members and friends at McMaster, especially, Vincent Azhikannickal, Dr. Naresh Balachandran, Simanga Gama, Maren Heimhalt, Lisset Liano Piedra for their encouragement, support and friendship. Finally, I would not be where I am today without the friendship, emotional support, and guidance of my family, Mahboobeh, Kamran, Bahar and Behrouz.

Table of Contents

List of Figures

List of Tables

List of Abbreviations

AP	alkaline phosphatase
APS	γ-aminopropylsilyl
ATP	adenosine triphosphate
BSA	bovine serum albumin
CI	confidence interval
Ct-SI	*C*-terminal domain of sucrase/isomaltase
ddH_2O	ultrapure water (resistivity ≥ 18Ω)
DEAE-Sephadex	diethylaminoethyl-Sephadex
EDTA	ethylenediaminetetraacetic acid
G6P	glucose-6-phosphate
G6PDH	glucose-6-phosphate dehydrogenase
GDH	glucose dehydrogenase
GH	glycoside hydrolase
GOx	glucose oxidase
HILIC	hydrophilic interaction liquid chromatography
IRC	intrinsic reaction coordinate
L	hydron (^2H or ^3H)
ME	maltose epimerase
MES	2-(*N*-morpholino)ethanesulfonic acid
PEP	phosphoenolpyruvate
Stdev	standard deviation
TLC	thin layer chromatography

Chapter 1 - Introduction

1.1. Overview

Diabetes has rapidly become a global epidemic. Among the available treatments are α-glucosidase inhibitors, which reduce postprandial hyperglycemia by inhibiting maltase/glucoamylase (MGAM) and sucrase/isomaltase (SI), which are responsible for converting non-absorbable dietary starch to absorbable monosaccharides, e.g. glucose. There are three α-glucosidase inhibitor drugs in use, each with limitations in absorption ability, inhibition efficacy and side effects. There is an urgent need for new, more specific inhibitors. Many of the best enzyme inhibitors are transition state (TS) analogs. The only technique that will provide direct information regarding the TS structure is the measurement and interpretation of kinetic isotope effects (KIEs). The comparison of experimental and calculated KIEs provides the geometric and electronic structure of the TS. The goal of this study is to elucidate the TS structure of enzyme- and acid-catalyzed maltose hydrolysis, the enzyme being the *C*-terminal domain of sucrase-isomaltase (Ct-SI).

1.2. Type 2 diabetes

Diabetes affects more than 3 million people in Canada alone, and this number is rising dramatically.[12] This increase is due to a number of factors, including the rise in obesity rates, increased sedentary lifestyles, and an ageing

population. Diabetes can cause complications leading to premature death, including: heart attack, stroke, kidney failure, blindness, and amputations. There is also a large financial cost: diabetes cost the Canadian health system $11.7 billion in 2010.[1,3]

There are two main forms of diabetes: Type 1 diabetes is due to the autoimmune system destroying the pancreatic β-cells, which store and release insulin, and accounts for 5% of diabetes cases. The only treatment is insulin injection and the disease cannot be prevented.[4,5]Type 2 diabetes is caused by loss of function in pancreatic β-cells. This impairs insulin release and glucose blood sugar homeostasis, which leads in turn to postprandial hyperglycemia, that is, the fast release of glucose into the bloodstream after a meal.[6] In the long run it can cause retino-, neuro-, and nephropathies.

Insulin is a hormone which is composed of two polypeptide chains that contain 51 amino acids. Its primary role is to regulate glucose metabolism in the body, and it causes glucose uptake into cells where it is converted into energy.[7]

Glucose and insulin levels are at their minimum during fasting. Postprandially, glucose uptake by muscle cells is the primary way to regulate the glucose levels, and insulin is required for delivering the glucose into muscle cells. Insulin decreases postprandial glycemia by (i) signaling tissues to increase their glucose uptake, and (ii) increasing glycogenesis (glycogen synthesis) in the liver, and (iii) inhibiting glucagon, a hormone which increases the blood glucose level.

Type 2 diabetic patients have a disconnect between the regulation of fasting and postprandial hyperglycemia, which requires them to need greater insulin levels to regulate the fasting and the postprandial glucose level in the blood.[8]

There are four anti-hyperglycemia treatments; they can be used individually, or in combination[8]. (1) Insulin secretagogues stimulate insulin release. (2) Insulin injections supplement low insulin levels. (3) Insulin sensitizers increase the sensitivity of tissue cells to insulin. (4) α-Glucosidase inhibitors delay postprandial hyperglycemia by slowing glucose release into the bloodstream.[8]

All these treatments have their own benefits and complications; however, the α-glucosidase inhibitors have the least toxicity and side effects compared to the others. Moreover, this group is independent of the other pharmacological therapies. Nonetheless, abdominal discomfort and diarrhea are severe enough side effects that some patients stop using them. The commercially available α-glucosidase inhibitors are acarbose (Precose), Miglitol (Glyset), and Voglibose (Basen)[8]. These drugs each have different absorption and inhibition ability. For instance, acarbose is a good inhibitor but its absorption is moderate and it is not specific to small intestinal α-glucosidases. In contrast, miglitol has better absorption, but its inhibitory ability is worse, and it is not specific to small intestinal α-glucosidases. Thus, it requires large dosages, which lead to side effects[9]. The ideal α-glucosidase inhibitor would be the one which is effective

enough for small intestinal α-glucosidases, but it does not alter other α-glucosidases enzymes.

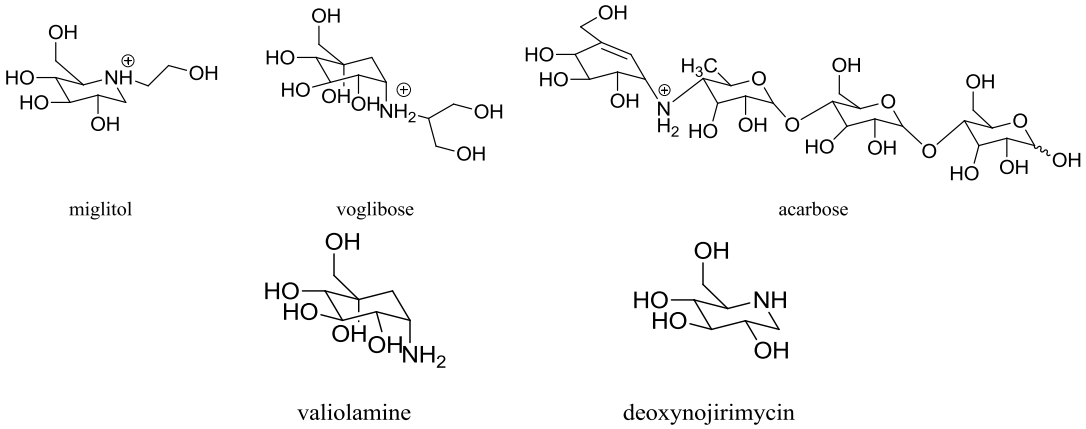

miglitol voglibose acarbose

valiolamine deoxynojirimycin

Acarbose is a non-cleavable pseudo-tetrasaccharide, which is a natural product[10–12]. Voglibose is an *N*-substituted derivative of valiolamine, which is a pseudo-amino sugar, or branched-chain aminocyclitol, and its *N*-substituted component is derived from glycerol[10,13]. Miglitol is a derivative of 1-deoxynojirimycin, which is a more potent α-glucosidase inhibitor with fewer gastrointestinal side effects[10,11].

1.3. MGAM and SI Enzymes

Enzymes work by decreasing the activation energy of a reaction by binding to its transition state. The enzymatic *O*-glycoside hydrolysis is a good example to illustrate enzymes' catalytic power. The nonenzymatic reaction has a half-life of about 5 million years,[14] while the enzymatic reactions have k_{cat} values

of up to 1000 s^{-1}. Enzymes are capable of producing rate enhancements up to 10^{19}- fold.[15]

There are four main human *O*-glycosidases that hydrolyze dietary starches and sugars. Salivary and pancreatic α-amylases are endo-glycosidases which hydrolyze internal glycoside bonds in complex polysaccharides, yielding maltose, and small oligosaccharides.

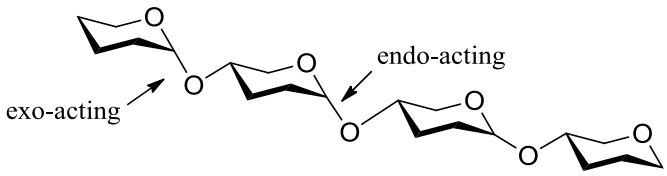

Figure 1.1. The endo- and exo-acting glycosidase.

The other two are maltase/glucoamylase (MGAM) and sucrase/isomaltase (SI); they are located in the small intestinal brush border membrane. They are exo-glycosidases; that is, they release absorbable monosaccharides (predominantly glucose and fructose) by hydrolyzing monosaccharides from the non-reducing ends of oligosaccharides.

As MGAM and SI are responsible for monosaccharide release, inhibiting them can prevent postprandial hyperglycemia. MGAM and SI are homologues, which mean they evolved from a common ancestor. Each enzyme contains duplicated catalytic domains, the *C*- and *N*-terminal domains (Figure 1.2). The *N*-terminal domains, Nt-MGAM and Nt-SI, share 60% sequence identity, as do the *C*-terminal domains. The *N*- and *C*-terminal domains of each protein (e.g., Nt-SI

and Ct-SI), share 40% sequence identity. Both are classified as glycoside hydrolase family 31(GH31) members in the carbohydrate enzyme database (CAZY) .[9,12,16] GH31 enzymes are specific to α-linkages, and retain that configuration in the products.

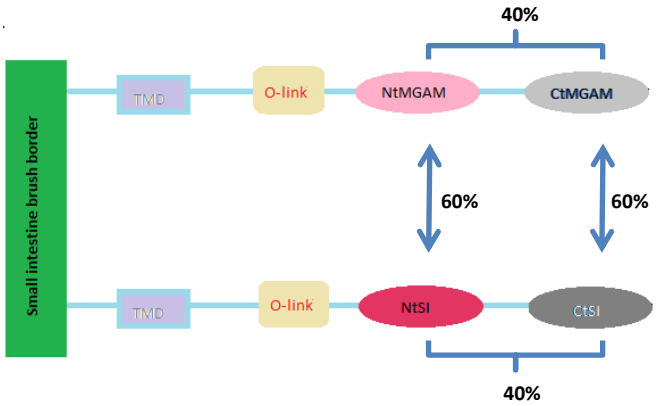

Figure 1.2. Protein organization for two human small intestinal brush border enzymes, SI and MGAM.

The above figure shows the protein organization for these two brush border enzymes. The transmembrane domain (TMD) is a cell membrane which contains around 20 residues, O-glycosylated Linker (O-link) connects TMD to the N-terminal domain of each enzyme and is 55 residues long, Nt-SI, Ct-SI, Nt-MGAM, and Nt-MGAM are each around 900 residues. Nt-SI and Nt-MGAM have 60% sequence identity with each other, as do Ct-SI and Ct-MGAM. The sequence identity between the *N*- and *C*-terminal domains are 40% in each protein. (Figure is from Figure 1 of reference [12]).

Each domain shows different substrate specificities. The α-(1→4) glycoside bond, which comprises ≈95% of the bonds in starches, is the main substrate for all domains (k_{cat} = 137 s^{-1} with Nt-SI, and 111 s^{-1} with Nt-MGAM). Nt-MGAM is more active against shorter starch molecules. Nt-SI has an additional hydrolytic activity against α-(1→6) glycoside bonds (k_{cat} = 97 s^{-1}), while Ct-SI is active against the α-(1→2) linkage of sucrose.[16,17]

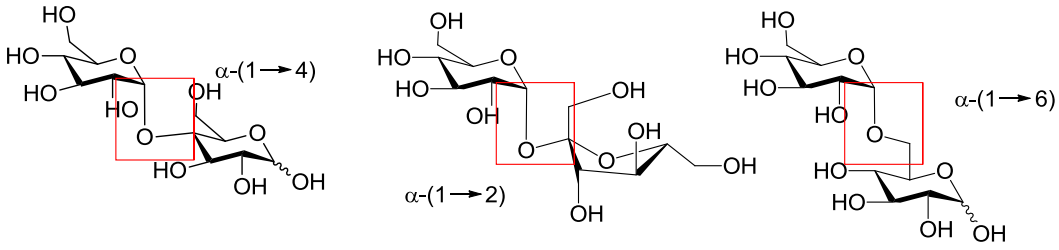

Maltose Sucrose Isomaltose

These specificity differences of each domain show the necessity of elucidating the structure and mechanism of these enzymes. This knowledge will enable us to design better inhibitors. For example, acarbose is an effective inhibitor of α-amylase and Ct-MGAM and Ct-SI, but a weaker inhibitor of Nt-MGAM and Nt-SI.[18,19] Thus, it is not an ideal drug, as it is not specific nor effective enough.

1.4. Glycoside Chemistry

There is a variety of natural or synthetic glycosidase inhibitors that are developed as potential inhibitors to be used for treatment of metabolic diseases,[20] cancer,[21] diabetes,[8] viral, and bacterial infections.[22,23] Designing strong selective inhibitors is only possible by having an understanding of structure and mechanism of these reactions and their respective enzymes. The information about these enzymes has increased greatly in the past decade, and a number of reviews have been written on this subject.[14,24–28]

An *O*-glycosidic bond is an acetal linkage between the anomeric carbon of a monosaccharide (the glycone) with an alcohol or carbohydrate (the aglycone) (Figure 1.3).[29]

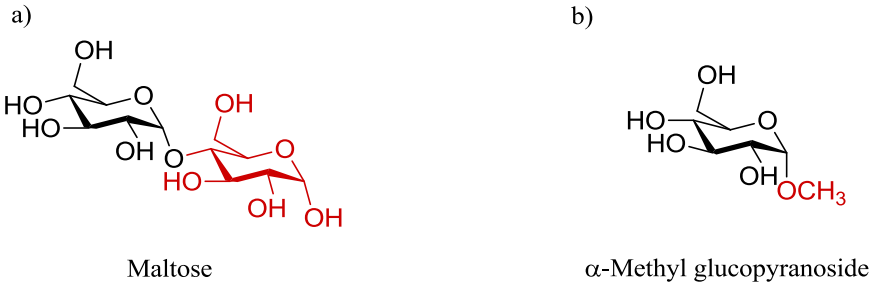

Figure 1.3. *O*-glycoside bonds.
a) *O*-glycosidic bond produced from condensation of two carbohydrates. b) *O*-glycosidic bond that produced from condensation of a carbohydrate and an alcohol. The aglycone portions have shown by red.

1.5. Glycoside Hydrolysis

Spontaneous *O*-glycoside bond hydrolysis is very slow, with a half-life of ≈5 million years,[15,30] but they are susceptible to general acid catalysis through protonation of the exocyclic glycosidic oxygen atom.[31] This promotes leaving group departure and also facilitates nucleophilic attack at the anomeric carbon atom.

1.5.1. Glycosidase Mechanisms: Inverting and Retaining

Glycoside hydrolases can be divided into two major classes, based on whether the product retains its anomeric configuration, or if it is inverted (Figure 1.4). A common feature of all glycosidases is that glycoside hydrolysis employs both general acid and general base catalysis[32,33]. Inverting glycosidases use water as the nucleophile, catalyzing a direct nucleophilic displacement of the leaving group by water, and leading to an inversion of stereochemistry. Retaining enzymes perform a double displacement reaction, first using a carboxylate

sidechain as a nucleophile to form a covalent enzyme-bound intermediate, then using water as a nucleophile to displace the carboxylate sidechain. This gives an overall retention of stereochemistry.

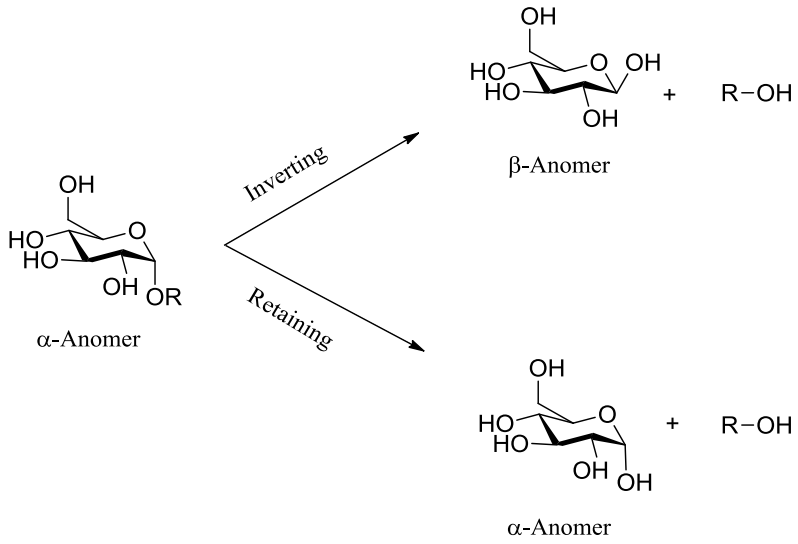

Figure 1.4. Inverting versus retaining reactions.
Glycoside hydrolases may invert the stereochemistry of the product relative to the substrate, giving a β-anomer configuration from an α-configured substrate, or an α-product from a β-substrate. Alternatively the stereochemistry of the substrate may be retained in the product.

In both mechanisms the general acid catalyst protonates the leaving group oxygen atom, promoting C-O bond cleavage, and both involve an oxacarbenium ion-like transition state structure (Figure 1.5 (a)). One difference is that the distance between the two carboxylic acid/carboxylate sidechains is about 5.5 Å in retaining mechanism enzymes, but about 10 Å in inverting enzymes, with the greater distance needed to accommodate the water nucleophile.[14,25,34]

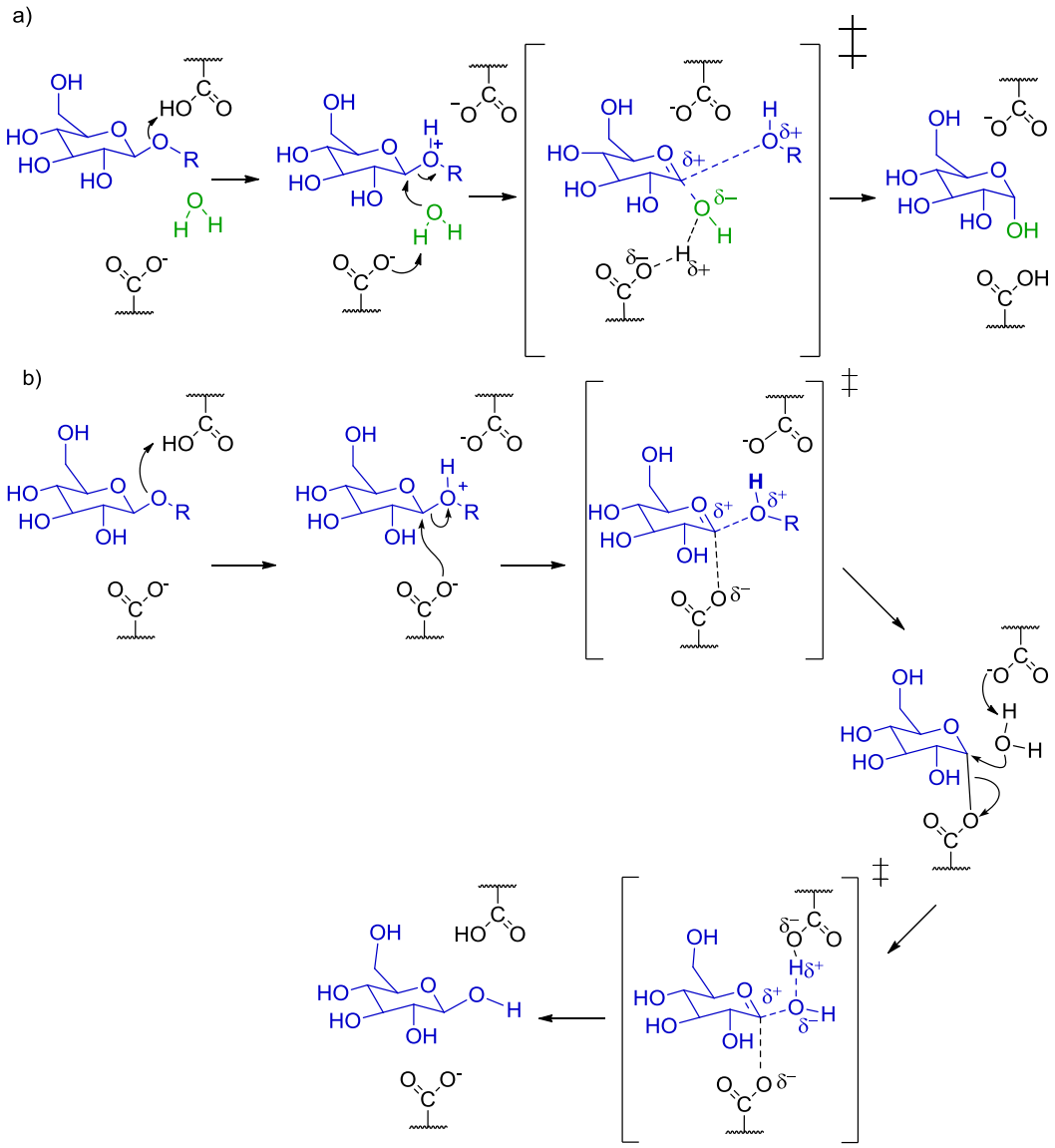

Figure 1.5. The two major mechanisms of enzymatic glycosidic bond hydrolysis. a) The inverting mechanism operates via a direct displacement mechanism. b) The retaining mechanism operates by a double displacement mechanism involving a glycosyl-enzyme intermediate.

In inverting enzymes, the general acid acts as a proton donor to facilitate the leaving group departure, and, concomitantly, the water molecule is activated by the general base to attack the anomeric carbon, thus creating the new C-O bond, with the inversion of configuration.

In the retaining mechanism, the carboxylic acid acts as a general acid to protonate the glycosidic oxygen atom concurrently with bond cleavage, while the carboxylate sidechain acts as a nucleophile, forming the covalent glycosyl-enzyme intermediate. This is the glycosylation step. In the second, deglycosylation step, the same sidechain that acted as the general acid catalyst now acts as a general base to deprotonate the incoming water molecule, which attacks at the anomeric center and displaces the carboxylate sidechain, yielding the final product.[25,33,34]

Other mechanisms have recently been discovered that do not follow the "normal" nucleophilic displacements described above. For example, an oxidation-elimination-addition-reduction sequence is proposed for family GH4,[35] or via an elimination reaction.[36,37]

1.6. Substrate Distortion

Sugar ring conformation and its distortion can affect glycoside bond reactivity; it also affects KIEs.[27,38–40] Glucopyranoses can adopt different conformations; each of which is described by a single letter: C for chair, H for half-chair, S for skewed, B for boat, E for envelope. Superscripted numbers on the left of the letter represent carbon atoms above the plane of the ring, while subscripted numbers to the right represent any carbon atoms below the plane of the ring (Figure 1.7).

$^4C_1$ is the lowest energy conformation for glucopyranoses. Several studies have suggested sugar ring distortion at the TS.[27,38–40] The oxacarbenium ion

character of the TS results in a positive charge on C1 of the pyranose ring, which causes the pyranose ring to be distorted away from the $^4C_1$ conformation toward ones which favour orbital overlap and electron delocalization of the ring oxygen lone-pair toward C1.[38]

Distortion of the sugar ring can accelerate the reaction in different ways. It can stabilize the electron-deficient anomeric carbon by positioning a ring oxygen atom lone pair near the C1 σ*-antibonding orbital to share its electrons.[40,41] It can facilitate nucleophilic attack by removing steric hindrance around C1. It can also bring the conformation of the sugar ring closer to the TS conformation.[41] For the TS conformation of the retaining glycosidase for the GH31 and GH27 α-glycosidase families, the following conformational itinerary during catalysis has been proposed: $^4C_1 \rightarrow {}^4H_3 \rightarrow {}^1S_3$ (Figure 1.6).[42] The reactant $^4C_1$ conformation is proposed to be converted to $^4H_3$ at the TS, followed by $^1S_3$ in the covalent glycosyl-enzyme intermediate.[38]

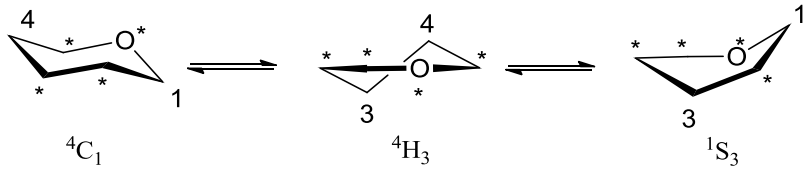

Figure 1.6. Proposed conformations for GH31 family for reactant, TS, and product.[42]
The coplanar atoms are shown by the asterisks.

Computations have shown that the glucopyranosyl oxacarbenium ion can adopt the ^3E, E_3, $^3H_4$, $^4H_3$, and E_4 conformations, so any one of these is plausible for the TS conformation.[43] Knowledge of the TS conformation is important for inhibitor design since creating inhibitors which match the TS conformation will

avoid the energetic cost of distorting the inhibitor into the TS conformation, which would decrease the inhibitor's affinity for the enzyme.[43] Acarbose, an α-glucosidase inhibitor, inhibits full length MGAM with a nanomolar K_i, but a micromolar range against Nt-MGAM,[18,44] exhibited a $^{2}H_{3}$ conformation in complex with Nt-MGAM.[45] The TS conformation is not known, so it is also not known whether there the acarbose ring must change conformation upon binding. Since acarbose might not be a TS mimic inhibitor for α-glucosidase, this conformation cannot be assumed to be the TS conformation for Nt-MGAM.

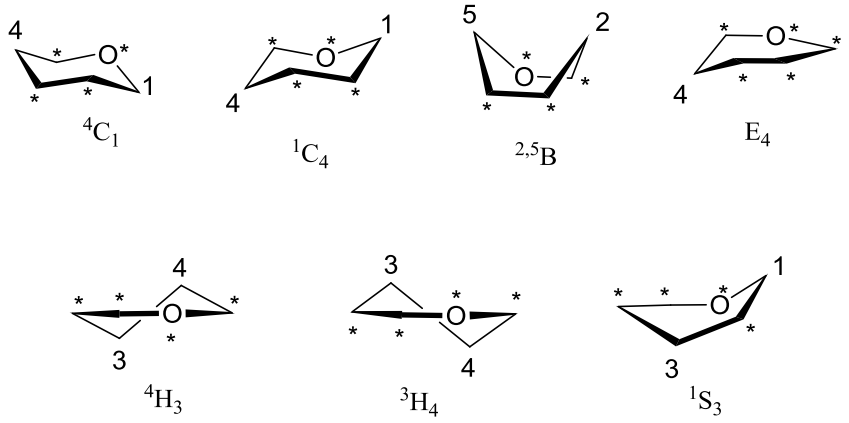

Figure 1.7. Some possible conformations of pyranoses.
Chair (C), boat (B), envelope (E), half-chair (H), and skew (S). The coplanar atoms are shown by the asterisks. All hydroxyl groups are omitted for clarity. Superscripted numbers indicate atoms which located above the plane and subscripted numbers are the ones below the plane.

1.7. Transition State Analysis of Enzymatic Reactions

Enzymes catalyze reactions by preferentially binding to the TS.[46] A common drug design technique is to create molecules that mimic the shape and charge distribution of the TS - i.e., TS analogs. However, the TS has a femtosecond lifetime, which makes TSs very difficult to study directly by common techniques such as x-ray crystallography, and linear free energy

relationship studies. TS analysis using kinetic isotope effects (KIE) is the only technique that is capable of providing detailed structural information about the TS in the solution phase, or for reactions involving more than a handful of atoms. TS analysis, in combination with structure, kinetic and inhibition studies can illuminate unanswered questions about an enzyme's catalytic mechanism.[47–49]

1.8. Enzymatic Versus Nonenzymatic Transition States

Some enzymes change the TS structure quite dramatically compared to the corresponding nonenzymatic reaction. For example, retaining glycosidases form a covalent substrate-enzyme intermediate that does not exist in nonenzymatic hydrolysis.[43,48] Other enzymes stabilize essentially the same TS as the corresponding nonenzymatic reaction; for example, NAD^+ hydrolysis by diphtheria toxin.[50–52] In contrast to reactions in aqueous solution, enzyme active sites have the ability to use both acid and base residues simultaneously. Enzymes are also able to use binding energies to counteract the entropic costs of bringing reactants together.[46,48,53] By comparing the TSs for enzymatic and the corresponding nonenzymatic reactions, it is possible to observe: how the interaction between the substrate and enzyme lowers the activation energy, what catalytic strategies are effective for a given reaction, and what role the intrinsic reactivity of the substrate plays in catalysis. [47–49]

1.9. Isotope Effects

A kinetic isotope effect (KIE) is defined as the ratio of the rate constants of isotopically labelled reactants (equation 1.1).

$$\mathbf{KIE} = {}^{\mathbf{light}}k \Big/ {}_{\mathbf{heavy}}\boldsymbol{k} \qquad \mathbf{(1.1)}$$

Equilibrium isotope effects (EIEs) are the ratios of equilibrium constants for isotopically labelled compounds (equation 1.2).

$$\mathbf{EIE} = {}^{\mathbf{light}}\boldsymbol{K}_{\mathbf{eq}} \Big/ {}_{\mathbf{heavy}}\boldsymbol{K}_{\mathbf{eq}} \qquad \mathbf{(1.2)}$$

The chemical meaning of KIEs and EIEs is that they reflect the changes in the "vibrational environment" between the reactant and the transition state (KIEs) or reactant and product (EIEs). The "vibrational environment" of each atom is the bonding forces (bond stretches, bends and torsions) affecting each atoms, and is reflected in the molecular vibrational frequencies.[54]

1.9.1. Origin of Isotope Effects

The concept of vibrational environment can be illustrated using a balls and spring model of a harmonic oscillator (Figure 1.8).

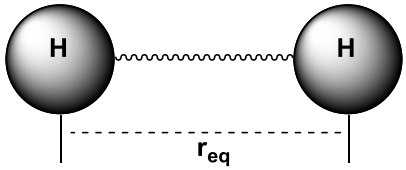

Figure 1.8. The balls and spring model for H_2

In this model the balls represent atoms, and the spring represents the massless bond between them. Based on Hooke's law for a simple harmonic oscillator, the vibrational frequency, ν, is a function of the reduced mass of the balls (μ), and the spring force constant (*k*) (equation 1.3)

$$\nu = \frac{1}{2\Pi}\sqrt{\frac{k}{\mu}} \quad \textbf{(1.3)}$$

$$\mu = \frac{m' + m''}{m' * m''} \quad \textbf{(1.4)}$$

The vibrational energy of a simple oscillator is given by:

$$E = \left(\nu + \tfrac{1}{2}\right) h\sqrt{\frac{k}{\mu}} \quad \textbf{(1.5)},$$

where h is Planck's constant and ν is vibrational quantum number. In this model, lighter atoms (balls) and stronger bond forces (springs) give higher vibrational frequencies, which in turn gives higher energies. Conversely, a weaker bond gives a lower vibrational energy.

Zero point energy is the vibrational energy in a harmonic oscillator when the quantum number, ν, is 0. Unlike macroscopic oscillators, the vibrational frequency of bonds is not zero at 0 K (Figure 1.9).

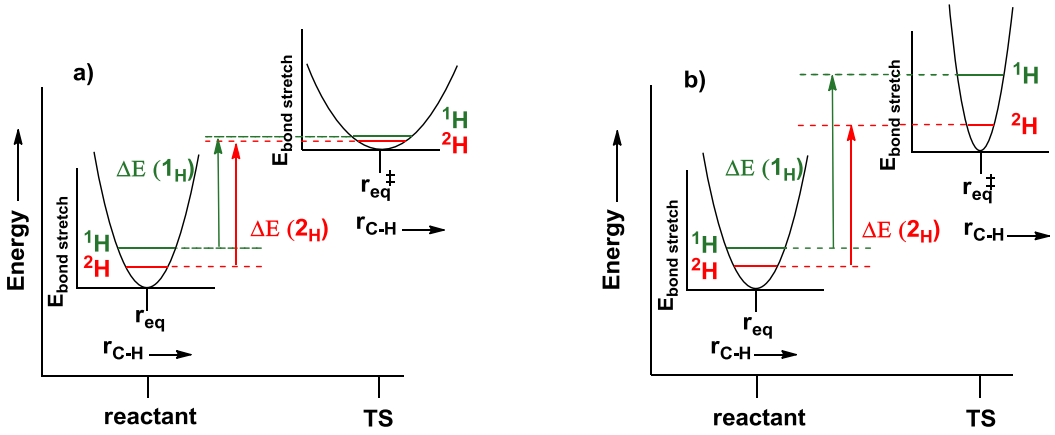

Figure 1.9. Vibrational energies for C-H and C-D bonds going from reactant to TS. The ZPE for secondary KIEs are shown. Differences in zero point energies cause differences in the activation energy. a) A normal KIE results when a weaker bond at the TS results in a "looser" vibrational environment. b) An inverse KIE results when a stronger bond at the TS results in a "tighter" vibrational environment.

The zero point energy of a bond containing a lighter isotope will have a higher frequency and a higher zero point energy than the same bond containing a heavier isotope. If the bond is weakened between reactant and TS, the zero point energy will decrease more for the light isotope than the heavy, which leads to a change in activation energies: ${}^{light}\Delta E_0 < {}^{heavy}\Delta E_0$. Thus, the light isotope would react faster, making it enriched in the product and depleted in the reactant. Conversely, if the bond strengthens, the heavy isotope will react faster.

IEs are the product of three values, the zero point energy contribution (ZPE), the excited state contribution, when the quantum number $v > 0$ (EXC), and mass and moments of inertia contribution (MMI). The largest contribution is generally ZPE:

$$IE = MMI \times ZPE \times EXC$$

The expression for each term is:

$$\mathrm{ZPE} = \frac{\left[\prod_{i}^{3N-6} e^{-(\mathrm{light}_{u_i} - \mathrm{heavy}_{u_i})/2}\right]_{\mathrm{final(TS)}}}{\left[\prod_{i}^{3N-6} e^{-(\mathrm{light}_{u_i} - \mathrm{heavy}_{u_i})/2}\right]_{\mathrm{initial}}},$$

where $u_i = h\nu_i/k_BT$ (h = Planck's constant, ν_i = frequency, k_B = Boltzman constant, T = absolute temperature), and 3N-6 is the number of normal vibrational modes in a non-linear molecule.

$$\mathrm{EXC} = \frac{\left[\prod_{i}^{3N-6} \frac{1-e^{(-\mathrm{heavy}_{u_i})}}{1-e^{(-\mathrm{light}_{u_i})}}\right]_{\mathrm{final(TS)}}}{\left[\prod_{i}^{3N-6} \frac{1-e^{(-\mathrm{heavy}_{u_i})}}{1-e^{(-\mathrm{light}_{u_i})}}\right]_{\mathrm{initial}}}$$

$$\mathrm{MMI} = \frac{\left[\left(\frac{\mathrm{light_M}}{\mathrm{heavy_M}}\right)^{3/2}\left(\prod_{i}^{n_{rot}} \frac{\mathrm{light_I}}{\mathrm{heavy_I}}\right)^{1/2}\right]_{\mathrm{final(TS)}}}{\left[\left(\frac{\mathrm{light_M}}{\mathrm{heavy_M}}\right)^{3/2}\left(\prod_{i}^{n_{rot}} \frac{\mathrm{light_I}}{\mathrm{heavy_I}}\right)^{1/2}\right]_{\mathrm{initial}}},$$

where M = mass and I= moment of inertia for each normal mode[55]. The equation could be presented as follows, where there is a moment of inertia for each axis.

$$\mathrm{MMI} = \frac{\left[\left(\frac{\mathrm{light_M}}{\mathrm{heavy_M}}\right)^{3/2} \frac{\mathrm{light_{I_x}light_{I_y}light_{I_z}}}{\mathrm{heavy_{I_x}heavy_{I_y}heavy_{I_z}}}\right]_{\mathrm{final(TS)}}}{\left[\left(\frac{\mathrm{light_M}}{\mathrm{heavy_M}}\right)^{3/2} \frac{\mathrm{light_{I_x}light_{I_y}light_{I_z}}}{\mathrm{heavy_{I_x}heavy_{I_y}heavy_{I_z}}}\right]_{\mathrm{initial}}}$$

The Teller-Redlich rule could express the MMI in term of vibrational product:

$$\mathrm{MMI} = \mathrm{VP} = \frac{\left(\prod_{i}^{3N-6} \frac{\mathrm{light}_{v_i}}{\mathrm{heavy}_{v_i}}\right)_{\mathrm{final(TS)}}}{\left(\prod_{i}^{3N-6} \frac{\mathrm{light}_{v_i}}{\mathrm{heavy}_{v_i}}\right)_{\mathrm{initial}}}$$

The equations are modified for KIEs because the final state, the TS, has only 3N-7 vibrational frequencies, rather than the 3N-6 in stable molecules (3N-5 in linear molecules) for EIEs.

The reaction coordinate motion also contributes to KIEs. The reaction coordinate has an imaginary frequency (ν^*), which is different from other vibrational frequencies because it lacks a restoring force. The reaction coordinate has zero force at the TS, and increasing forces that push the oscillator *away* from the TS before and after the TS.[47,48,56]

The relationship between KIEs and structure is explained by how changes in structure cause changes vibrational frequencies, as explained by the Pauling bond order and Badger's law. The Pauling bond order is given by:

$$n_{ij} = e^{\frac{(r_1 - r_{ij})}{0.3}} \quad \textbf{(1.6)},$$

where n_{ij} is the Pauling bond order between atom i and j, r_{ij} is the bond length, and r_1 is the length of a typical single bond between atoms i and j. For example, r_1 for a C-C bond is 1.526 Å, C-O is 1.41 Å, C-H is 1.1 Å, and O-H is 1.01 Å.[54] There is a general empirical relationship that relates the bond order to bond stretching force constant. This simple estimate of calculating the force constant is made by using Badger law.[54] This relationship is relevant for mostly diatomic compounds; for polyatomic molecules the stretching force constant is

complicated due to coupling of vibrational modes. In this study, force constants were derived directly from the vibrational frequencies in the computational structures which made the evaluation of force constant of polyatomic molecules possible, and Badger's law was not used directly.[57] Based on these two laws, if there is a change in the bond lengths, there will be a change in the force constant, and therefore in vibrational frequencies.[47,54]

1.9.2. Meaning of KIEs

A normal KIE (KIE > 1, $^{light}k > {}^{heavy}k$) indicates a "looser" vibrational environment for the labelled atom at the TS. Conversely, an inverse KIE (KIE < 1.0, $^{light}k < {}^{heavy}k$) indicates a "tighter" vibrational environment.

Primary KIEs involve the atoms that are undergoing bond breaking or making. Secondary KIEs are KIEs at any position not directly involved in the chemistry.

The bond orders and motions of the leaving group and nucleophile define the mechanism of the reaction. In an A_ND_N, or S_N2 reaction, both leaving group bonding and nucleophile bonding are present and in concerted motion at the TS. A_N indicates the nucleophile association and D_N means the nucleofuge dissociation.[58]

S_N1 reactions are stepwise, with an oxacarbenium ion intermediate. The intermediate could exist long enough to diffusionally separate from the leaving group, giving a D_N+A_N mechanism, or it could be too short-lived to diffusionally

separate, giving a D_N*A_N mechanism. The D_N*A_N mechanisms can be differentiated based on the partitioning of the oxacarbenium intermediate to at least two transition states, ($D_N*A_N^{\ddagger}$) and ($D_N^{\ddagger}*A_N$).

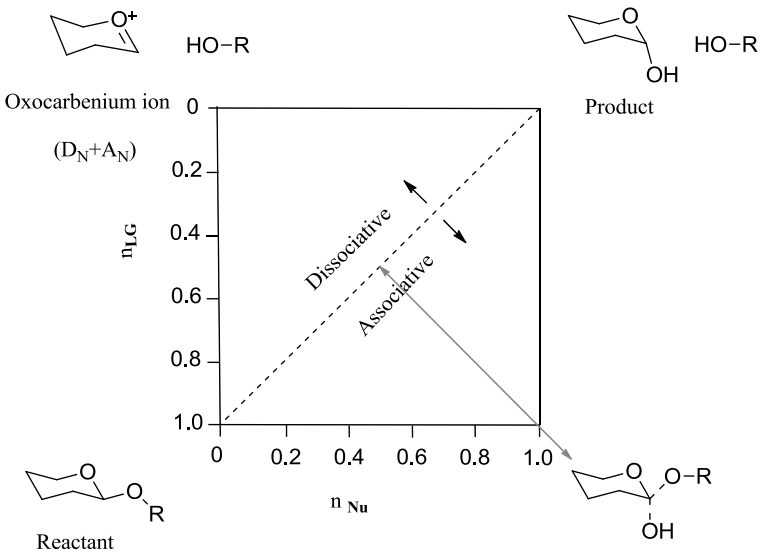

Figure 1.10. A More O'Ferrall-Jencks diagram.
The axes are the bond orders to the leaving group and the nucleophile. Dissociative TSs are defined as ones where (n_{LG} + n_{Nu}) < 1, and are the only realistic values for nucleophilic substitutions at carbon centres.

The primary, anomeric carbon KIE for D_N*A_N (or D_N+A_N) reactions are close to unity or slightly inverse. (1-^{14}C KIE = 1.00–1.02 ($D_N*A_N^{\ddagger}$) or ^{14}C KIE = 1.01 – 1.02 ($D_N^{\ddagger}*A_N$)).[47,48,59] However, KIEs higher than this range has been calculated ($D_N^{\ddagger}*A_N$ 1'-^{14}CKIE =1.052 for an *N*-glycoside hydrolysis reaction).[60] A_ND_N reactions usually give larger primary KIEs than D_N*A_N reactions because of the contribution from the reaction coordinate motion, which contains contributions from both the nucleophile and the nucleofuge. This number usually ranges around 1-^{14}C KIE = 1.025 - 1.139, and the number is larger for more synchronous (i.e., less dissociative) reactions.[48,59]

The α-secondary hydron KIE (hydron = L = ^{2}H or ^{3}H), provides information on the amount of oxacarbenium ion character at the TS. Oxacarbenium ion-like TSs (highly dissociative A_ND_N or $D_N{*}A_N$) have large, normal α-secondary hydron KIEs. The anomeric carbon's sp^2 hybridization in an oxacarbenium ion creates a less crowded vibrational environment. For a more crowded synchronous A_ND_N transition state, the KIE would be small or inverse.

The β-secondary hydron (2-^{3}H) KIE can give conformational information.[48] If the KIE is large, then the TS is oxacarbenium ion-like, and the conformation allows hyperconjugation (see below) at C2. If the KIE is small, then either the TS is oxacarbenium ion-like but the conformation prevents hyperconjugation, or it is not oxacarbenium ion-like.[47,48]

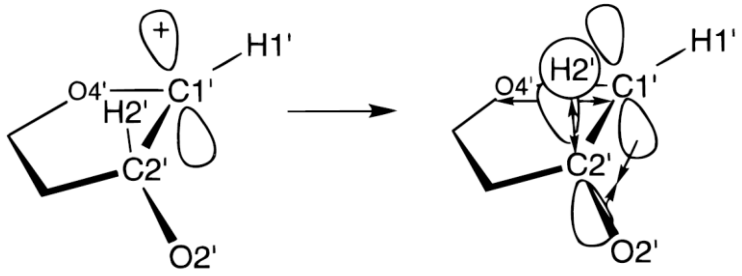

Figure 1.11. Hyperconjugation at H2′ for a furanosyl ring.
The figure shows the interaction of the p-orbital of C1' of the oxacarbenium ion with the occupied p-orbital of C2' leads to C1'-C2' π-bonding. Concomitant with increased $n_{C1\text{-}C2}$ are decreases in $n_{C2'\text{-}H2'}$ and $n_{C1'\text{-}O4'}$. Which leads to a large, normal 2'-^{3}H KIE. Hyperconjugation in pyranoses will be essentially the same. Reprinted from Figure 2 of reference [50].

Hyperconjugation is the formation of C1-C2 π-bonding, with the electrons being donated from the C2-L σ-bond. This can only occur if the C2-L bond is aligned with the empty p-orbital of C1. Hyperconjugation stabilizes the TS via electron delocalization, and results in a weaker C2-L σ-bond, leading to a large,

normal KIE. We can take advantage of this specificity to determine the probable conformation of the sugar ring. Remote KIEs could also give some information about the TS conformation.

The glycosidic oxygen (leaving group) ^{18}O KIE would give information on the extent of glycone-aglycone bond cleavage at the TS, with the cleavage being roughly proportional to the ^{18}O-KIE.

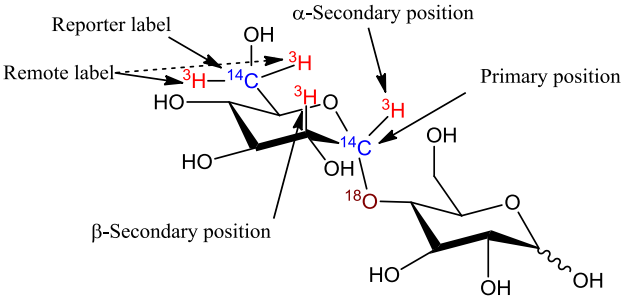

Figure 1.12. Important KIEs for TS analysis of maltose hydrolysis.
The important positions that would provide key information concerning the TS structure and conformation are shown. The 1-^{14}C and 4'-^{18}O KIEs are primary KIEs, while the secondary KIEs include 1-^{3}H (α-secondary), 2-^{3}H (β-secondary), 6-^{14}C and 6,6-$^{3}H_2$ (remote).

1.9.3. Competitive vs. noncompetitive KIEs

KIEs can be measured using non-competitive (direct) and competitive (isotope discrimination) methods.[47,61] For the former, each isotopologue substrate's rate is measured individually, then the KIE (ratio of the rate constants) is calculated. For competitive KIEs, labelled and unlabelled substrates compete with each other for the enzyme, and the KIE reflects the second order rate constant, k_{cat}/K_M.[47,48] k_{cat}/K_M reflects the steps up to and including the first irreversible step, i.e., the energetic difference between the free substrate in solution and the first irreversible TS. KIEs are only useful for systems where

chemistry is the first irreversible step, rather than non-chemical steps such as conformational changes, or substrate binding

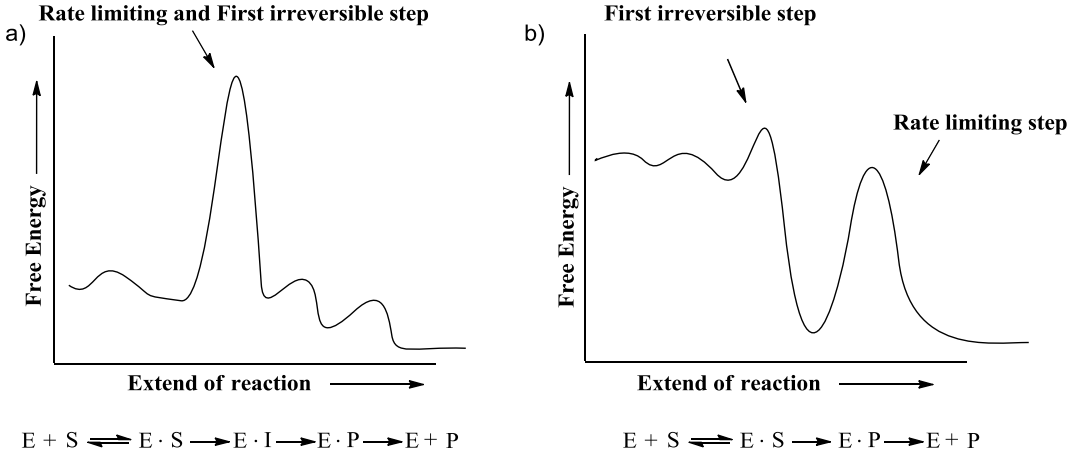

Figure 1.13. Free energy profile for enzyme catalyzed reactions. a) The rate limiting and the first irreversible step are the same. b) The first irreversible step preceding the rate limiting step.

The figures are adopted from Fig 2 of reference[48]

The non-competitive approach has the major disadvantage that it is not normally precise enough for TS analysis, as its accuracy is in the range of experimental errors on rate measurements, typically ≈5%. In the competitive reaction, this source of error is eliminated by measuring isotope ratios rather than rates directly. This gives the ratio of rate constants, which allows KIEs to be measured with accuracy of 0.2-0.5%.[48]

1.9.4. Measuring KIEs

A number of KIE measurement techniques have been developed, including whole- molecule mass spectrometry, spectrophotometry, and NMR.[48] However, the most common method employs radiolabels and liquid scintillation

counting to detect changes in isotope ratios.[48,61] One of the major disadvantages of this method is the need to synthesize complex molecules isotopically labelled at every position of interest in extremely high radioisotopic purity. For complex reactants like maltose, it is necessary to use enzymatic syntheses.

Measuring KIEs with radiolabels requires two radiolabels: the label of interest, and a remote label. For example, measuring the 1-^{3}H KIE involves making a mixture of [1-^{3}H]maltose, the label of interest, and [6-^{14}C]maltose, the remote label. In measuring the KIE, we are attempting to determine KIE = $^{1}k/^{3}k$; however, ^{1}H is not radioactive. Instead, the 6-^{14}C label, which is assumed to have no KIE, is used to report on 1-^{1}H. Assuming that there is a normal KIE at the 1-^{3}H position, the glucose product will be relatively depleted in 1-^{3}H while the residual reactant will be enriched in 1-^{3}H. This change in the ^{1}H/^{3}H ratio will be observed experimentally as a change in the ^{14}C/^{3}H isotope ratio. The change in isotope ratio can be measured in either residual maltose, or in the product, glucose.

It is necessary to correct the observed isotope ratios for the extent of reaction. This is because the reactant starts to become depleted in the faster reacting isotope as soon as the reaction begins. This decreases the relative concentration of the faster reacting isotope, and therefore incrementally shifts the reaction toward the slower reacting isotope as the extent of reaction increases. Several equations have been formulated to compensate for this effect;[61–63] the two

equations used in this study were equation 1.7, for isotope ratios in the residual substrate[51] and equation 1.8 for the products.[63]

$$\text{KIE (substrate)} = \frac{\ln\left[\frac{(1-f)\left(1+\frac{1}{R_0}\right)}{\left(1+\frac{1}{R_i}\right)}\right]}{\ln\left[\frac{(1-f)(1+R_0)}{(1+R_i)}\right]} \qquad \textbf{(1.7)}$$

$$\text{KIE(product)} = 1 + \frac{\ln\left[1+\left[\frac{{}^{A_0}/_{A_0'} - {}^{X}/_{X'}}{{}^{A_0}/_{A_0'}}\right]\left[\frac{f\left[\frac{1+{}^{A_0}/_{A_0'}}{1+{}^{X}/_{X'}}\right]}{1-f\left[\frac{1+{}^{A_0}/_{A_0'}}{1+{}^{X}/_{X'}}\right]}\right]\right]}{\ln\left[1-f\left[\frac{1+{}^{A_0}/_{A_0'}}{1+{}^{X}/_{X'}}\right]\right]} \qquad \textbf{(1.8)}$$

1.10. KIEs for Glycoside Hydrolysis

A number of KIEs for glycoside hydrolysis have been measured for enzymatic and acid-catalyzed reactions.[43,64–68]

1.10.1. Enzymatic

A number of KIEs were measured for glycosidase using different substrates including: α-fluoro-glucoside (**1**),[64] α-D-glucopyranosyl isoquinolinium bromide (**2**),[65] α-D-glucopyranosyl pyridinium bromide (**3**),[65] α- and β-methyl glucopyranoside (**4**, **5**).[43,66]

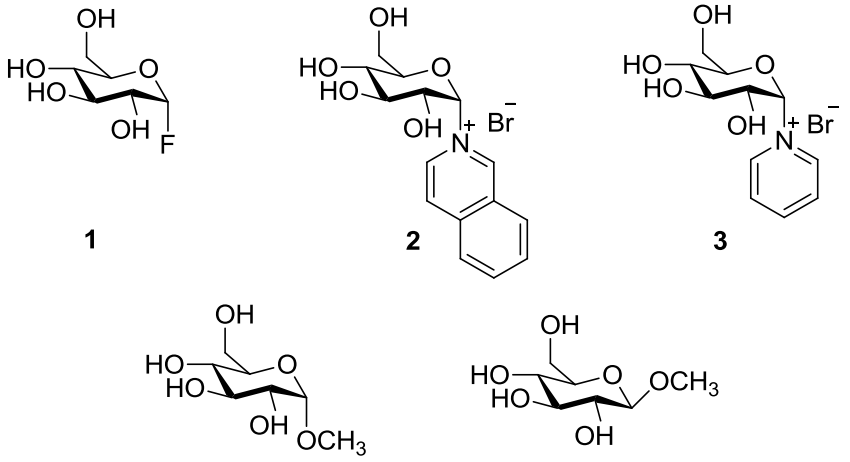

1 **2** **3**

4 **5**

Table 1.1. KIEs on enzyme-catalyzed glycoside hydrolysis.

Compound	KIE type	Enzyme	1-^{14}C	1-^{3}H	2-^{3}H	6,6-^{3}H$_2$
1[67]	k_{cat}/K_M	α-glucosidase (beet)	1.014	1.103	1.039	1.033
1[67]	k_{cat}/K_M	α-glucosidase (rice)	1.014	1.045	-	1.023
1[67]	k_{cat}/K_M	α-glucosidase (*Aspergillus niger*)	1.005	1.030	-	1.033
2[65]	k_{cat}	α-glucosidase (yeast)	1.036[a]	-	1.039[b]	-
3[65]	k_{cat}	α-glucosidase (yeast)	1.053[a]	-	1.169[b]	-
4[43]	k_{cat}/K_M	α-glucosidase (yeast)	1.0189[a]	-	-	-
5[43]	k_{cat}/K_M	β-glucosidase	1.061[a]	-	-	-

(almond)

[a] Converted from the ^{13}C KIE using the Swain-Schaad relationship: $(^{13}CKIE)^{1.89}=(^{14}CKIE)$.[47]

[b] Converted from the ^{2}H KIE using the Swain-Schaad relationship: $(^{2}HKIE)^{1.442}=(^{3}HKIE)$.[47,69]

Based on the 1-^{14}C KIEs, reactions of **1** in Table 1.1 appear to proceed through D_N*A_N mechanisms, which typically have 1-^{14}C KIEs of 1.00 – 1.02.[47,60] The other reactions are more likely A_ND_N, where the expected KIEs would be in the range of 1.025-1.139.[47]

The α-secondary deuterium KIEs for sucrase-isomaltase and isolated isomaltase domain with p-chloro-phenyl-α-D-glucopyranoside were measured by Cogoli et al.[70], and for sucrase isomaltase it was between 1.16 - 1.21 and 1.14 for isolated isomaltase. These large KIEs indicated a change from sp^3- to sp^2-hybridization around anomeric carbon, which strongly suggests an oxacarbenium ion-like TS.[70]

1.10.2. Nonenzymatic hydrolysis

Acid-catalyzed KIEs have been reported for **1**,[64] **4**,[43,66] **5**,[43,66] β-fluoro-glucoside (**6**),[64] methyl-5-thio-α-xylopyranoside (**7**),[68] methyl α-xylopyranoside (**8**),[68] and α-D-glucopyranosyl 4′-bromoisoquinolinium bromide (**9**).[65]

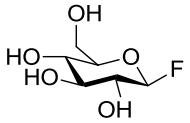

6

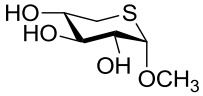

7

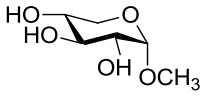

8

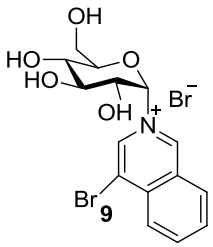

9

Table 1.2. KIEs on spontaneous and acid-catalyzed glycoside hydrolysis.

Compound	1-^{14}C[a]	1-^{3}H[a]	2-^{3}H[a]	6,6-$^{3}H_2$[a]
1[64]	1.061	1.208	1.088	-
4[66]	1.010	1.203	1.107	0.981
4[43]	1.013	-	-	-
5[66]	1.016	1.131	1.065	0.958
5[43]	1.019	-	-	-
6[64,b,c]	1.032	1.126	1.043	0.969
7[68]	1.059	1.211	1.089	0.998
8[68]	1.011	1.189	1.129	0.979
9[65,c]	1.009	1.283	1.138	-

[a] All the experimental KIEs were ^{2}H and ^{13}C KIEs. They were converted to ^{14}C and ^{3}H KIEs According to the Swain-Schaad relationships: (^{14}C KIE) = (^{13}CKIE)$^{1.89}$, (^{3}HKIE) = (^{2}HKIE)$^{1.44}$.[69]
[b] The experiments performed at 50°C (rest of the experiments done at 80°C).
[c] These experiments refer to spontaneous hydrolysis.

The 1-^{14}C KIEs showed that nonenzymatic hydrolysis of **1**, **6**, and **7** likely occurred via an A_ND_N mechanism, while **4**, **5**, **8**, and **9** proceeded through a D_N*A_N mechanism.

The information obtained from nonenzymatic reactions would be useful, since they show the different possible mechanisms of a reaction, and the effect of different leaving groups on the reaction.

1.11. Radioactivity Counting

Radioactive isotopes in KIE experiments are quantified by liquid scintillation counting, in which the radioactive sample is mixed with a scintillation cocktail. The scintillation cocktail contains solvent(s), emulsifier, and a fluor.[71] Liquid scintillation counting works by transferring kinetic energy from the emitted β-particles to electronically excite the solvent molecules. The excited solvent molecules excite the fluor molecules, which then emit photons in the UV

range. The photons are detected by the two photomultiplier tubes (PMT) which surrounded the vial. The PMTs must differentiate photons resulting from β-decay from other photons, including chemiluminescence and electronic noise in the PMTs. A given β-particle generally excites more than one fluor molecule, and the resultant photons are emitted in all directions equally. Thus, in order to accept an event as a radioactive decay, both PMTs must detect photons simultaneously.

^{3}H and ^{14}C have different counting efficiencies due to the different kinetic energies of their β-particles. ^{14}C β-particles have a 9-fold greater E_{max} (0.158 MeV) than ^{3}H (0.018 MeV).[7273] The greater a β-particle's kinetic energy, the greater the probability that the energy will be transferred to solvent or fluor molecules, and the greater the number of photons generated per radioactive decay. This difference in photons generated per radioactive decay is used to differentiate between ^{3}H and ^{14}C.

Quenching is any process that interferes with detection of a β-particle. It results in fewer counts and/or a shift in the energy distribution toward lower energies. There are three types of quenching: (1) Chemical quenching occurs when the emitted energy is not transferred to the solvent or the fluor, but is instead absorbed by other substances. Some electrophilic materials like halogens cause chemical quenching. (2) Colour quenching is caused by chromophores absorbing the photons that have been emitted by the fluor. (3) Physical quenching is caused by anything that physically blocks light, such as particles in the solution.[74,75]

One measure of quenching is the H-number, which is calculated and reported by the instrument. [76] The goal in KIE measurements is to have a constant, and preferably low H-number in all samples. Preparing all samples in an identical manner helps to minimize variability in H numbers.[61]

Fluor molecules can be excited by heat, room- or sunlight, and static charges, leading to luminescence. This can be avoided by avoiding those conditions, and by letting samples sit for a couple of hours before counting them.[77]

1.12. Computational Chemistry

Computational chemistry is used in TS analysis to interpret the experimental KIEs. Post-Hartree Fock methods are needed to give sufficiently accurate frequencies for TS analysis.[78,79] The least computationally expensive post-Hartree Fock methods are density functional theory (DFT) and hybrid DFT methods, so they are the most commonly used methods for KIE calculations. KIEs are a simple function of force constants[47,63,80,81] which are, in turn, simple functions of vibrational frequencies. The program QUIVER converts force constants and atomic masses into the reduced isotope partition function ratio (Q or $Q^{\ddagger}$) for each isotope of interest.[81,82] KIEs are calculated as KIE = $Q_{initial}/Q^{\ddagger}$.

If the calculated KIEs for a computational TS structure match the experimental values, then this is considered the experimental TS.[48,56] Since vibrational frequencies calculated by hybrid DFT methods are generally an accurate reflection of the molecular structure, the calculated KIEs will also be

accurate reflections of the molecular structures. Thus, a good match of computational to experimental KIEs is considered sufficient evidence for the TS structure.[47,78,79,83] If the computational TS structure is not correct, whether due to limitations in the level of theory, solvation/environmental effects, or other factors, then the calculated KIEs will not match the experimental values.

Chapter 2 - Materials and Methods

2.1. General

^{3}H- and ^{14}C-labelled glucoses were purchased from American Radiolabeled Chemicals (St. Louis, MO) and were lyophilized prior to use. All commercially available enzymes and reagents were purchased from Sigma-Aldrich or Bioshop Canada (Burlington, ON) and were used without further purification. Ultrapure water (ddH_2O) with resistivity $\geq$ 18 MΩ was used throughout. The *C*-terminal domain of sucrase/isomaltase (Ct-SI) was generously provided by Dr. David Rose (University of Waterloo).

2.2. Purification of the radiolabelled glucose

The radiolabelled glucoses contained impurities that inhibited hexokinase in the enzymatic synthesis of maltose, and were a source of contamination in the KIE experiments. Therefore, the radiolabelled materials were purified prior to maltose synthesis. Initially, all ^{3}H- and ^{14}C-labelled glucoses were purified by reversed phase C18-silica TLC's (Aldrich catalogue #Z293032) with 12:1.5:1 CH_3CN:ddH_2O:MeOH (v:v:v) as the solvent system. The method was later changed to HPLC purification (see below).

HPLC Purification of the radiolabelled glucose

Radiolabelled glucose (5 to10 µCi, 0.09 to 0.18 µmoL of ^{14}C, or 20 to 30 µCi, 1.3 to 2 nmoL of ^{3}H) was lyophilized, redissolved in ddH_2O, and purified by HPLC on a γ-aminopropylsilyl (APS) column (Supelcosil LC-NH2, 25 cm ×

4.6 mm ID, 5 μm particles). Two methodologies were developed to purify glucose, an isocratic and a gradient method.

In the isocratic elution method, the mobile phase was 75:8:17 MeCN:iPrOH:ddH_2O, at a flow rate of 0.5 mL/min. Glucose eluted at 10 - 13.5 min, and maltose eluted at 13.5 - 20 min, as detected by the elution of radioactivity (see below). It was also possible to detect standard injections of glucose and maltose by A_{190}, but detection was not sensitive enough for routine detection during syntheses.

The gradient elution method involved maintaining the column at 6 °C in a water bath, with the starting solvent composition of 75:8:17 MeCN:iPrOH:ddH_2O being changed to 98:2:0 over 9 min, then back to 75:8:17 over 1 min, which was maintained for the remainder of the purification. Glucose eluted at 10.5 - 13 min, while maltose eluted at 20 - 26 min. Fractions containing glucose were dried down using a rotary evaporator. The purified glucose was resuspended in ddH_2O and stored at -20 °C.

Eluted radioactivity was detected by mixing an aliquot of each fraction with 10 mL of Biosafe II scintillation fluid in scintillation vials and counting the radioactivity with a Beckman LS 6500 scintillation counter. For ^{14}C samples, a wide range program was used, with the window set to 0 to 1000 channels (arbitrary units). ^{3}H samples were counted with the window set to 0 to 460 channels.

2.3. Glucose 6-phosphate synthesis

The first step of maltose synthesis was the phosphorylation of glucose to glucose 6-phosphate (G6P) using hexokinase (Figure 2.1). A typical reaction contained 1.8 mM ^{14}C or ^{3}H glucose. For ^{14}C reactions, 10 μCi was used with no added cold glucose. For ^{3}H reactions, which had higher specific activities 20-30 μCi was used, with added unlabelled glucose as a carrier, to maintain 1.8 mM glucose. The reaction mixtures contained glucose, plus 0.8 mM adenosine triphosphate (ATP), 10 mM phosphoenolpyruvate (PEP), 24 units of rabbit muscle pyruvate kinase (PK), 8 units of *Saccharomyces cerevisiae* hexokinase, 6 mM $MgCl_2$, and 50 mM 2-(*N*-morpholino) ethanesulfonic acid (MES), pH 7.3, in a volume of 40 μL. The reaction mixture was incubated 18 h at room temperature, then quenched by heating at 95°C for 5 min. Precipitated proteins were removed by centrifugation at 16,000 ×g for 15 min.

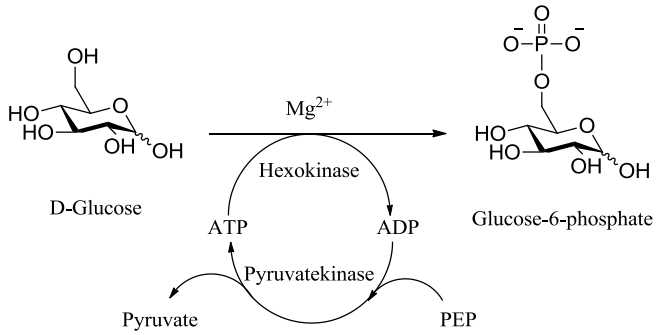

Figure 2.1. D-Glucose phosphorylation reaction.
D-Glucose is phosphorylated to G6P (glucose-6-phosphate) by using ATP (adenosine triphosphate), Mg^{2+}, and hexokinase enzyme. The ATP is regenerated from ADP (adenosine diphosphate) using pyruvate kinase enzyme and PEP (phosphoenol pyruvate).

2.4. Maltose synthesis

Glucose 6-phosphate from the above reaction was used without further purification to synthesize maltose. To the glucose 6-phosphate reaction mixture was added 2 mM $MgCl_2$, 10 mM 7-methylinosine, 0.1 mM glucose 1,6-bisphosphate, 0.37 units of purine nucleoside phosphorylase, 1.5 units of *Lactococcus sp.* β-phosphoglucomutase, 0.12 units *Enterococcus sp.* maltose phosphorylase and unlabelled glucose to bring the final glucose concentration to 2.5 mM in a final volume of 68 µL (Figure 2.2). The glucose 1,6-bisphosphate was needed to "kick start" β-phosphoglucomutase. The reaction was incubated at room temperature for 18 h, and stopped by heating at 95 °C for 5 min.

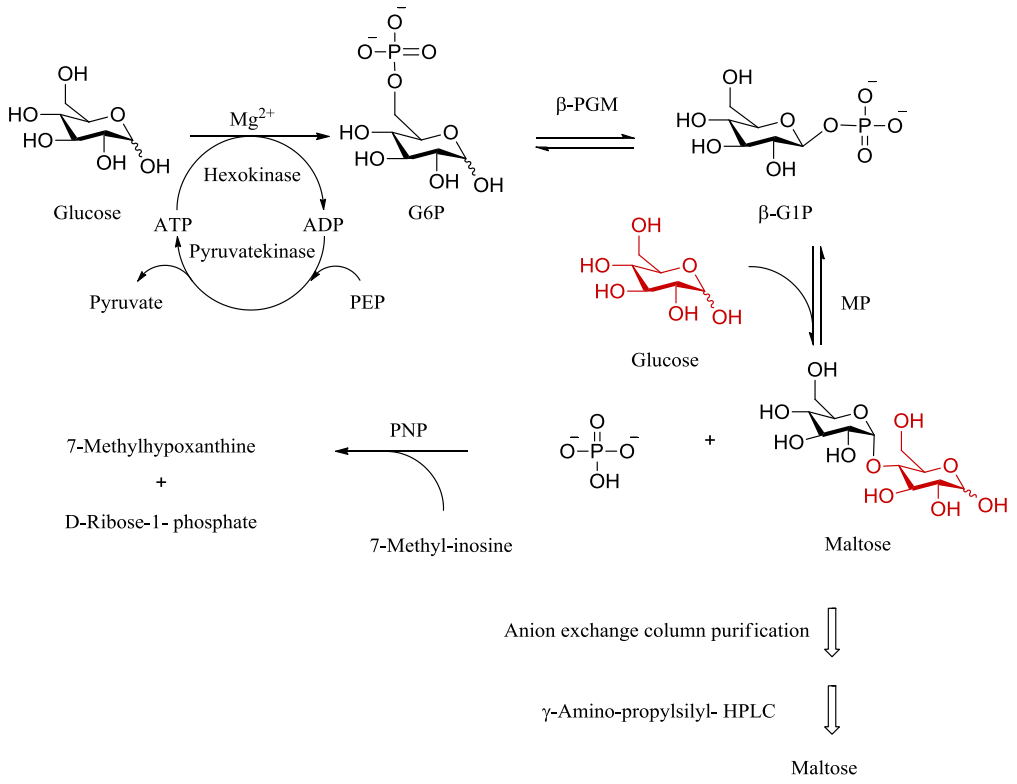

Figure 2.2. Maltose Synthesis.
Maltose synthesis is performed in two steps. First, glucose phosphorylation. Second ,maltose synthesis. ATP: adenosine triphosphate, ADP: adenosine diphosphate, PEP:

phosphoenolpyruvate, G6P: glucose-6-phosphate, β-G1P: beta- glucose-1-phosphate, β-PGM: beta-phosphoglucomutase, MP: maltose phosphorylase, PNP: purine nucleoside phosphorylase.

2.5. Sucrose Synthesis

In sucrose synthesis, 2 mM $MgCl_2$, 10 mM 7-methylinosine, 0.37 units of purine nucleoside phosphorylase, 3 units of rabbit muscle α-phosphoglucomutase, 0.025 units *E. coli* sucrose phosphorylase and 125 mM unlabelled fructose was added to the glucose 6-phosphate reaction mixture, in a final volume of 55 µL (Figure 2.3). The reaction was incubated at room temperature for 18 h, and stopped by heating at 95 °C for 5 min.

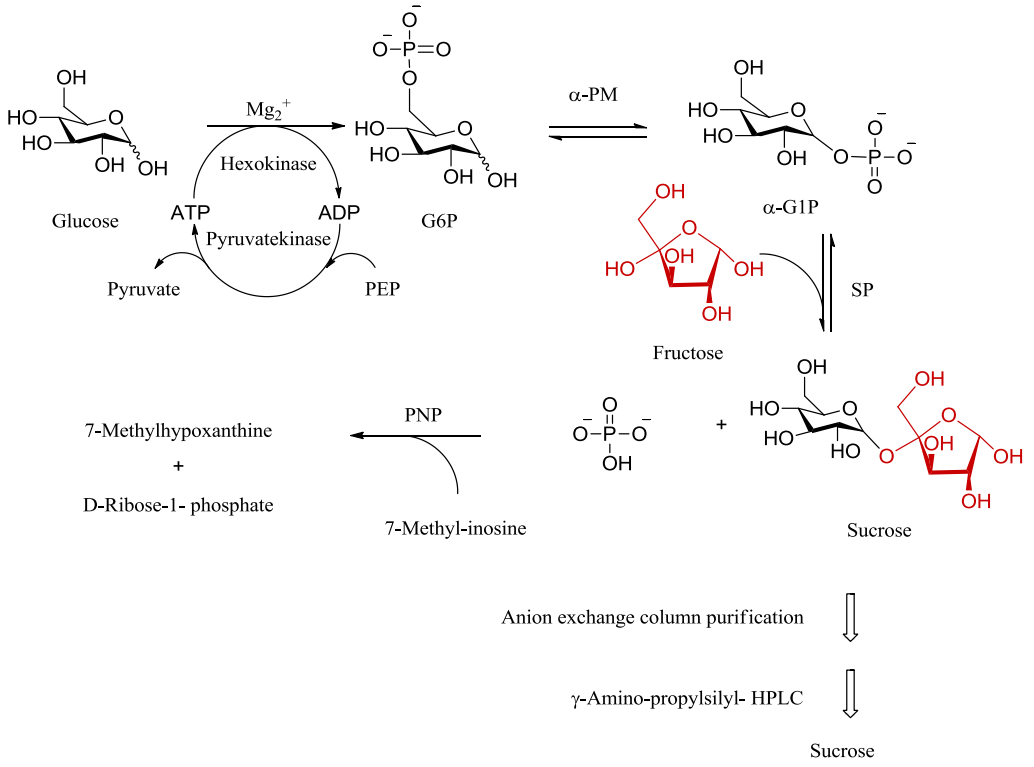

Figure 2.3. Sucrose synthesis

Sucrose synthesis is performed in two steps. First, glucose phosphorylation. Second ,sucrose synthesis. ATP: adenosine triphosphate, ADP: adenosine diphosphate, PEP: phosphoenolpyruvate, G6P: glucose-6-phosphate, α-G1P: alpha- glucose-1-phosphate, α-PM: alpha-phosphoglucomutase, SP: sucrose phosphorylase, PNP: purine nucleoside phosphorylase.

2.6. Maltose purification

Maltose was purified in two steps; anion exchange chromatography removed G6P and other phosphorylated compounds, then APS chromatography separated maltose from glucose and other uncharged compounds.

Maltose was purified by anion exchange column on a Mono-Q 5/50 GL column (1 mL column volume) using stepwise elution, starting with 10 mM ammonium acetate, pH 8.6, for 8 min, then a step to 400 mM NaCl, 6 mM ammonium acetate, pH 8.6, for 8 min, at a flow rate of 1 mL/min. The maltose-containing low salt eluate was lyophilized and redissolved in ddH_2O.

This mixture was further purified by APS chromatography using the gradient elution method described above. The maltose-containing fractions were dried down on a rotary evaporator and resuspended in water.

Sucrose Purification

Sucrose purification was done in the same manner as maltose. An anion exchange chromatography followed by purification with APS HPLC.

2.7. Enzymatic KIE reaction

KIEs were measured by making a mixture of ^{3}H- and ^{14}C-labelled maltose, allowing the hydrolysis reaction to proceed to ≈50% to allow the enzyme to discriminate between the isotopologues, then re-isolating the residual substrate and/or product, and measuring the change in the ^{3}H:^{14}C ratio relative to the reference sample. The reference sample was unreacted maltose (0% reaction)

when the isotope ratios in residual maltose were being measured. When isotope ratios were measured in G6P (the phosphorylated product of Ct-SI) the reference sample was G6P from the 100% reaction.

Purification of Substrates

A mixture of ^{3}H- and ^{14}C-labelled maltose containing 5×10^{5} to 7.5×10^{5} counts per minute (cpm) of each isotope was made and repurified by APS chromatography, as described above. The radioactivity-containing fractions were dried down on a rotary evaporator, then redissolved in ddH_2O.

2.8. Enzyme-catalyzed KIE reaction mixture

To the repurified maltose was added 50 mM MES buffer, pH 7.3, and 1 unit *Lactobacillus sp*. maltose epimerase in a final volume of 60 μL. The mixture was divided into two fractions; 20 μL was used as the reference sample and 40 μL was used for the partial reaction.

For the partial reaction, 50 to 80 nM Ct-SI and 0.1 to 0.16 mg/mL of bovine serum albumin (BSA) were added. The reaction progress was monitored by APS chromatography with the gradient elution method. The reaction was stopped at ≈50% completion (ca. 3-5 h) by heat quenching at 95 °C for 5 min.

2.9. KIE measurement: Residual substrate method

When isotope ratios were measured in the residual maltose, then residual maltose in the partial reaction was separated from glucose by APS chromatography. The 0% reaction sample was similarly chromatographed. Both

isocratic and gradient APS chromatography were tested (Section 2.2). Fractions of 30 s were collected around the expected elution times for the isocratic method, with 1 min fraction for the rest of the run, while 1 min fractions were collected with the gradient method throughout the run.

For the isocratic method, each fraction was made to 1.06 g with mobile phase, as necessary, to ensure the same solvent composition, then 15 g of scintillation fluid (Ecoscint A, National Diagnostics, USA) was added. In the gradient method, all fractions were 1 mL, and therefore not adjusted. The blank and ^{14}C standard samples (see below) were made using as solvent the eluate from a blank injection on the APS column collected at the glucose and maltose elution times. All the fractions were counted for 1 min, and those without radioactivity were discarded. The remaining fractions were counted for multiple 10 min cycles, and isotope ratios were then determined (see below).

2.10. KIE measurement: Products method

If the isotope ratios were to be measured on the products, then the reference sample was the reaction taken to completion. For both the partial and 100% reactions, the product glucose was converted to G6P with hexokinase and separated from maltose by anion exchange chromatography. Maltose in the 100% reaction was hydrolysed to glucose by the addition of 3 units of *Saccharomyces cerevisiae* α-glucosidase, 1 unit maltose epimerase, 50mM MES, pH 7.3, and overnight incubation at room temperature.

After the partial and 100% reactions were complete, glucose was converted to G6P by addition of 0.8 mM adenosine triphosphate (ATP), 10 mM phosphoenolpyruvate (PEP), 24 units of pyruvate kinase, 8 units of hexokinase, and either 6 mM $MgCl_2$ (partial reaction) or 14 mM $MgCl_2$ (100% reaction, α-glucosidase contained ethylenediaminetetraacetic acid (EDTA)) in a final volume of 75 μL (Figure 2.1). Reactions were incubated for 18 h at room temperature, and stopped by heating at 95 °C for 5 min. Control experiments showed that hexokinase did not phosphorylate maltose. G6P was then separated from maltose by Mono-Q anion exchange chromatography, as described above, with 1ml (1 min) fractions collected.

Each chromatographic fraction was weighed, and the Mono-Q mobile phase was added, as necessary, to give 1.06 g, then 15 g of scintillation fluid (Ecoscint A) was added. All the fractions were counted for 1 min, and those without radioactivity were discarded, and the remaining samples were counted for multiple cycles of 10 min each. The isotope ratios were then determined (see below).

2.11. KIE measurement: Acid-catalyzed maltose hydrolysis

Radiolabelled maltose was prepared as for the enzymatic reactions. The HPLC repurified mixture of ^{3}H- and ^{14}C-maltoses was redissolved in 15 μL of ddH_2O. A 10 μL aliquot was then added to 9 μL of 4.32 M HCl and the volume was brought to 20 μL with ddH_2O then was reacted at 80 °C for 20 min to reach

≈50% hydrolysis. The reaction was stopped by adding 13 µL of 4 M KOH, and 5 µL of 250 mM MES buffer, pH 7.3, in a final volume of 38 µL.

The remaining 5 µL was used for the 0% reaction. It was added to 9 µL of 4.32 M HCl and the volume was brought to 20 µL with ddH_2O and quenched immediately after acid addition with 13 µL of 4 M KOH, and 5 µL of 250mM MES, pH 7.3, in a final volume of 38 µL.

Glucose and maltose were separated using the gradient APS chromatography method. Fractions (1 min) were collected in scintillation vials. Each fraction was weighed and the liquid weights of the fractions were adjusted to be equal and then 15 g of scintillation fluid was added to each vial. The blank and ^{14}C standard samples (see below) were made by doing a blank injection on the APS column, and collecting the eluate at the times corresponding to glucose and maltose elution, and using the eluate as solvent for the blank and standard samples.

2.12. Isotope ratio measurement and KIE calculation

Isotope ratios were determined using dual channel LSC analysis. The principle is that the lower energy window (Win1, 0 - 460 channels) contains >99.99% of the ^{3}H counts, plus some of the ^{14}C counts. The higher energy window (Win2, 461 - 1000 channels) contains only ^{14}C counts. The Win1:Win2 ratio is measured for a standard containing ^{14}C only. Using this ratio, it is possible to convert the Win1:Win2 ratio to ^{3}H:^{14}C for each sample. Blank samples which had the same solvent composition as the samples were used to

determine background counts. After subtracting the background counts, ^{3}H and ^{14}C were calculated from Win1 and Win2 using equations 2.1 and 2.2 (all in units of counts per minute (cpm)):

$$^{3}\mathrm{H} = \mathrm{Win1} - \left[\mathrm{Win2} \times \left(\frac{\mathrm{Win1}}{\mathrm{Win2}}\right)_{^{14}\mathrm{C_{std}}}\right] \quad \textbf{(2.1)}$$

$$^{14}\mathrm{C} = \mathrm{Win2} \times \left[1 + \left(\frac{\mathrm{Win1}}{\mathrm{Win2}}\right)_{^{14}\mathrm{C_{std}}}\right] \quad \textbf{(2.2)}$$

KIEs were calculated based on the substrate or product isotope ratios. Equation 1.7 is for residual substrate:

$$\mathrm{KIE\ (substrate)} = \frac{\ln\left[\frac{(1-f)\left(1+\frac{1}{\mathrm{R}_0}\right)}{\left(1+\frac{1}{\mathrm{R}_i}\right)}\right]}{\ln\left[\frac{(1-f)(1+R_0)}{(1+R_i)}\right]} \quad \textbf{(1.7)}$$

where R_i is the ratio light: heavy for the partial reaction, R_0 is the same ratio for the 0% reaction, and f is the fractional extent of reaction.[51] For a ^{3}H KIE measurement, light:heavy is ^{14}C:^{3}H because ^{14}C is a reporter on ^{1}H.

KIEs based on the product isotope ratio were calculated with equation 1.8:

$$\mathrm{KIE(product)} = 1 + \frac{\ln\left[1 + \left[\frac{{}^{A_0}/_{A'_0} - {}^{X}/_{X'}}{{}^{A_0}/_{A'_0}}\right]\left[\frac{f\left[\frac{1 + {}^{A_0}/_{A'_0}}{1 + {}^{X}/_{X'}}\right]}{1 - f\left[\frac{1 + {}^{A_0}/_{A'_0}}{1 + {}^{X}/_{X'}}\right]}\right]\right]}{\ln\left[1 - f\left[\frac{1 + {}^{A_0}/_{A'_0}}{1 + {}^{X}/_{X'}}\right]\right]} \quad \textbf{(1.8)}$$

where A_0 and A'_0 are the light and heavy isotopes, respectively, in the 100% reaction, X and X' are the light and heavy isotopes, respectively, in the partial reaction, and the *f* is the fractional extent of the reaction.[63]

2.13. Computational

The electronic structure optimization, frequency and force constant calculations were done with Gaussian 09[84] using hybrid density functional theory (DFT), with Becke's exchange functional, Perdew and Wang's correlation functional, and 6-31+G** as the basis set (RB3PW91/6-31+G**). The QST3 method was used to calculate the TS model, using as starting structures the optimized reactant and product structures, and a guess TS structure based on a potential energy scan of the reaction. Frequency calculations confirmed that the TS model had only one imaginary frequency. Further, intrinsic reaction coordinate (IRC) calculations were performed to confirm the correct reaction

motion for the leaving group. The vibrational frequency and force constants plus the masses of the atoms, and the temperature were used in the program called QUIVER[81] to determine the reduced isotope fractionation factors for each isotope (Q or $Q^{\ddagger}$ for reactant or TS, respectively) using equations 2.3 and 2.4.

$$EIE = Q_{initial}/Q_{final} \quad \textbf{(2.3)}$$

$$KIE = Q_{initial}/Q^{\ddagger}_{TS} \times ({}^{light}\nu^*/{}^{heavy}\nu^*) \quad \textbf{(2.4)}$$

The ratio of the imaginary frequencies (${}^{light}\nu^*/{}^{heavy}\nu^*$) is known as the Teller-Redlich product.[56] Moreover, Bell's tunnelling corrections were also used in calculations.

All the calculations were done on α-methyl glucopyranoside with $^4C_1$ conformation. The KIEs and EIEs were only calculated for the first step, i.e., departure of the leaving group.

Chapter 3 - Results

3.1. General

The goal of this study was to elucidate the TS structure of enzyme- and acid-catalyzed maltose hydrolysis, the enzyme being the *C*-terminal domain of sucrase-isomaltase (Ct-SI). The study required pure radiolabelled maltose as substrate; the substrate synthesis yields were optimized, and a purification method was developed. As for the KIE measurements, they were made using three different methods, and the results were compared with each other. Different attempts were made to achieve complete separation of glucose and maltose in the partial reaction mixture.

3.2. Purification

Labelled glucoses and maltoses were initially purified by reverse phase C18 TLC (RP TLC). Later, APS HPLC methods were developed, which improved the separation.

3.2.1. Reverse Phase TLC Purification Method

Radiolabelled glucoses were not radioisotopically pure, and the contaminants co-migrated with maltose on RP TLC. Therefore, glucoses are purified prior to maltose synthesis (Figure 3.1). The glucose was still not completely pure, and the purification yield was only 50%, so an APS HPLC purification was developed.

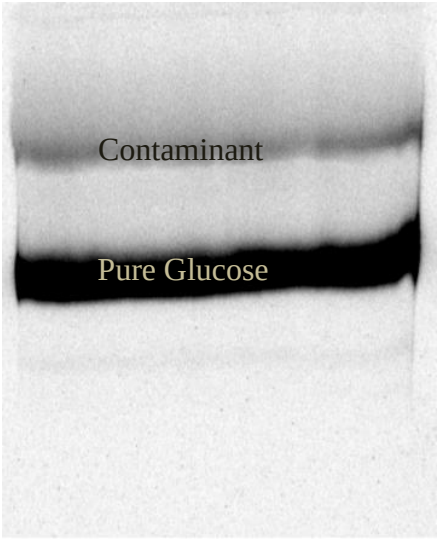

Figure 3.1. The TLC for purification of radiolabelled D-glucose
The purification of radiolabelled glucose by RP TLC with 12:1.5:1 (CH_3CN:ddH_2O:CH_3OH) as a running solvent.

3.2.2. Purification Methods Using γ-aminopropylsilyl (APS) Chromatography

RP TLC purification of glucose did not adequately remove the contamination, so an APS HPLC purification method was developed for both glucose and maltose. Solute elution was monitored by following the eluted radioactivity, or through the A_{190}. Absorbance detection was insensitive and the background absorbance was high (Figure 3.2), so radioactivity was more commonly monitored.

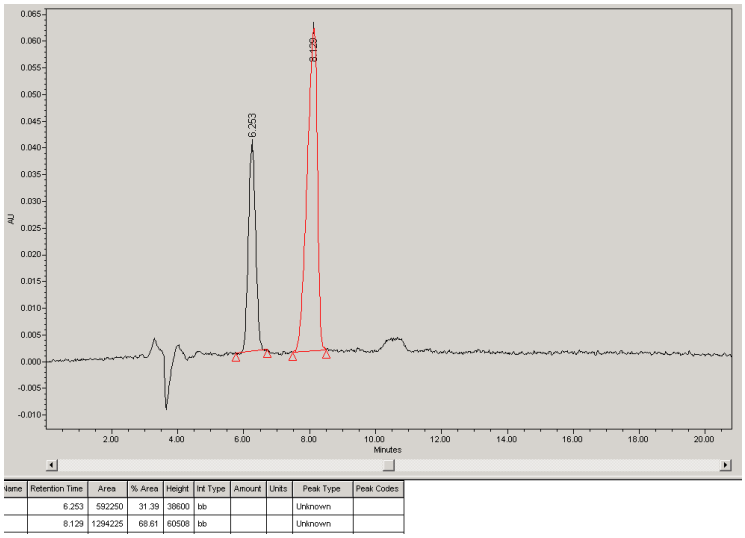

Name	Retention Time	Area	% Area	Height	Int Type	Amount	Units	Peak Type	Peak Codes
	6.253	592250	31.39	38600	bb			Unknown	
	8.129	1294225	68.61	60508	bb			Unknown	

Figure 3.2. Elution of unlabelled D-glucose and maltose standards on HPLC with detection at 190 nm.

Injection of standard D-glucose (6.2 min) and maltose (8.1 min) with isocratic elution in 75:25 MeCN:ddH_2O. A_{190} was used for detection. 1.11 µmol of each analyte was injected.

As method development progressed, the elution conditions for glucose purification changed from isocratic elution with 75: 25 MeCN:ddH_2O (Figure 3.3, Figure 3.4) to isocratic elution with 75:8:17 MeCN:iPrOH:ddH_2O (Figure 3.5), to gradient elution (Figure 3.6). Isocratic elution with 75: 25 MeCN:ddH_2O gave apparently acceptable purification of glucose from its contaminants, primarily eluting between 7 and 12 min (Figure 3.3), but did not give complete separation of glucose and maltose (Figure 3.4).

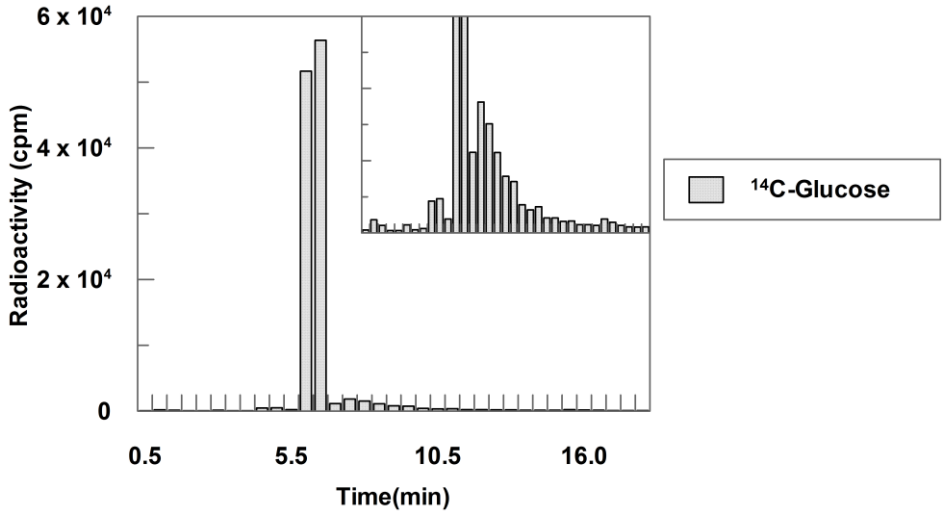

Figure 3.3. Distribution of radioactivity for HPLC purification of [^{14}C]-glucose.
Distribution of radioactivity for HPLC purification of [^{14}C]glucose with isocratic 75:25 MeCN:ddH_2O. The contaminant peak eluted between 7- 12 min.

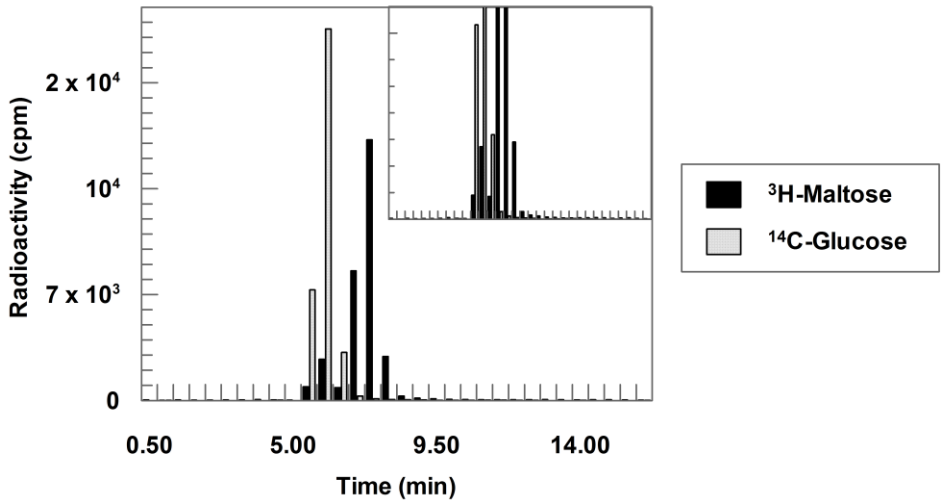

Figure 3.4. Distribution of radioactivity for HPLC purification of [^{14}C]glucose and [^{3}H]maltose.
Distribution of radioactivity for HPLC purification of [^{14}C]glucose and [^{3}H]maltose with isocratic 75:25 MeCN:ddH_2O. Glucose eluted at 6.5 – 7.5 min, and maltose peak time eluted at 7.5 - 10 min.

Isopropanol was added to improve the separation of D-glucose from maltose (Figure 3.5). Changing to gradient elution improved the separation further (Figure 3.6).

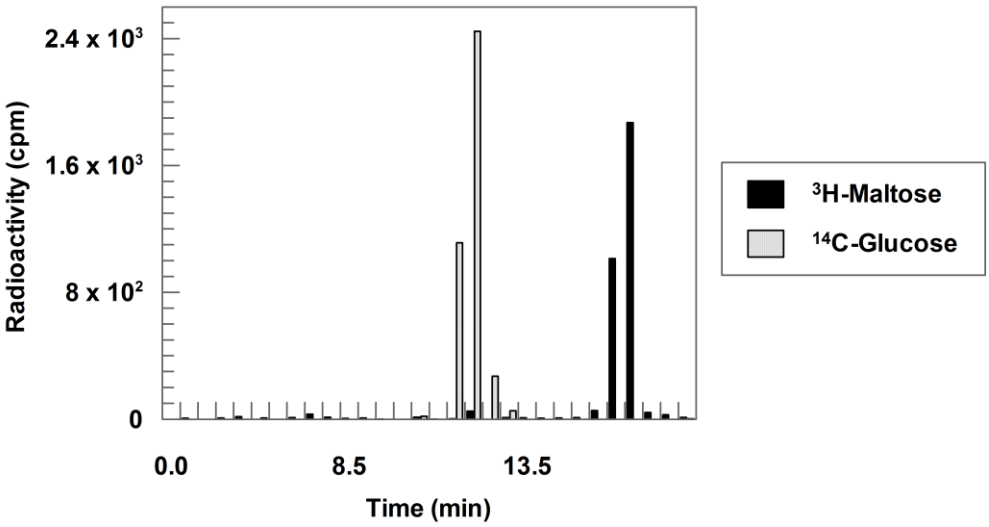

Figure 3.5. Distribution of radioactivity for isocratic APS HPLC purification of [^{14}C]glucose and [^{3}H]maltose using isopropanol in the solvent.

Distribution of radioactivity for APS HPLC purification of [^{14}C]glucose and [^{3}H]maltose with isocratic 75:8:25 MeCN:iPrOH:ddH_2O. Glucose eluted between 10 – 14.5 min, and maltose peak eluted at 14.5 - 19 min.

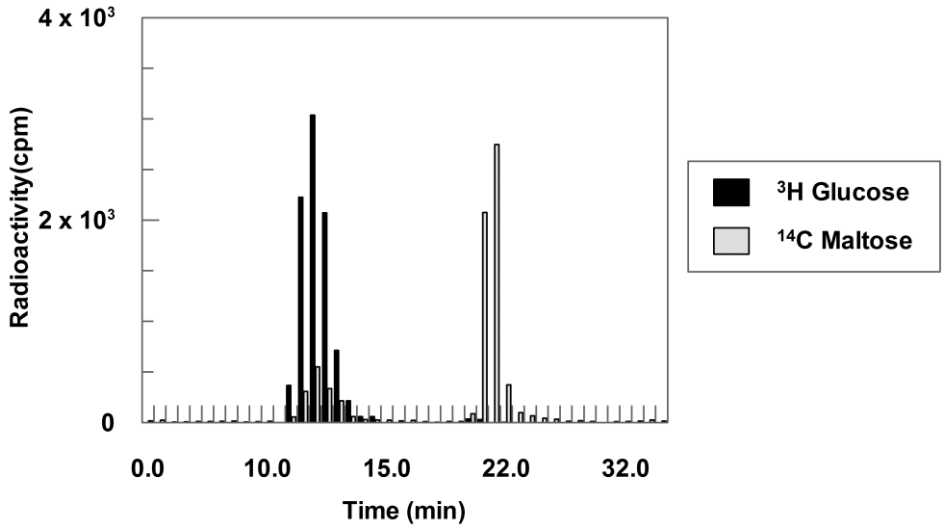

Figure 3.6. Distribution of radioactivity for gradient APS HPLC purification of [^{3}H]glucose and [^{14}C]maltose.

[^{3}H]glucose and [^{14}C]maltose were purified with a gradient method starting from 75:8:25 MeCN:iPrOH:ddH_2O, which changed to 98:2:0 over 9 min, then back to 75:8:17 over 1 min. Glucose eluted between 11.5 – 15.5 min, and maltose eluted between 21.5 - 26 min.

3.3. Maltose and Sucrose Synthesis

Maltose and sucrose syntheses had already been developed prior to my arrival, though the yields were poor. The yields were increased from 20% to 90% by changing the reactant concentrations, the enzymes used, the reaction times, and the purification methods. Initially, G6P was purified by anion exchange chromatography immediately after synthesis. In order to improve the synthetic yield, G6P was used immediately after synthesis for maltose synthesis by adding the maltose synthetic enzymes and reagents directly to the G6P synthetic mixture. Anion exchange was then used to remove all phosphorylated compounds, right before APS HPLC purification. For radiolabelled maltose, the synthesis was optimized with respect to both the glycone and aglycone residues, while sucrose was synthesized with only the glycone radiolabelled.

3.4. Conducting a KIE Measurement

Mixtures of [^{3}H]- and [^{14}C]-labelled maltoses for KIE measurements were repurified by APS HPLC chromatography immediately before KIE measurement. KIEs were measured by running the reaction to ≈50% completion, which allows the enzyme to discriminate between the light and heavy isotopes. The isotope ratio is then measured and compared to the original value before reaction, that is, in the 0% or 100% reaction. Different amounts of Ct-SI were tested to find the best concentration and time to achieve the 50% reaction (Figure 3.7). In this example, the enzyme reached 50% reaction after 5h.

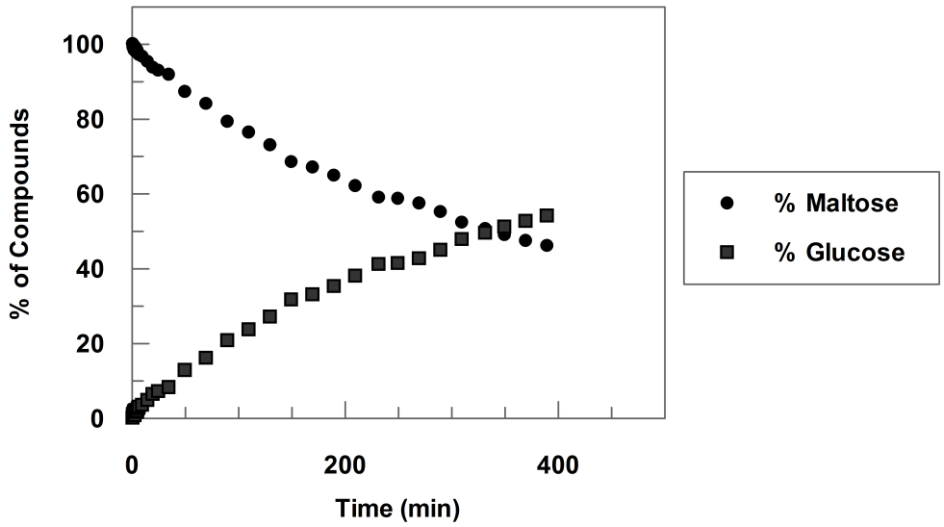

Figure 3.7. Radiolabelled maltose hydrolysis by Ct-SI.
50% hydrolysis was achieved after letting 200nCi [^{14}C]maltose react with 5 nM Ct-SI for≈5h at 37°C. The reaction progress was monitored by normal phase TLC (Section 2.2) with a storage phosphor-autoradiography, and band quantification with the ImageJ program.

Once the basic reaction conditions were found, the progress of routine KIE reactions were monitored by APS HPLC.

3.5. KIE Purification Methods Using γ-Aminopropylsilyl Column

The first KIE reaction was separated with isocratic APS HPLC using 75:8:17 MeCN:iPrOH:ddH_2O as the mobile phase (Figure 3.8 and Figure 3.9).

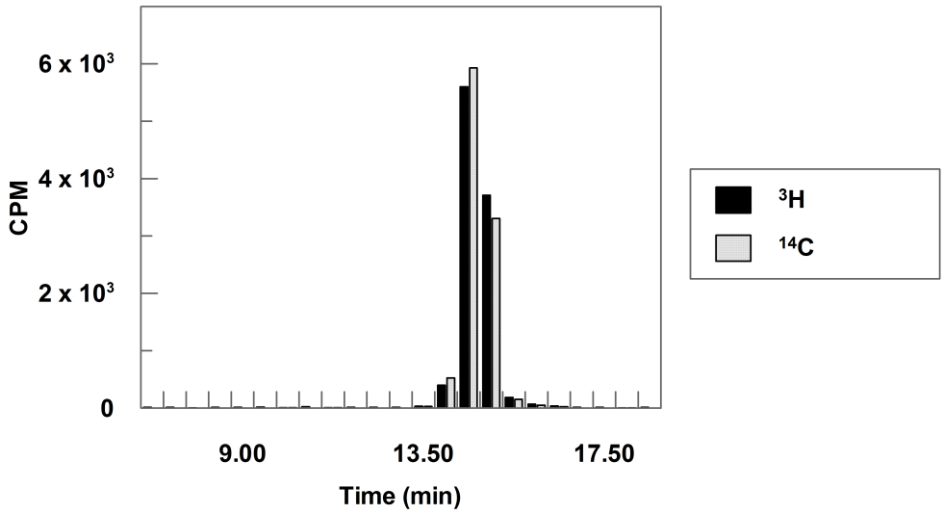

Figure 3.8. Reference KIE reaction mixture (0% reaction) separated using isocratic APS HPLC.

Isocratic APS HPLC chromatogram of the 0% reaction mixture, run in 75:8:17 MeCN:iPrOH:ddH_2O. The reaction mixture consisted of a mixture of [1-^{3}H]- and [6-^{14}C]maltose.

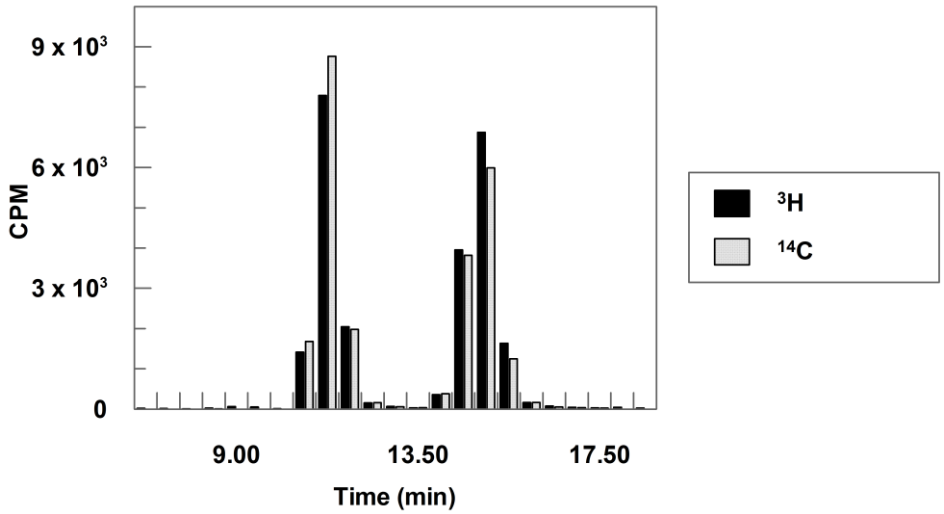

Figure 3.9. Partial KIE reaction (50% reaction) separated using isocratic APS HPLC.

Isocratic APS HPLC chromatogram of the 50% reaction mixture, run in 75:8:17 MeCN:iPrOH:ddH_2O. The initial reaction mixture consisted of a mixture of [1-^{3}H]- and [6-^{14}C]maltose. Glucose eluted at 11 to 13.5 min, while maltose eluted at 13.5 to 17.5 min.

The separation appeared sufficient for KIE determination; however, after multiple KIE measurements, the variability in the observed KIE values was too

large to be useful for TS analysis. The KIEs for Ct-SI-catalyzed hydrolysis at three different positions were measured, namely the 1-^{3}H (α-secondary) KIE (Table 3.1), the 6-^{3}H (remote) KIE (Table 3.2), and the 1-^{14}C (primary) KIE (Table 3.3). All three values were in the range expected for different mechanisms,[43,47] though the 95% confidence intervals (95% CI) for each KIE were too large to be useful in TS analysis.

Table 3.1. Experimental 1-^{3}H KIEs for Ct-SI-catalyzed maltose hydrolysis, with post-reaction purification by isocratic APS HPLC chromatography.

Trial	cycles[a]	KIE (substrates)[b]	KIE (products)[c]
1	41	1.177	1.166
2	16	1.141	1.152
3[d]	22	1.177	1.152
4	11	1.144	1.149
5	17	1.135	1.201
Average		1.155	1.174
Stdev		0.020	0.025
95% CI		0.025	0.031

[a] Each sample was counted for 10 min each per cycle, for the number of cycles indicated.
[b] Eq. (1.7**)**, calculated using the isotope ratios in the maltose substrate.
[c] Eq. (1.8), calculated using the isotope ratios in the glucose product.
[d] Purified samples were rotary evaporated to dryness, then resuspended in 15 g of Ecoscint A scintillation fluid.

Table 3.2. Experimental 6-^{3}H KIEs for Ct-SI-catalyzed maltose hydrolysis, with post-reaction purification by isocratic APS HPLC chromatography.

Trial	cycles[a]	KIE (substrate)[b]	KIE (product)[c]
1	18	1.001	1.054
2	16	1.024	1.053
3	17	1.054	1.045
4	31	1.013	1.052
5	6	1.179	1.102
Average		1.054	1.061
Stdev		0.073	0.023
95% CI		0.090	0.028

[a] Each sample was counted for 10 min each per cycle, for the number of cycles indicated.
[b] Eq. (1.7**)**, calculated using the isotope ratios in the maltose substrate.
[c] Eq. (1.8**)**, calculated using the isotope ratios in the glucose product.

Table 3.3. 1-^{14}C KIE for Ct-SI-catalyzed maltose hydrolysis, with post-reaction purification by isocratic APS HPLC chromatography.
The 1-^{14}C KIEs were not corrected for the 6,6-$^{3}H_2$ labelling.

Trial	cycles[a]	KIE (substrate)[b]	KIE (product)[c]
1[d]	5	1.034	0.932
2	24	1.030	0.999
Average		1.032	0.966
Stdev		0.003	0.048
95% CI		-[e]	-[e]

[a] Each sample was counted for 10 min each per cycle, for the number of cycles indicated.
[b] Eq. (1.7**)**calculated using the isotope ratios in the maltose substrate.
[c] Eq. (1.8**)**, calculated using the isotope ratios in the glucose product.
[d] Purified samples were rotary evaporated to dryness, then resuspended in 15 g of Ecoscint A scintillation fluid.
[e] There were too few independent experiments to calculate a 95% confidence interval.

The gradient method was later developed to improve the separation of glucose and maltose (Figure 3.10, Figure 3.11). However, in the partial reaction an extra peak appeared that eluted later than maltose (Figure 3.11). Adding 0.3 mM unlabelled maltose prior to heat quenching reduced but did not eliminate the peak (Figure 3.12).

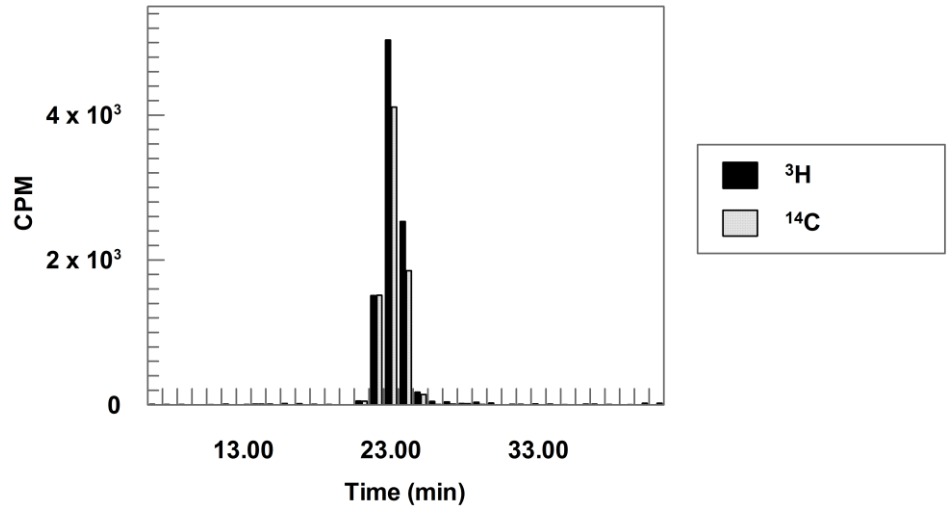

Figure 3.10. 0% reaction mixture separated by gradient APS HPLC chromatography.

Maltose eluted at 21 to 26 min.

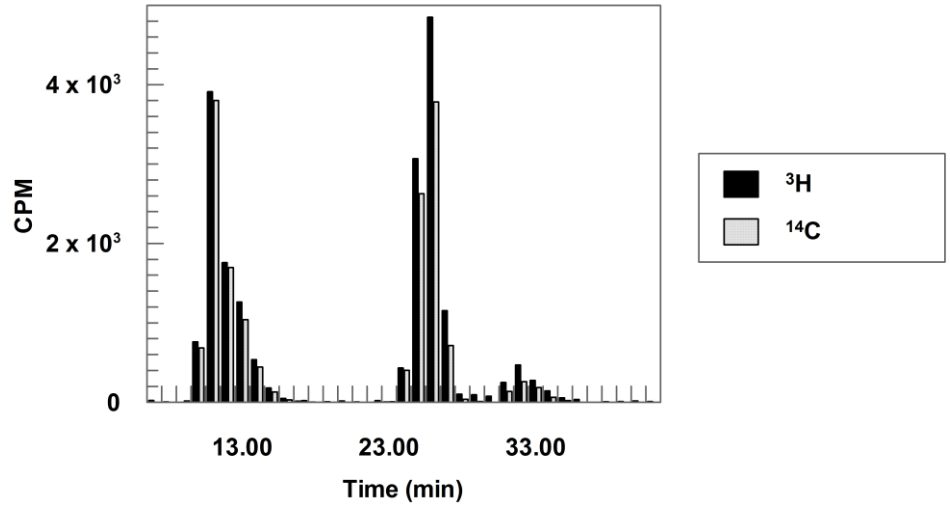

Figure 3.11. Partial KIE reaction mixture separated by gradient APS HPLC chromatography.

Glucose eluted at 10 - 17 min; maltose eluted at 23 - 26 min. An extra peak consistently appeared after maltose that was not present in other samples. Its source is unknown.

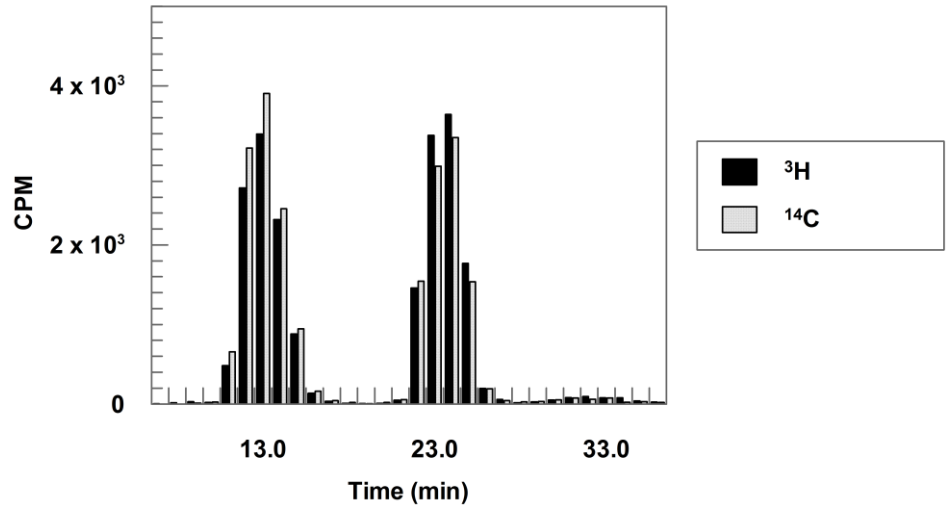

Figure 3.12. Partial KIE reaction with added unlabelled maltose, then separated using APS HPLC chromatography.

Unlabelled maltose (0.3 mM) was added to the partial reaction mixture before heat quenching.

The Ct-SI-catalyzed 1-^{3}H KIE was measured again using the gradient APS HPLC method for the post-reaction purification (Table 3.4). The average value was higher than the isocratic method, but still within the range of values observed previously.[43,47] The 95% confidence interval was similar to the isocratic method.

Table 3.4. Ct-SI-catalyzed 1-^{3}H KIEs for maltose hydrolysis, with post-reaction purification by gradient APS HPLC chromatography.

Trial	cycles[a]	KIE (substrate)[b]	KIE (product)[c]
1	5	1.164	1.211
2	7	1.156	1.290
3	12	1.155	1.230
4	9	1.168	1.223
5	17	1.155	1.230
6	7	1.257	1.241
7	9	1.306	1.223
8	4	1.121	1.262
9	6	1.143	1.188
10	5	1.158	1.261
Average		1.179	1.237
Stdev		0.057	0.028
95% CI		0.041	0.020

[a] Each sample was counted for 10 min each per cycle, for the number of cycles indicated.
[b] Eq. (1.7**)**, calculated using the isotope ratios in the maltose substrate.
[c] Eq. (1.8**)**, calculated using the isotope ratios in the glucose product.

KIEs were also measured for the remote, 6,6-$^3H_2$, label by the same method (Table 3.5). The measured KIE for this position with the gradient purification, 1.16 ± 0.08, was higher than with isocratic purification, 1.05 ± 0.09. Moreover, this KIE is higher than expected for a remote position.

Table 3.5. 6,6-$^{3}H_2$ KIEs for Ct-SI-catalyzed maltose hydrolysis, with post-reaction purification by gradient APS HPLC chromatography.

Trial	cycles[a]	KIE (substrate)[b]	KIE (product)[c]
1	7	1.270	1.027
2	7	1.220	1.071
3	11	1.132	1.127
4	8	1.203	1.252
5	27	1.003	1.053
6	9	1.158	1.168
7	6	1.096	1.097
Average		1.155	1.113
Stdev		0.088	0.077
95% CI		0.082	0.071

[a] Each sample was counted for 10 min each per cycle, for the number of cycles indicated.
[b] Eq. (1.7**)**, calculated using the isotope ratios in the maltose substrate.
[c] Eq. (1.8**)**, calculated using the isotope ratios in the glucose product.

The 2-^{14}C KIE was also measured, but the data were not considered reliable because of the high variability (Table 3.6). Also, few experiments were done for this position and the existing ones had low number of cycles.

Table 3.6. 2-^{14}C KIEs for Ct-SI-catalyzed maltose hydrolysis, with post-reaction purification by gradient APS HPLC chromatography.

Trial	cycles[a]	KIE (substrates)[b]	KIE (products)[c]
1	6	1.063	1.056
2	7	1.017	1.011
Average		1.040	1.034
Stdev		0.033	0.032
95% CI		-[d]	-[d]

[a] Each sample was counted for 10 min each per cycle, for the number of cycles indicated.
[b] Eq. (1.7**)**, calculated using the isotope ratios in the maltose substrate.
[c] Eq. (1.8**)**, calculated using the isotope ratios in the glucose product.
[d] There were too few independent experiments to calculate a 95% confidence interval.

3.5.1. KIE Purification of Acid Catalyzed Hydrolysis Using γ-Aminopropylsilyl Column

Given the poor reproducibility of the Ct-SI-catalyzed KIEs, and evidence that the "extra" peak in the gradient elution (Figure 3.11) was due to the enzyme, KIEs for acid-catalyzed maltose hydrolysis were measured using the gradient method. Figure 3.13 and Figure 3.14 show separation of the reference and the partial acid-catalyzed KIE reactions using the gradient method.

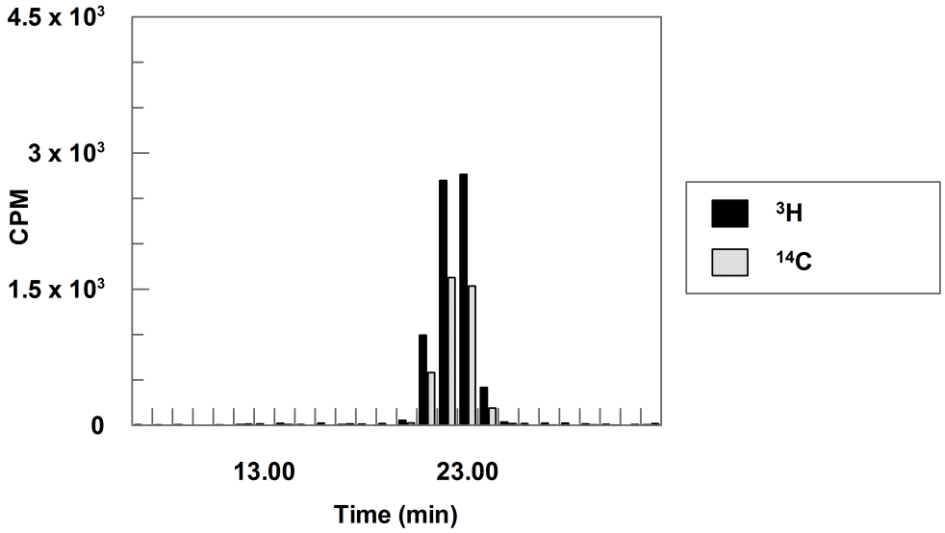

Figure 3.13. Separation of reference (0% reaction) acid-catalyzed reaction using gradient APS HPLC.

The 0% reaction shows similar elution time to the 0% enzyme catalyzed reactions.

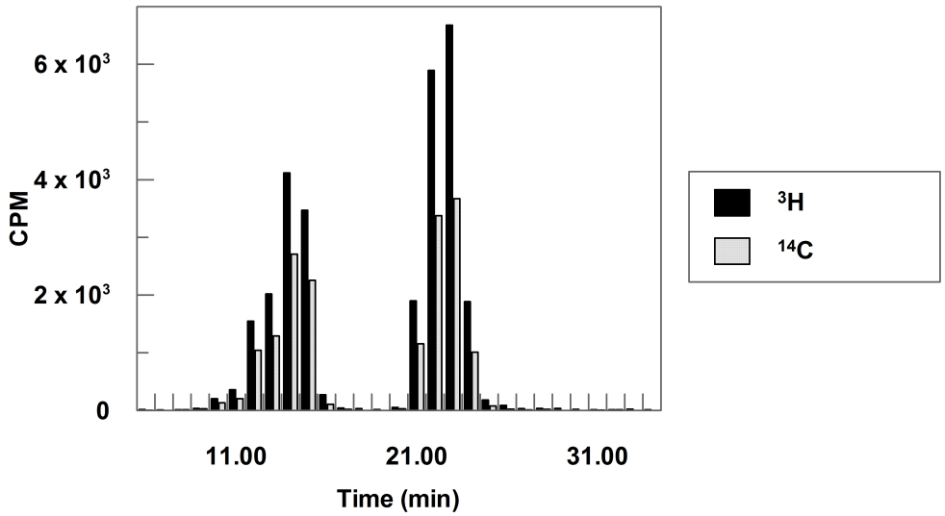

Figure 3.14. Separation of partial acid-catalyzed KIE reaction using gradient APS HPLC.

The partial reaction for the acid-catalyzed reaction showed a similar retention time for the maltose, but slightly earlier elution time for the glucose peak compared with the enzymatic reaction.

The KIEs were measured using isotope ratios in both the substrate and the product (Table 3.7). The observed 1-^{3}H KIE fell into the range of values observed previously; however, the large confidence intervals make the data unusable for TS analysis.

Table 3.7 1-^{3}H KIE for acid-catalyzed maltose hydrolysis, with post-reaction purification by gradient APS HPLC chromatography

Trial	cycles[a]	KIE (substrate)[b]	KIE (product)[c]
1	11	1.213	1.233
2	3	1.235	1.241
3	9	1.198	1.240
4	23	1.163	1.180
Average		1.202	1.223
Stdev		0.030	0.029
95% CI		0.049	0.046

[a] Each sample was counted for 10 min each per cycle, for the number of cycles indicated.
[b] Eq. (1.7), calculated using the isotope ratios in the maltose substrate.
[c] Eq. (1.8), calculated using the isotope ratios in the glucose product.

The 6,6-$^{3}H_2$ KIE was also measured for the acid-catalyzed reaction (Table 3.8). Again, the large confidence interval made the data uninterpretable.

Table 3.8 6-^{3}H KIE for acid-catalyzed maltose hydrolysis, with post-reaction purification by gradient APS HPLC chromatography

Trial	cycles[a]	KIE (substrate)[b]	KIE (product)[c]
1	5	0.980	0.968
2	18	1.014	0.959
3	14	0.964	1.040
4	18	1.026	0.965
5	19	1.013	1.096
6	28	1.023	0.953
Average		1.003	0.997
Stdev		0.025	0.058
95% CI		0.026	0.061

[a] Each sample was counted for 10 min each per cycle, for the number of cycles indicated.
[b] Eq. (1.7), calculated using the isotope ratios in the maltose substrate.
[c] Eq. (1.8), calculated using the isotope ratios in the glucose product.

3.6. KIE Purification Method Using an Anion Exchange Column

Use of an anion exchanger column was one of the first methods were used to separate the KIE reactions. In this method, the glucose product was phosphorylated to glucose-6-phosphate (G6P), then separated from residual maltose by anion exchange on a Mono-Q column.

In test reactions, [1-^{14}C]G6P was synthesized from [1-^{14}C]glucose and applied to the Mono-Q column (Figure 3.15). A smear of radioactivity eluted at low salt concentration. The early fractions peak corresponded to 5% of the total radioactivity. The 5% early eluting peak is too high to be corrected as contamination for KIE.

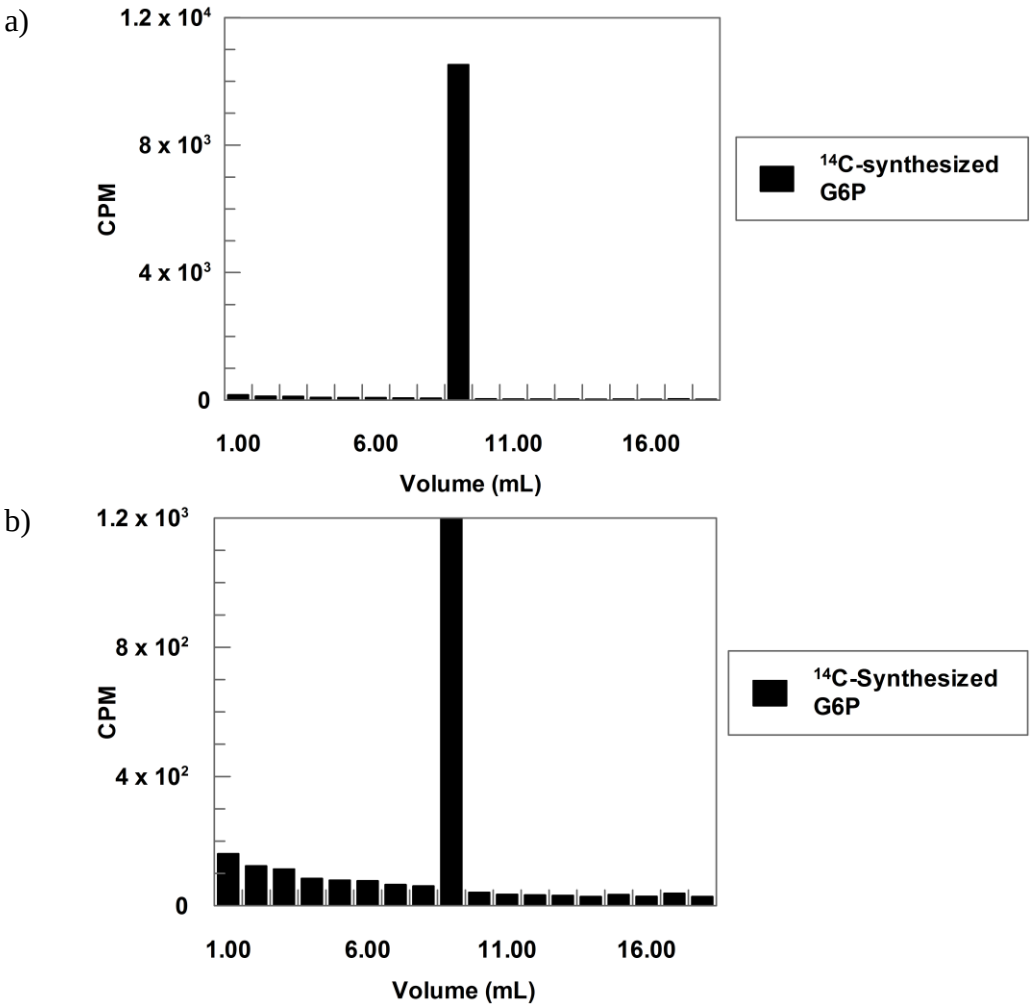

Figure 3.15. [1-^{14}C]G6P was synthesized from [1-^{14}C]glucose and separated on a Mono-Q column.

a) Chromatogram of a Mono-Q purification of 11500 cpm of [1-^{14}C]G6P. Around 600 cpm (5% of the total) eluted with low salt. b) Rescaled to show early eluting radioactivity.

Different test reactions were done to investigate the source of the early peak, and eliminate it. A test purification of ≈12 000 cpm [γ-^{33}P]G6P on the Mono-Q column was performed to check whether the early eluting peak was G6P, or if some other species was eluting early (Figure 3.16). No radioactivity eluted with the low salt buffer in this test.

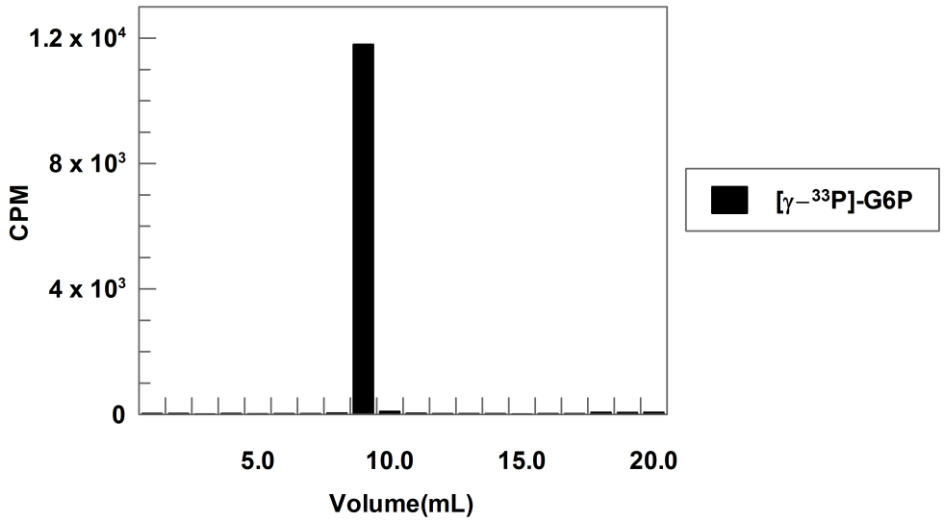

Figure 3.16. Mono-Q chromatogram of [γ-^{33}P]G6P.
[γ-^{33}P]G6P was synthesized from [γ-^{33}P]ATP. No early elution of G6P was detected.

The possibility that G6P was being hydrolyzed back to glucose by hexokinase was tested. Incubating G6P and hexokinase together for 24 h produced no detectable phosphate. However incubation of a mixture of G6P, HK, $MgCl_2$, and ATP did produce phosphate due to ATP hydrolysis (Figure 3.17). This result demonstrated that hexokinase was not hydrolyzing the G6P back to glucose.

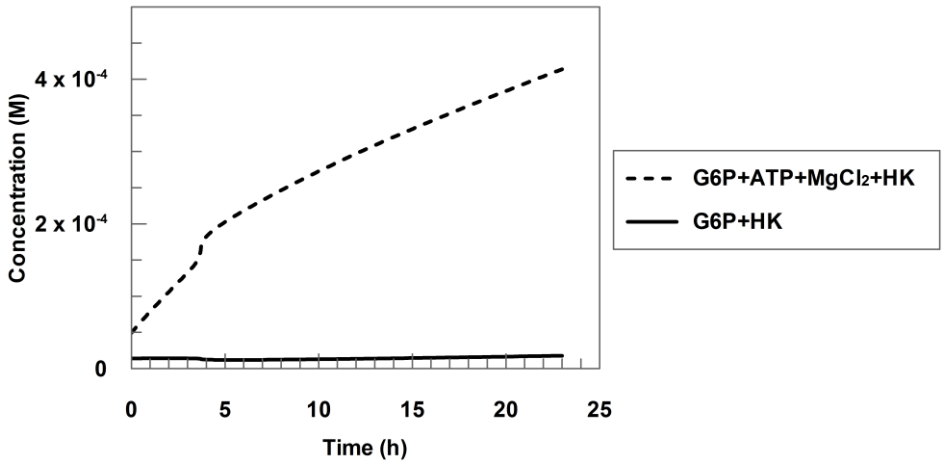

Figure 3.17. Phosphate production in reaction mixtures containing G6P and hexokinase (HK).

Phosphate concentrations were determined using the Malachite Green/ammonium molybdate colorimetric assay for inorganic phosphate.[85]

One possibility that was considered was that the reaction was not going to completion because of either product inhibition by ADP, or because the reaction was not sufficiently exergonic to go to completion on its own. To address these possibilities, a regeneration system for ATP was added (Figure 3.18).

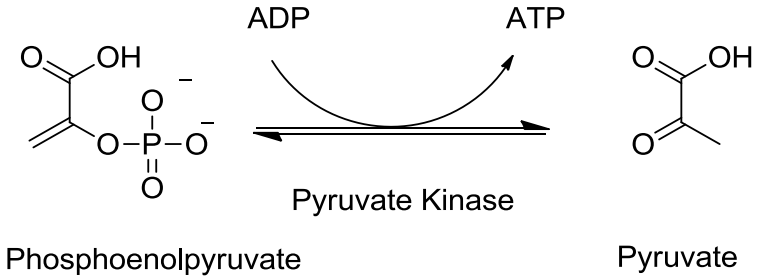

Figure 3.18. ATP generation system using pyruvate kinase (PK).

Another strategy was used to try to ensure that glucose phosphorylation went to completion, by oxidizing G6P to 6-phosphogluconate (Figure 3.19). No improvement was detected with this test reaction.

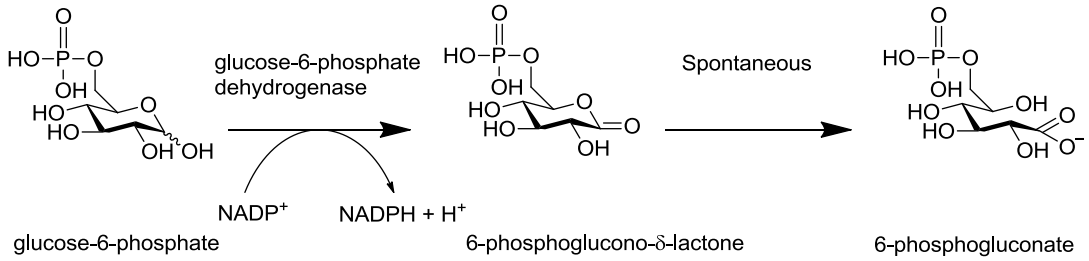

Figure 3.19. Coupled reaction used to drive the hexokinase reaction to completion by oxidizing G6P to 6-phosphogluconate, using glucose 6-phosphate dehydrogenase (G6PDH).

Since it was not possible to drive the phosphorylation of glucose to completion, and since G6P was shown by the experiment with [γ-^{33}P]G6P not to elute early, it was posited that whatever was eluting early was a non-glucose

contaminant. A KIE measurement was tried using Mono-Q separation of G6P from residual maltose. Samples of the 0%, partial, and 100% reaction mixtures were subjected to Mono-Q chromatography (Figure 3.20, Figure 3.21, Figure 3.22). The reaction mixture itself was re-purified by APS HPLC chromatography immediately before use.

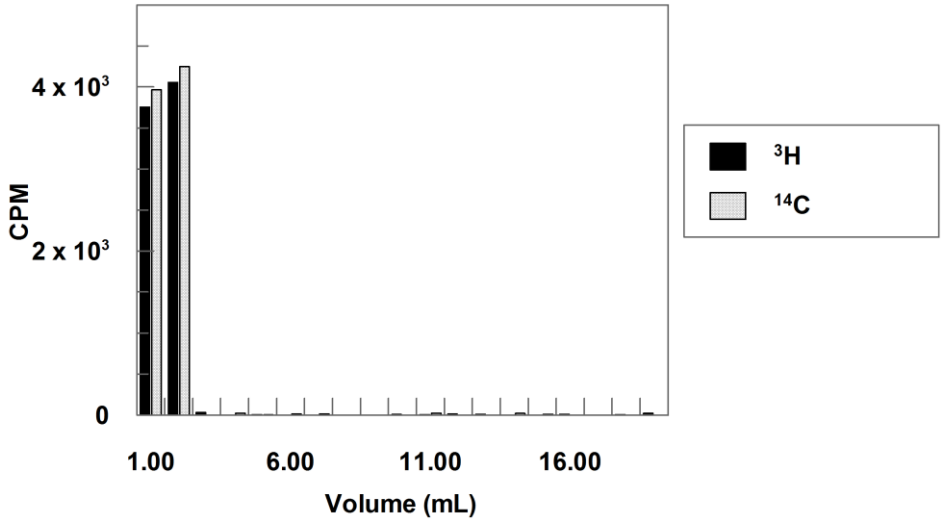

Figure 3.20. Separation of the 0% enzymatic KIE reaction mixture by Mono-Q chromatography.

The first 8 mL were collected with low salt (10 m M NH_4OAC, pH 8.5) and the second 8 mL were high salt eluate (400 mM NaCl, 6 mM NH_4OAC, pH 8.5).

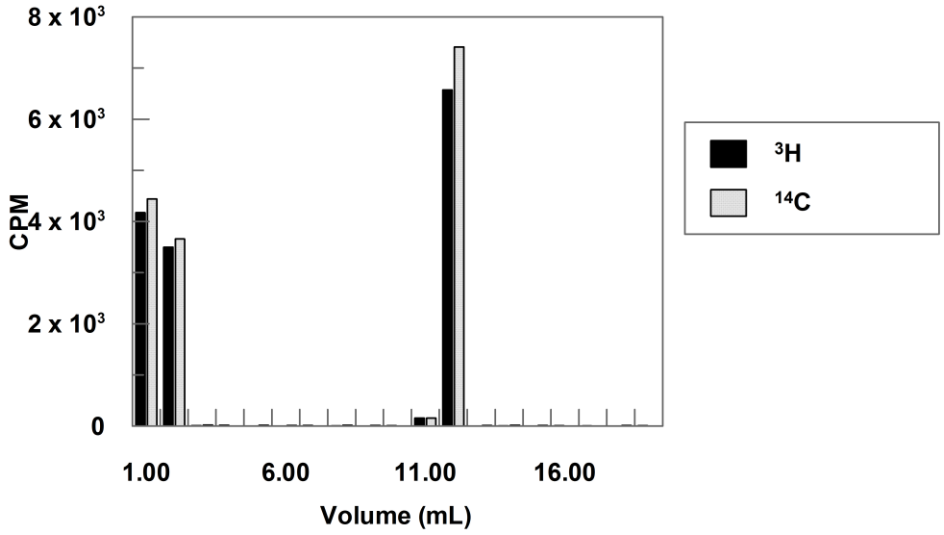

Figure 3.21. Separation of the partial enzymatic KIE reaction mixture by Mono-Q chromatography.

The elution method is the same as the 0% reaction separation. One of the advantages of this method is that the substrate and product elutes in fewer fractions compared to APS column separation methods.

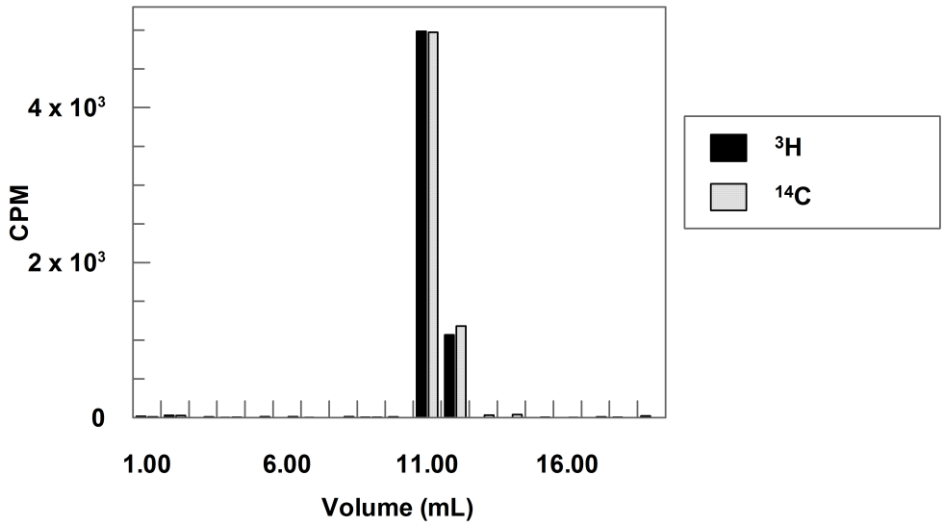

Figure 3.22. Separation of the 100% enzymatic KIE reaction mixture by Mono-Q chromatography.

The 100% reaction mixture was hydrolyzed to completion with 3 units of α-glucosidase, then phosphorylated in the same reaction as the Ct-SI reaction mixtures. Around 100 cpm eluted with the early peak, 1% of the total radioactivity.

KIEs were measured for maltose hydrolysis at the 1-^{3}H position, initially without prior re-purification of maltose (Table 3.9), then with re-purification

(Table 3.10), and at the 2-^{14}C position (Table 3.11). All KIE measurement showed too high variability to be useful.

Table 3.9. 1-^{3}H KIE for Ct-SI-catalyzed maltose hydrolysis, without repurification prior to the KIE reaction, and with post-reaction purification by Mono-Q HPLC chromatography.

Trial	cycles[a]	KIE (substrate)[b]	KIE (product)[c]
1	22	1.367	1.222
2	32	1.466	1.201
3	16	2.359	1.282
4	11	1.032	1.172
5	11	1.526	1.254
6	14	1.454	1.249
Average		1.534	1.230
Stdev		0.441	0.040
95% CI		0.463	0.042

[a] Each sample was counted for 10 min each per cycle, for the number of cycles indicated.
[b] Eq. (1.7), calculated using the isotope ratios in the maltose substrate.
[c] Eq. (1.8), calculated using the isotope ratios in the glucose product.

Table 3.10. 1-^{3}H KIE for Ct-SI-catalyzed maltose hydrolysis, with repurification prior to the KIE reaction, and post-reaction purification by Mono-Q HPLC chromatography

Trial	cycles[a]	KIE (substrate)[b]	KIE (product)[c]
1	37	1.129	1.151
2	18	1.138	1.070
3	25	1.045	1.131
4	14	1.073	1.117
5	28	1.110	1.112
6	15	1.099	1.111
Average		1.099	1.115
Stdev		0.035	0.027
95% CI		0.037	0.028

[a] Each sample was counted for 10 min each per cycle, for the number of cycles indicated.
[b] Eq. (1.7), calculated using the isotope ratios in the maltose substrate.
[c] Eq. (1.8), calculated using the isotope ratios in the glucose product.

Table 3.11. 2-^{14}C KIE for Ct-SI-catalyzed maltose hydrolysis, with repurification prior to the KIE reaction, and post-reaction purification by Mono-Q HPLC chromatography

Trial	cycles[a]	KIE (substrate)[b]	KIE (product)[c]
1	26	1.106	0.984

[a] Each sample was counted for 10 min each per cycle, for the number of cycles indicated.
[b] Eq. (1.7), calculated using the isotope ratios in the maltose substrate.
[c] Eq. (1.8), calculated using the isotope ratios in the glucose product.

Later experiments demonstrated the nonspecific glucose binding to the Mono-Q column in the presence of G6P (Figure 3.23); most of the radioactivity was eluted with the high salt concentration. Addition of the maltose to the mobile phase helped to improve the separation and minimized the effect of nonspecific binding (Figure 3.24). AMP and PEP were also tested, and they showed similar effects to G6P.

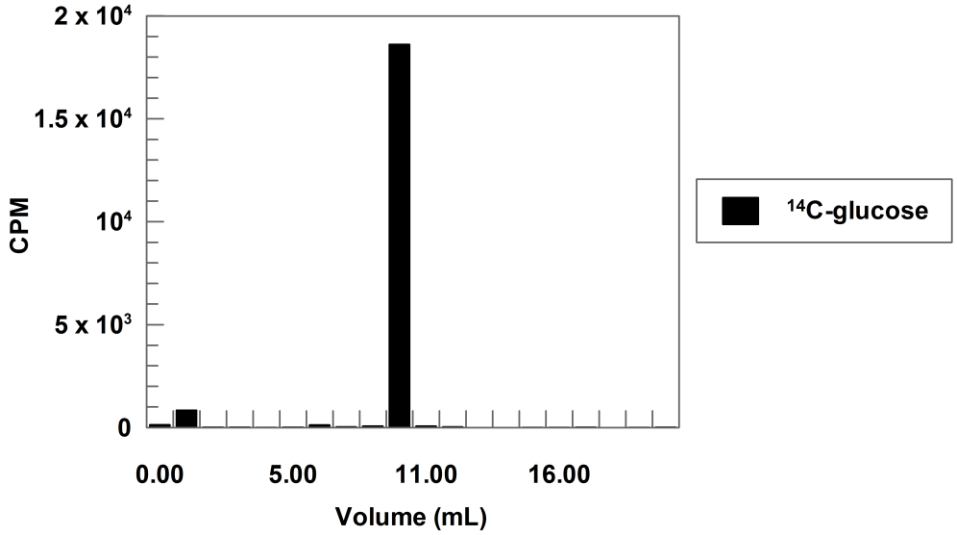

Figure 3.23. Nonspecific glucose binding to the Mono-Q column in the presence of G6P.
The chromatogram shows the elution of synthesized cold G6P with radiolabelled glucose.

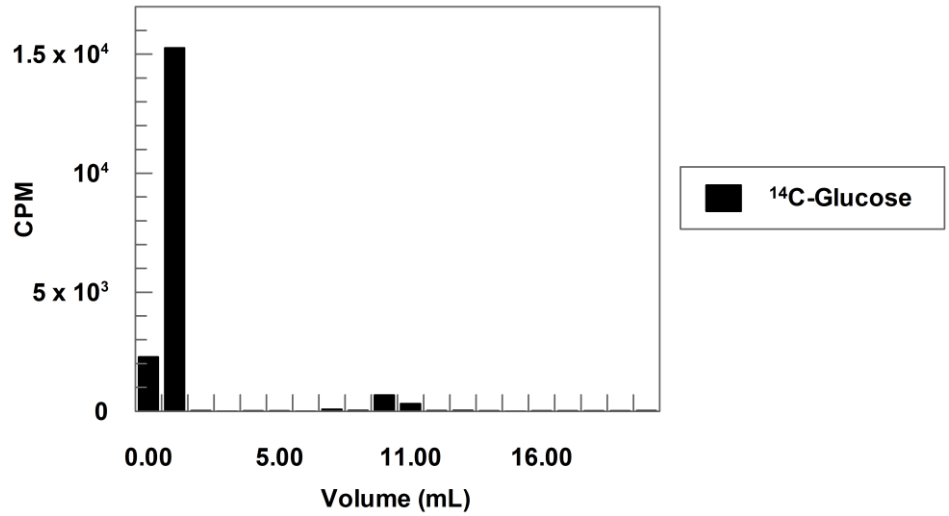

Figure 3.24. Nonspecific glucose binding to the Mono-Q column in the presence of G6P was alleviated by addition of 10 mM maltose to the mobile phase.
The chromatogram shows the elution of radiolabelled glucose on the Mono-Q column in the presence of 1.7 mM G6P and 10 mM maltose.

3.7. Radioactivity Counting

KIEs are calculated from experimental isotope ratios (i.e., ^{3}H:^{14}C). ^{3}H and ^{14}C are distinguished experimentally by their β-particles' kinetic energy. The energy spectra for ^{3}H and ^{14}C standards were obtained by scanning each isotope over the energy range of 0 - 1000 channels (0-2000 keV) individually (Figure 3.25). ^{3}H counts appear in channels 0 - 460, while ^{14}C counts were between channels 0 - 650. Radioactive counts were collected in two "windows", with Win1 (channels 0 - 460) containing all the ^{3}H counts, and Win2 (channels 460 - 1000) containing only ^{14}C counts. A ^{14}C standard with an identical solvent composition to the KIE samples was used to determine the Win1/Win2 ratio, thus allowing the ^{3}H:^{14}C ratio to be measured.

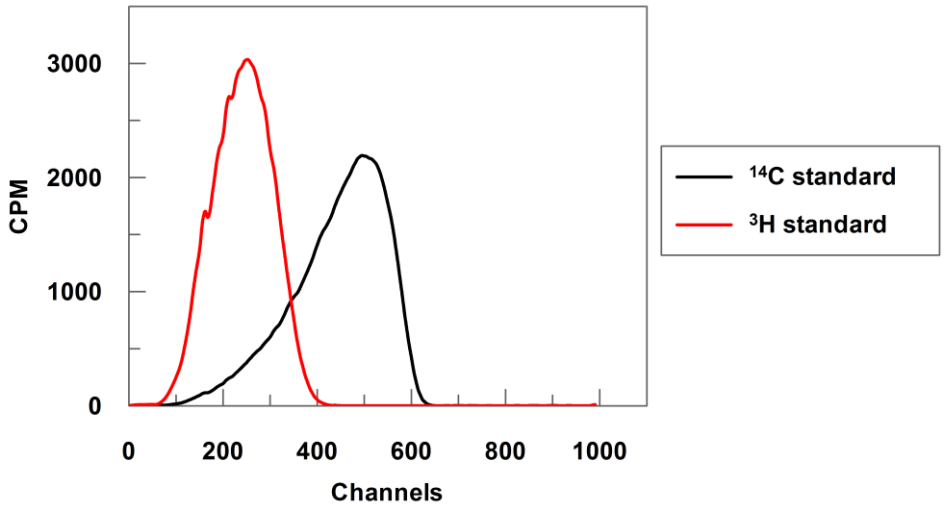

Figure 3.25. Energy distribution for ^{3}H and ^{14}C β-particles.
Energy spectra of ^{3}H and ^{14}C standards, with glass vials and Ecoscint A as scintillation fluid.

Each mobile phase from each different separation method was tested for compatibility with the liquid scintillation; all the mobile phases produce clear solutions (Figure 3.26). The ratios are different between each method's mobile phases; however the ratios are close enough for the buffers to be used in the same experiment.

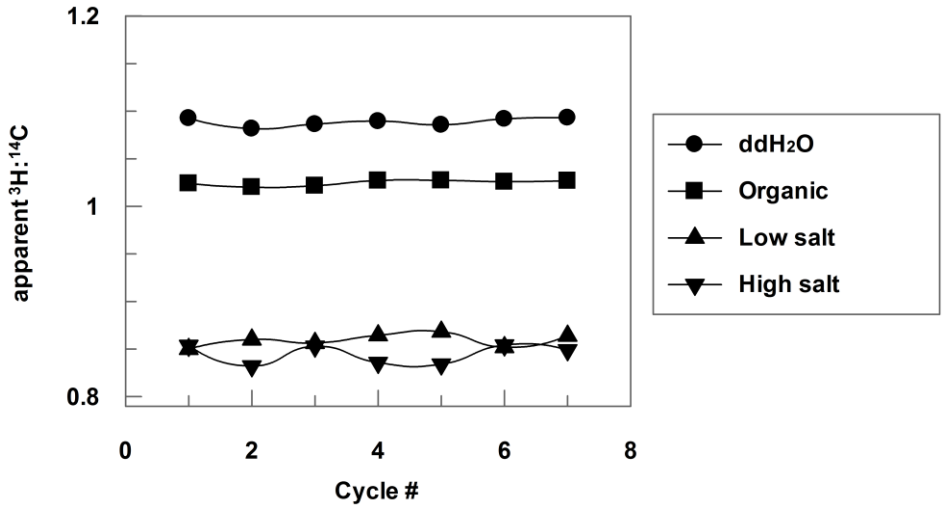

Figure 3.26. $^{3}H:^{14}C$ ratios for different mobile phases with Ecoscint A scintillation fluid.

All samples contained 200 μL of ^{3}H and ^{14}C in water, plus 17 g Ecoscint A. The *Organic* sample also contained 0.4 g of 75:8:17 MeCN:iPrOH:ddH_2O. The *Low salt* sample contained 4 g of 10 mM NH_4OAc, pH 8.5, or while the *High salt* sample contained 4 g of 6 mM NH_4OAc, pH 8.5, 400 mM NaCl.

Another experiment was designed to test the linearity of observed versus expected $^{3}H:^{14}C$ isotope ratios in standard samples (Figure 3.27). A roughly 1:1 mixture of ^{3}H and ^{14}C was made and aliquoted, then a known, small, amounts of ^{14}C were added to the aliquots.

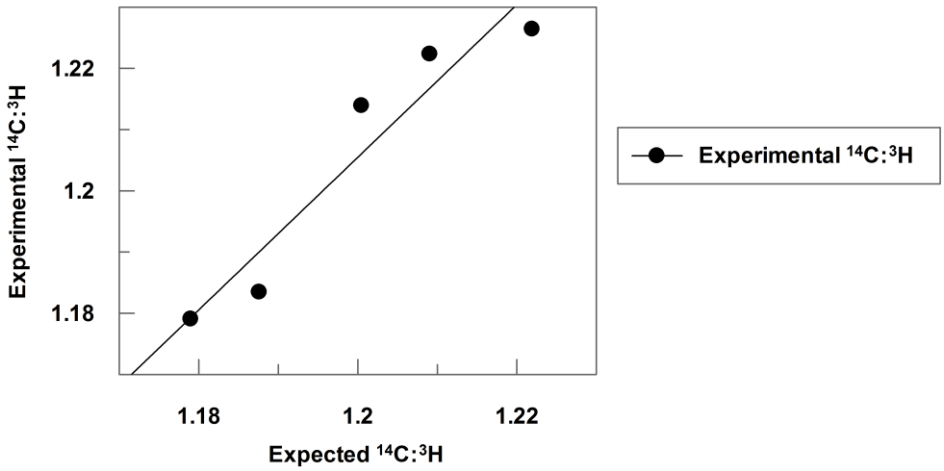

Figure 3.27. Linearity of $^{14}C:^{3}H$ isotope ratio with standard samples.
Samples were aliquoted from a mixture with a known ratio and set, small, amounts of ^{14}C were added, then counted. This experiment was done with 3 g 75:8:17 MeCN:iPrOH:ddH_2O and 15 g Ecoscint A scintillation fluid.

The effect of the mobile phase composition in gradient APS chromatography on the apparent $^{3}H:^{14}C$ isotope ratio was tested. Fractions were collected at the glucose and maltose elution times in a blank run, and a $^{3}H:^{14}C$ mixture was added to each fraction (Figure 3.28).

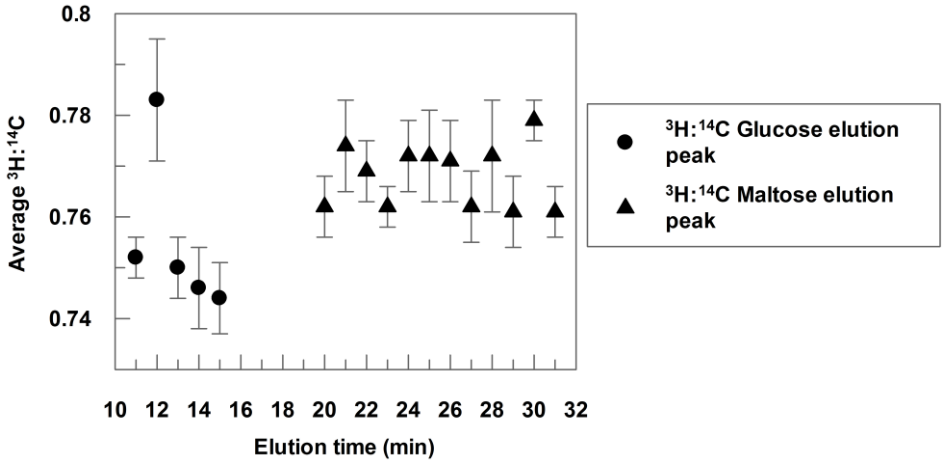

Figure 3.28. Changes in the $^{3}H:^{14}C$ ratio with varying mobile phase composition in gradient APS HPLC chromatography.

Similarly, the H numbers (a measure of quenching) were measured for fractions during gradient APS HPLC chromatography (Figure 3.29) and isocratic

APS HPLC chromatography (Figure 3.30). In the former case, there was a noticeable but small change in H numbers throughout the chromatogram, but not in the latter case.

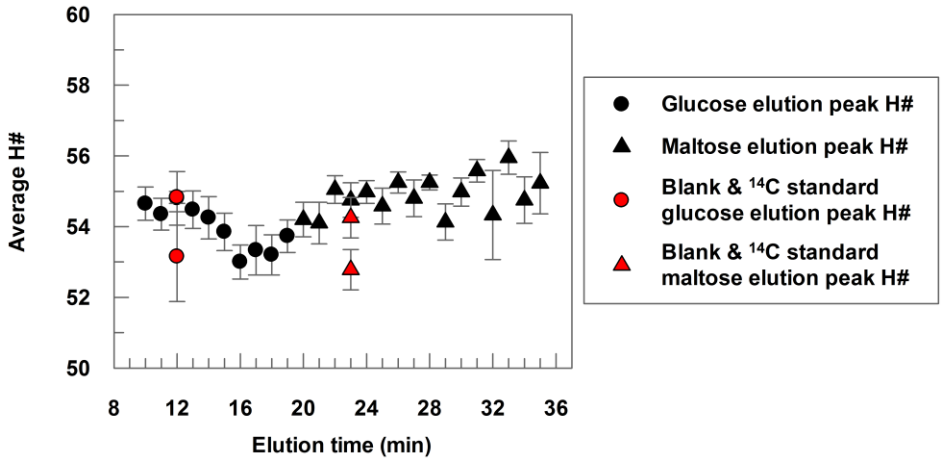

Figure 3.29. H numbers for gradient APS HPLC chromatography.
Fractions were collected for injection of a partially (≈50%) hydrolyzed mixture of ^{3}H and ^{14}C (≈20000CPM of both isotopes), and H numbers were measured for each fraction. Blank and ^{14}C standard were each made from a blank run.

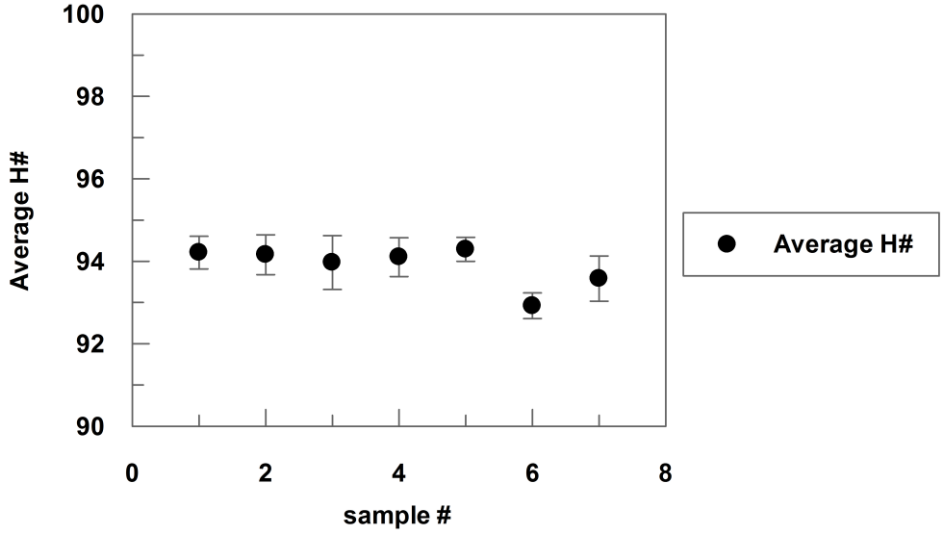

Figure 3.30. H numbers for isocratic APS HPLC chromatography.
Fractions were collected for a blank isocratic run with 75:8:17 MeCN:iPrOH:ddH_2O as the mobile phase; ^{3}H and ^{14}C added, and H numbers were measured for each fraction.

3.8. Computational Chemistry

KIEs were calculated for one potential transition state for maltose hydrolysis, namely methanol departure in the first step of a $D_N{*}A_N$ (S_N1) mechanism, as well as the EIEs for forming the intermediates, the glucose oxacarbenium ion and methanol. Structures were optimized using Gaussian 09,[84] then the vibrational frequencies and force constants were calculated. These were then entered into the program QUIVER,[81] which calculated the isotope partition function ratio (Q or $Q^{\ddagger}$) for each isotopic label. The Q values were then used to calculate KIEs and EIEs.

The starting points for TS optimization were the optimized structures of the reactant, α-methyl glucopyranoside, the products, glucose oxacarbenium ion, and methanol (Figure 3.31).

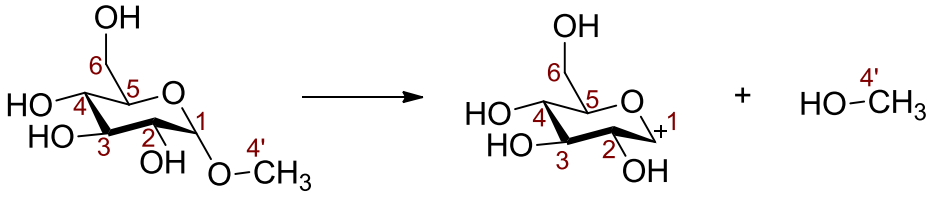

Figure 3.31. α-Methyl glucopyranoside.
The reactant, α-methyl glucopyranoside and the products of the first step, the oxacarbenium ion of glucopyranoside, and methanol, are shown.

Departure of the leaving group ($D_N^{\ddagger}$) was the first TS tested. The potential energy surface was obtained by gradually increasing the distance of the C_1-$O_{4'}$ bond. The calculation was done in vacuum (Figure 3.32) and with SCRF (continuum) solvation (Figure 3.33).

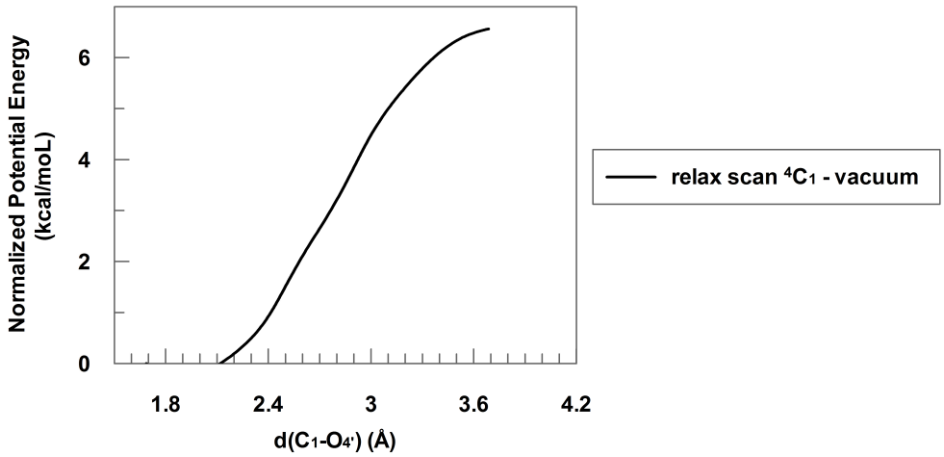

Figure 3.32. The ionization energy for relaxed scan done in vacuum for $^4C_1$ conformation of α-methyl glucopyranoside

The potential energy scan for α-methyl glucopyranoside protonated on the bridging oxygen. The energy was normalized with the energy of the optimum structure.

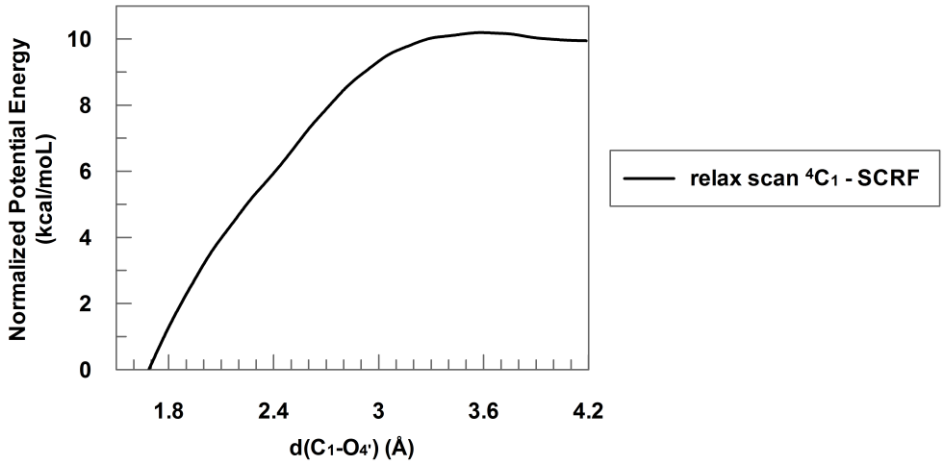

Figure 3.33. The ionization energy for relaxed scan done in SCRF for $^4C_1$ conformation of α-methyl glucopyranoside.

The potential energy scan for α-methyl glucopyranoside protonated on the bridging oxygen. The energies were normalized with the energy of the optimum structure.

A potential transition state for C1-O4' bond breakage was found using SCRF solvation. The candidate structure was used as the initial TS guess in a QST3 transition state optimization done in vacuo in Gaussian 09. QST3 method requires the reactant and product structures, plus an initial guess at the TS structure. The initial guess structure was the structure with the highest potential

energy from the potential energy scan, with the C1-O4' bondlength, $d_{C1\text{-}O4'}$, fixed at 3.69 Å. The optimized TS structure had $d_{C1\text{-}O4'}$ = 3.97 Å and a reaction coordinate frequency of 34.63*i* cm^{-1} (Figure 3.34).

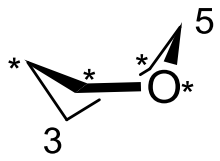

$^5S_3$

Figure 3.34. The $^5S_3$ conformation observed for the calculated TS structure for leaving group departure ($D_N^{\ddagger}$).

In the $^5S_3$ conformation, the C5 atom is located above the plane of the ring, and C3 is below. The coplanar atoms are shown by the asterisks. Only the pyranose ring is shown for simplicity.

The TS structure had a $^5S_3$ conformation, starting from a reactant $^4C_1$ conformation (Figure 3.35). This was very similar to the previously reported E_3 conformation for the oxacarbenium ion of glucopyranose.[43] In the present TS structure, the C5 atom was slightly higher above the plane of the ring, causing it to be $^5S_3$ rather than E_3. The TS conformation was similar to the oxacarbenium ion, which was also $^5S_3$. To date, TSs of glycoside hydrolysis have been highly oxacarbenium ion-like, and the calculated TS here also had high oxacarbenium ion character.

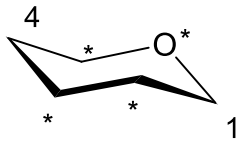

$^4C_1$

Figure 3.35. The $^4C_1$ conformation used as starting conformation for the reactant.
In the $^4C_1$ conformation, the C4 atom is located above the plane of the ring, and C1 is below. The coplanar atoms are shown by the asterisks. Only the pyranose ring is shown for simplicity.

Given the extremely low reaction coordinate frequency, it was necessary to use intrinsic reaction coordinate calculations (IRC) to ensure that the reaction coordinate in the TS structure really corresponded to C1-O4' bond breakage. The IRC calculation follows the reaction path toward reactants and products through the steepest downhill path. IRC uses initial force constants of the optimized possible TS to begin the calculations.[86] The IRC calculations showed that the reaction coordinate did correspond to C1-O4' bond breakage.

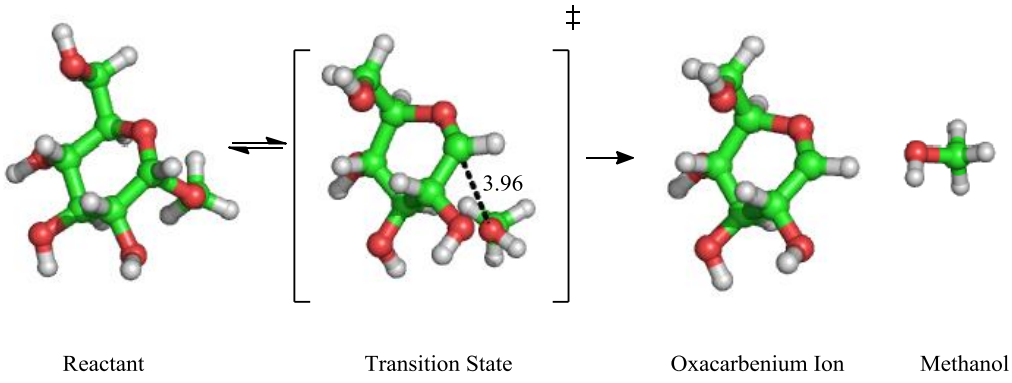

Figure 3.36. Optimized structures from electronic structure optimization for departure of the methanol leaving group methanol ($D_N^{\ddagger}$).
Methanol departure corresponds to the D_N step of a $D_N{*}A_N$ (S_N1) reaction mechanism. The reactant for the overall reaction was α-methyl glucopyranoside, as it would be in solution. In the TS optimization calculations, the starting structure was α-methyl glucopyranoside protonated on the glycosidic oxygen atom. The C1-O bondlength, in Ångstroms, is shown for the TS structure.

The Pauling bond orders were calculated for the reactant, TS and the products (Table 3.12). There was a big decrease in $n_{C1\text{-}O4'}$ which changed from 0.997 in the reactant to 0.002 in the TS. There were increases in $n_{C1\text{-}C2}$, from 0.98 to 1.21and $n_{C1\text{-}O5}$, from 1.03 to 1.67. These bond orders reflected the rehybridization of C1 toward sp^2 as the oxacarbenium ion character increases. The increase in $n_{C1\text{-}C2}$, decrease in $n_{C2\text{-}O2}$ and $n_{C2\text{-}H2}$ were consistent with hyperconjugation stabilizing the cationic centre. There were also big decreases in $n_{C2\text{-}C3}$ and $n_{C5\text{-}O5}$, which may have been caused by increased π-bonding at C1-C2 and C1-O5.

Table 3.12. Pauling bond orders for different positions in reactant, TS and products.

Pauling bond order (n^1)	Reactant	TS	Oxacarbenium	Methanol
C1-O4′	0.997	0.0002	--	--
C1-O5	1.029	1.670	1.673	--
C1-C2	0.982	1.209	1.169	--
C2-O2	0.974	1.061	1.050	--
C2-H2	0.983	0.944	0.958	--
C2-C3	1.003	0.894	0.897	--
C3-O3	0.969	1.026	1.051	--
C3-C4	1.021	0.991	0.986	--
C4-O4	0.974	1.010	1.019	--
C4-C5	0.990	0.951	0.952	--
C5-O5	0.927	0.740	0.743	--
C5-C6	1.036	1.041	1.038	--
C6-O6	0.974	0.987	0.986	--
C6-H6a	0.967	0.976	0.976	--

[1] Total Pauling bond order $n = e^{\frac{[d_1 - d_{ij}]}{b}}$, d_1 is reference bond length, d_{ij} is experimentally measured bond length. b=0.3 is a constant. d_1(C-C) =1.526, d_1(C-H) =1.09, d_1(C-O) = 1.41.

C6-H6b	0.974	0.970	0.970	--
O4′-C4′	0.966	0.935	--	0.978

The KIEs and EIEs for C1-O4' bond breakage were calculated (Table 3.13). The EIEs and KIEs at each position were very similar to each other, since the structure of the TS was very similar to the product (oxacarbenium). The 1-^{14}C KIE might be expected to be larger (or less inverse) than the EIE because of the reaction coordinate contribution; however, the reaction coordinate frequency was so low, 34*i* cm^{-1}, that it had little effect on the KIE.

Table 3.13. Calculated KIEs and EIEs for departure of methanol from α-methyl glucopyranose.

Position of the Isotope	Calculated KIE	Calculated EIE
1-^{14}C	0.979	0.977
2-^{14}C	1.014	1.015
3-^{14}C	1.014	1.010
4-^{14}C	1.007	1.006
5-^{14}C	1.013	1.012
6-^{14}C	1.005	1.003
5-^{18}O	0.999	0.994
4′-^{14}C	1.006	--
4′-^{18}O	1.032	--
1-^{3}H	1.406	1.397
2-^{3}H	1.189	1.156
3-^{3}H	0.866	0.939
4-^{3}H	0.972	0.977
5-^{3}H	0.951	0.943
6-^{3}H	1.029	1.027
6,6-$^{3}H_2$	1.012	1.001
4′-^{3}H	1.045	--
4′-O-^{3}H	0.961	--

Chapter 4 - Discussion

4.1. Maltose and Sucrose Synthesis

The maltose synthesis method was initially developed by Jason Thomas, a postdoctoral fellow, and Adam Mepham, a summer student. Contaminants in commercial radiolabelled D-glucoses co-migrated with maltose, so D-glucoses were purified prior to maltose synthesis. Glucose and maltose purifications were initially performed by TLC, but contaminants were still present in the synthesized maltose (Figure 3.1), so an additional purification step was developed by Adam. In this method, D-glucose was phosphorylated to G6P, which was then purified by anion exchange chromatography. However, the maltose synthesis step was inhibited by high residual salt from the anion exchange step. Moreover, maltose purification by TLC gave poor recovery. Therefore, an γ-aminopropylsilyl (APS) HPLC purification was developed.

Effective separation of carbohydrates is challenging because they are uncharged, highly polar, and poor chromophores. These challenges introduced some limitations in separation and detection methods. For instance, even though elution of glucose and maltose standards could be monitored by absorbance at 190 nm, they were such poor chromophores, and the amounts of radiolabelled compounds were so low, that separations could only be monitored by counting the radioactivity fractions.

With HPLC purification, the purity and recovery of glucose improved (Figure 3.3, Figure 3.4).

The maltose and sucrose syntheses which were developed prior to my arrival had yields around 20%, which is improved to 90% for maltose. The first approach was to optimize each enzyme concentration, then reactant concentrations, and finally the optimum reaction time was found. The same optimization procedure was applied to the sucrose synthesis for radiolabels in the glycone ring. Optimization of the aglycone ring for the sucrose still needs to be performed.

4.2. Purity in KIE Reaction

Radioactive contamination can change the observed isotope ratios; a radioactive impurity as small as 0.2% can cause errors as large as 1% in the observed KIE.[61] An error this large would make the observed KIEs uninterpretable. For this reason, the method for purifying the residual substrate in the KIE reaction mixture from the product should be tested for the level of purity and reproducibility.[61] After testing different methods for purification and KIE measurement, the necessity of repurifying the substrates before KIE measurement became clear. Once this was realized, labelled maltoses were repurified by gradient APS HPLC chromatography before all KIE measurements.

4.3. Purification Methods by APS HPLC Chromatography

An HPLC purification method was developed for maltose purification and KIE measurement using APS HPLC chromatography. APS is a hydrophilic interaction liquid chromatography (HILIC) column.[87] Using APS chromatography improved the purity of glucose and increased its recovery from ≈50% to 80%.

The first method used isocratic elution with 75:25 MeCN:ddH_2O as the mobile phase. In this method, complete baseline resolution between glucose and maltose was not achieved (Figure 3.3 and Figure 3.4). This method was an enormous improvement for synthesis, but not good enough for KIE measurements. Addition of different organic solvents, including ethanol, methanol, and isopropanol were tested in an attempt to improve resolution.[87] The best result was achieved with 75:8:17 MeCN:iPrOH:ddH_2O. The new method was capable of baseline separation of glucose and maltose at low concentrations and small injection volumes. This method was used for maltose purification since we could afford compromising quantity for purity by collecting only the middle of the peaks. Other changes to improve peak resolution, including decreasing the flow rate from 1 mL/min to 0.5 mL/min and decreasing fraction sizes from 2 min to 0.5 min, varying the injection volume and the injection concentration (smaller was better for both); all slightly helped the separation. However, this still did not achieve complete baseline resolution, and the end of the glucose peak overlapped the beginning of the maltose peak; causing at least one fraction to have mixture of maltose and glucose. However, the fraction containing both glucose and maltose

consisted of ≈200 of the total radioactivity, so KIE measurements were attempted (Table 3.1, Table 3.2, Table 3.3). KIEs were calculated based on the isotope ratios in both the substrate and product. The measured 1-^{3}H KIEs were in the range of values observed previously for the α-secondary position[47] for glycoside hydrolysis (Table 3.1), so none of the values were obviously incorrect. The situation was the same for the remote, 6-^{3}H KIE (Table 3.2).

In order to improve compound separation, a gradient APS HPLC chromatographic method was developed. In HILIC chromatography, carbohydrate separation depends on at least three processes: adsorption, surface tension and partitioning.[88] Carbohydrate retention can be caused by the competition between water and carbohydrate molecules for hydrogen bonding with the amino groups of the stationary phase. Increasing the water percentage in the solvent decreases retention of highly polar (larger oligosaccharides) analytes. The gradient method was designed to first elute the less polar glucose by using less water in the initial elution solvent, then suddenly increasing the water percentage to elute the molecule with more polar groups, i.e., maltose. This gradient method was able to increase the difference in the retention times of the two analytes. Different gradient conditions were tested and the best one was chosen. The gradient method that was chosen starts with 75:8:17 MeCN:iPrOH:ddH_2O as initial condition, and gradually changes to 98:2:0 MeCN:iPrOH:ddH_2O in 9 min, and then suddenly goes back to the initial conditions, and stays there till the run is over. The separation between glucose and

maltose improved, but they were still not baseline resolved. The next approach was to change the temperature. Published methods use both high and low temperatures.[89] A water bath was used to test temperatures from 6 °C to 45 °C. The effect of decreased temperature could be an increase in the viscosity of the mobile phase and decrease in the analyte diffusivity, which diminishes kinetic and transport characteristics;[90,91] however, the best separation was achieved at 6 °C (Figure 3.10 and Figure 3.11).

KIEs were measured at several positions with this method. The observed 1-^{3}H KIEs had different averages depending on whether the isotope ratios were measured in the residual substrate, or the product, though both fell into the range of previously observed values (Table 3.4). For the remote 6,6-$^{3}H_2$ position, the KIE of 10-15% was higher than observed previously (Table 3.5). Also, the large confidence interval meant that the values were not useful for TS analysis. The 2-^{14}C KIE was 3-4%, with high variability (Table 3.6).

In later KIE measurements using the gradient APS HPLC method, a small extra peak eluting after maltose appeared during maltose purification and separation of the KIE partial reaction mixtures (Figure 3.11). This extra peak was absent in acid-catalyzed reaction mixtures (Figure 3.14), indicating that it was unique to reactions which contained proteins (i.e., Ct-SI-catalyzed maltose hydrolysis, or maltose synthesis). To further investigate the effect of enzymes on the presence of the extra peak, different test reactions which varied with regard to the proteins present (Ct-SI, maltose epimerase (ME), bovine serum albumin

(BSA)), incubation time and heat quenching were tested, but no correlation was found. The use of Tween-20 (a nonionic polyoxyethylene surfactant, which used for enzyme stability during the reaction) was stopped to eliminate its possible adverse effect on separation. The existence of a possible side reaction that could produce larger molecular weight molecules via transglycosylation was tested. A Ct-SI hydrolysis reaction mixture containing a 10-fold higher cold maltose concentration was tested, but no second peak was observed. Thus, the production of maltotriose or higher oligomers was considered unlikely.

Another possibility was that the gradient method was capable of separating the α- and β-anomers of maltose. To test this, maltose was reacted with ME, which interconverts, and therefore equilibrates β- and α-maltose. The extra peak still appeared after treating the maltose with ME. Also, α-glucosidase, which hydrolyzes α-maltose to D-glucose was used. With α-glucosidase, half of the maltose was hydrolyzed to D-glucose, but no extra peak was obtained, which was an indication of the extra peak being specific to the Ct-SI-catalyzed KIE partial reaction.

Heat quenching to denature and precipitate the proteins in the partial reaction mixture before injection on the APS HPLC column was another difference between the Ct-SI- and acid-catalyzed reactions. The hypothesis was that radiolabelled maltose and/or glucose could be adsorbing or otherwise reacting with the proteins, and that trace amounts of denatured protein was being injected onto the APS column. To test this possibility, a large excess of cold maltose was

added to the KIE reaction mixtures immediately before heat quenching in order to out-compete radiolabelled maltose. This eliminated the second peak in some cases (Figure 3.12), but this was not completely reproducible.

4.3.1. KIE Measurement for Acid-Catalyzed Hydrolysis Using the γ-Aminopropylsilyl Column

The reaction mixtures for the acid-catalyzed KIE measurements were separated using the gradient APS HPLC method. (Figure 3.13, and Figure 3.14). There is no extra peak after the maltose peak. The 1-^{3}H and 6,6-$^{3}H_2$ KIEs were measured for acid-catalyzed hydrolysis (Table 3.7 and Table 3.8). The observed KIEs were within ranges observed previously, but the variability was too large to be usable for TS analysis.

4.4. Purification Method Using an Anion Exchange Column

One common method in carbohydrate separation is use of derivatives, such as phosphate groups, or hydrophobic substituents, to improve their separation. An enzymatic reaction with hexokinase was used to phosphorylate the glucose product of the KIE reaction. In this method, the glucose was phosphorylated to G6P while maltose did not react. The mixture then was separated by anion exchange chromatography. In theory, the maltose should elutein low salt conditions, and G6P at high salt. However, in practice, chromatography of ^{3}H- or ^{14}C-radiolabelled G6P always resulted in an early eluting peak in anion exchange chromatography (Figure 3.15). There were three

possible sources for the early eluting peak. First, a portion of the G6P could be eluting early due to a chromatographic problem. Second, there could be an uncharged contaminant in the radiolabelled glucose that was not phosphorylated by G6P. Third, the hexokinase reaction was not proceeding to completion.

Different anion exchangers were used to check whether the chromatography was the source for the early peak. Q-Sepharose, Dowex 1X2, Dowex 1X8, and Mono-Q columns were tested, but the problem persisted with all of them. Variable bed volumes were used to eliminate the probability of overloading the column, but the problem remained. In another test, [γ-^{33}P]G6P was synthesized from [γ-^{33}P]ATP and cold glucose, and was run on the Mono-Q column. In this experiment, ^{33}P should only exist in forms of G6P or ATP, so any early eluting radioactivity would be a sign of chromatographic problems. No radioactivity was detected in the low salt eluting fractions, which demonstrated that the column was able to quantitatively retain G6P under low salt conditions (Figure 3.16).

The next possibility tested was a radioactive contaminant in D-glucose that could not be phosphorylated. Different glucoses were tested, namely [6,6-$^{3}H_2$]- and [1-^{14}C]glucose, and both gave an early eluting peak. Similarly, radiolabelled glucose was purified, then used to synthesize maltose, which was purified, then hydrolyzed back to glucose with α-glucosidase. This twice-purified glucose was then phosphorylated with hexokinase and subjected to anion exchange chromatography. The early eluting peak persisted.

As a final attempt to rule out contaminants, [2-^{14}C]- and [6,6-$^{3}H_2$]G6P was synthesized from glucose that had been previously phosphorylated and purified, so that every molecule of glucose was, in principle, capable of being phosphorylated. Thus, G6P was synthesized from the glucose liberated from maltose hydrolysis, purified by anion exchange chromatography on DEAE Sephadex, then hydrolyzed back to glucose using alkaline phosphatase. The resulting glucose was purified again on DEAE Sephadex, eluted in a low concentration of a volatile buffer, 10 mM ammonium formate, pH 9, and lyophilized to dryness. This multiply purified glucose was then phosphorylated with hexokinase and subjected to anion exchange chromatography on a Mono-Q column. Again, radioactivity was observed to elute in the low salt fraction.

The phosphorylation reaction catalyzed by hexokinase was then examined. Different concentrations of hexokinase were used, but no change was detected. Changes in the concentrations of the other reactants, i.e., ATP, glucose, $MgCl_2$, also did not affect the reaction. The reaction time was optimized, and the best result was achieved with 18 h, which gave as little as 0.8% of the early eluting peak. Nevertheless, this is still too much contamination for KIE measurements. Normally, *Saccharomyces cerevisiae* (yeast) hexokinase was used, but human hexokinase, and glucokinase were also tested. Yields with different species of the enzyme were not better than the yeast hexokinase. Sodium tungstate was used at up to 50 mM to help eliminate any phosphatase contaminant which might be hydrolyzing G6P. No improvement was obtained in the results.

Hexokinase was also checked for its ability to hydrolyze G6P back to glucose and inorganic phosphate. This was checked using the Malachite Green/ammonium molybdate colorimetric assay for inorganic phosphate.[85] This assay showed that hexokinase slowly hydrolyzes ATP to ADP in the absence of glucose, but it did not hydrolyze G6P (Figure 3.17). In case hexokinase was being inhibited by its ADP product, the reaction was also run using catalytic amounts of ATP, with stoichiometric amounts of phosphoenolpyruvate (a source of high energy phosphate) and pyruvate kinase to regenerate ATP via the reaction: ADP + PEP → ATP + pyruvate (Figure 3.18). This did not eliminate the early-eluting peak. In case glucose phosphorylation was not going to completion due to product inhibition, G6P dehydrogenase was used to oxidize G6P to 6-phosphogluconate to further drive the reaction to completion (Figure 3.19). This also did not remove the early eluting peak. Although the origin of the low salt elution radioactivity remained undetermined, KIE experiments were separated using this method.

Comparison of the KIEs obtained from APS and Mono-Q columns indicates smaller confidence intervals for separation with the Mono-Q. This was one of the reasons that we reconsider this method after development of APS separation methods and measurement of multiple KIEs with them. However this time, all the mixtures of radiolabelled maltoses were purified prior to the hydrolysis reaction using APS column with gradient method.

In experiments undertaken after those described above, it was found that the Mono-Q column was incapable of eluting the glucose completely in the

presence of glucose 6-phosphate (Figure 3.23), though addition of cold maltose in the mobile phase improved the situation (Figure 3.24). No effect was detected on maltose elution in the presence of phosphate. None of the KIEs that were measured previously with Mono-Q contained cold maltose in their mobile phase. However, this should not create any problem for KIE measurements, and it could even inadvertently help. In both the partial and 100% reaction mixtures, only the product in any form, glucose or G6P, should elute at the high salt concentrations.

KIEs that were measured with using anion exchange chromatography before routine repurification of the substrates were not usable for TS analysis (Table 3.9). Table 3.10 and Table 3.11 are the KIEs that were measured with pre-purified mixtures. The KIE for [1-^{3}H]maltose was in the acceptable range; however, the variability was too high. Not enough replicates of the [2-^{14}C]maltose KIE were done to make a judgment about its reliability.

4.5. Radioactivity Counting

The energy scan was performed to divide the windows such that 99.99% of the ^{3}H β-particles were detected in Win1. The window sizes were tested with each mobile phase since the composition of the mobile phase could change the emission energies (Figure 3.25). Window ranges of 0 - 460 (Win1) and 460 - 1000 (Win2) were suitable for all the methods. One of the challenges we faced was to have a mobile phase which is compatible with the scintillation cocktail (low H# and homogenous, translucent solution).[61]

4.6. Computational Chemistry

The TS structures for acid-catalyzed glycoside hydrolyses are oxacarbenium ion-like, as are the enzymatic TSs characterized to date.[43,48] Therefore, the structures for leaving group departure and oxacarbenium ion formation were optimized first. The EIEs for product (oxacarbenium ion and methanol) formation were also determined. When the experimental KIEs become available, they will be compared with the calculated KIEs, and their similarity will determine whether the calculated TS structure matches the experimental TS. If the KIEs do not match, other possible catalytic mechanisms will be modelled; including approach of the nucleophile to the oxacarbenium ion, and the concerted, A_ND_N mechanism.

α-Methyl glucopyranoside was used as a model to decrease the computational cost relative to maltose. The first attempt to find the highest potential energy point for α-methyl glucoside's C1-O4' bond cleavage by performing a relaxed scan (i.e., constraining $d_{C1\text{-}O4}$ at increasing values and optimizing the rest of the structure) failed because of hydrogen bonding between the methanol's hydroxyl proton and the C2 hydroxyl group. Instead, a constrained scan, where methanol's proton was prevented from approaching the C2 hydroxyl group, was performed (Figure 3.32). This scan demonstrated that there was no barrier to C1-O4' bond formation, and therefore no TS would be found. A self-consistent reaction field (SCRF), that is, a continuum solvation model, calculation was performed, which solved the problem, finding a local maximum in energy at

a C1-O4' bond length of ≈3.6 Å (Figure 3.33). This local maxima was used as a guess structure to find the TS using a QST3 calculation. The TS structure obtained had a $^{5}S_{3}$ conformation with the C1-O4′ bond length of 3.97 Å. The frequency calculations for TS showed only one imaginary frequency. Intrinsic reaction coordinate calculations were used to confirm any displacement around this imaginary frequency led to the reactant and the products.

Force constants obtained from frequency calculations were used to calculate isotope effects (Table 3.13). The calculated KIEs for the computational TS structure showed an inverse 1-^{14}C KIE, which is consistent with the expectation for a stepwise TS.[47,48] The calculated 4'-^{18}O (leaving group) KIE was large and normal, as expected given the loss of the bond to C1. The calculated 2-^{3}H KIE was large and normal, indicating that there was hyperconjugation between C2 and C1.

Chapter 5 - Concluding Remarks

5.1. Conclusions

Radiolabelled glucose was purified successfully using the gradient APS HPLC chromatography. The purified radiolabelled glucoses were used to synthesize the radiolabelled maltoses. The radiolabelled maltose synthesis was also optimized. The development of the gradient method of APS chromatography improved the separation of the maltose and glucose. The method was sufficient for purification of synthesized radiolabelled maltose.

For enzymatic KIE reactions, the reactions were successfully done while the reaction progress was monitored by HPLC on APS column with gradient elution method. Acid-catalyzed KIE reactions were also done with success.

The purification of the KIE mixtures for enzymatic reactions was done using three different methods: isocratic and gradient elution with an APS HPLC column, and stepwise elution with an anion exchange column (Mono-Q).

KIEs were measured at several positions with each method. Most of the measured KIEs were in the range of values previously observed for glycoside hydrolysis reactions; however, in every case the variability in measured KIEs was too large to be use to determine the TS structures. It was not possible to determine the source of this variability, but it will be necessary to do so.

KIEs and EIEs were calculated for all the positions for the departure of the leaving group, methanol, from α-methyl glucoside. The $^{4}C_{1}$ conformation was used for the reactant's conformation and the TS structure had a $^{5}S_{3}$ conformation.

These KIEs and EIEs could be used and compared to the experimental ones when the KIEs are measured.

5.2. Future work

All the methods that were developed for KIE measurements lack reproducibility. This means revision is required in order to be able to use these methods. For instance, in APS column the gradient method, the source of the extra peak that appears next to the maltose peak should be defined and eliminated. Also, in separation with the Mono-Q column, the source of the early eluting peak in the 100% reaction should be determined and refined.

New methods can be tested for the separation of the KIE reaction. One method is high-pH anion exchange chromatography. Since carbohydrates are weak acids, with high pH their hydroxyl groups are deprotonated, allowing these compounds to be separated. In this method, the retention time increases with decrease of the pK_a. The number of the hydroxyl group and the degree of polymerization are some of the factors that are influencing the separation.[92,93]

The other method that can be tried is to use glucose oxidase (GOx) or glucose dehydrogenase (GDH) enzymes to convert glucose in the mixture to gluconic acid and separate it by an anion exchange chromatography (Figure 5.1). This method of separation has some limitations. In this method, we would not be able to measure the α-secondary hydron KIE, since the anomeric position would lose its hydrogen. Also, most of the GOx enzymes have α-glucosidase contamination inside them or even have activity toward disaccharides, which

would make them oxidize maltose as well. However, some studies suggested that the use of Tris buffer mixture will inhibit the activity of these enzymes toward disaccharides.[94,95] GDH is also active toward maltose, but its K_m value is 45-fold higher than glucose's. Also, the substrate specificities changes based on the species that the enzyme is from, which has been suggested for both enzymes.[96,97]

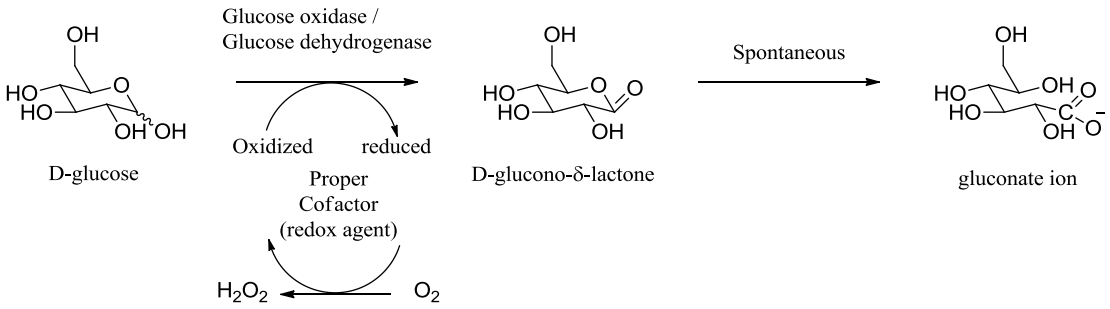

Figure 5.1. General mechanism of reaction with glucose oxidase and glucose dehydrogenase enzymes.

The other method is use of different derivatives. One of the common reactions used is reductive amination to make carbohydrate derivatives. And then it can be purified by a regular C18 column. Another benefit of these derivatives is that some of them are UV active.[98]

After finding a separation method which is promising and gives precise enough KIEs, the method should be used to measure a series of 1-^{3}H KIEs, since this is normally a large number, and it would be a good evidence for the validity of the experimental method. Once the method is finalized, experimental KIE will be measured for different positions in maltose and sucrose substrates, and for all four subunits (Nt, Ct-SI and Nt, Ct-MGAM).

Last is the comparison of the calculated KIEs with the experimental KIEs. In the case that the already calculated KIEs do not match, different possible mechanisms should be evaluated.

References

(1) Canadian Diabetes Association. (2009) The prevalence and costs of diabetes. *Consult. Novemb.*, pp 1–2.

(2) Canadian Diabetes Association. (2014) Canadian Diabetes Association About Diabetes. *http://www.diabetes.ca/about-diabetes/what-is-diabetes*.

(3) Canadian Diabetes Association. (2011) Diabetes: Canada at the Tipping Point: Charting a New Path, p 58.

(4) Tisch, R., and McDevitt, H. (1996) Insulin-dependent diabetes mellitus: review. *Cell 85*, 291–297.

(5) Centers for Disease control and prevention. (2011) DIABETES Successes And Opportunities for Population-Based Prevention and Control. Atlanta.

(6) Groop, L. C. (1997) The molecular genetics of non-insulin-dependent diabetes mellitus. *J. Intern. Med. 241*, 95–101.

(7) Aronoff, S. L., Berkowitz, K., Shreiner, B., and Want, L. (2004) Glucose Metabolism and Regulation: Beyond Insulin and Glucagon. *Diabetes Spectr. 17*, 183–190.

(8) Lebovitz, H. E. (2002) Treating hyperglycemia in type 2 diabetes: new goals and strategies. *Cleve. Clin. J. Med. 69*, 809–20.

(9) Jones, K., Sim, L., Mohan, S., Kumarasamy, J., Liu, H., Avery, S., Naim, H. Y., Quezada-Calvillo, R., Nichols, B. L., Pinto, B. M., and Rose, D. R. (2011) Mapping the intestinal alpha-glucogenic enzyme specificities of starch digesting maltase-glucoamylase and sucrase-isomaltase. *Bioorg. Med. Chem. 19*, 3929–34.

(10) Asano, N. (2003) Glycosidase inhibitors: update and perspectives on practical use. *Glycobiology 13*, 93R–104R.

(11) Gloster, T. M., and Vocadlo, D. J. (2012) Developing inhibitors of glycan processing enzymes as tools for enabling glycobiology. *Nat. Chem. Biol. 8*, 683–94.

(12) Sim, L., Quezada-Calvillo, R., Sterchi, E. E., Nichols, B. L., and Rose, D. R. (2008) Human intestinal maltase-glucoamylase: crystal structure of the N-terminal catalytic subunit and basis of inhibition and substrate specificity. *J. Mol. Biol. 375*, 782–92.

(13) Chen, X., Zheng, Y., and Shen, Y. (2006) Voglibose (Basen, AO-128), one of the most important alpha-glucosidase inhibitors. *Curr. Med. Chem. 13*, 109–16.

(14) Zechel, D. L., and Withers, S. G. (2000) Glycosidase mechanisms: anatomy of a finely tuned catalyst. *Acc. Chem. Res. 33*, 11–8.

(15) Wolfenden, R., and Snider, M. J. (2001) The depth of chemical time and the power of enzymes as catalysts. *Acc. Chem. Res. 34*, 938–945.

(16) Ren, L., Cao, X., Geng, P., Bai, F., and Bai, G. (2011) Study of the inhibition of two human maltase-glucoamylases catalytic domains by different α-glucosidase inhibitors. *Carbohydr. Res. 346*, 2688–92.

(17) Sim, L., Willemsma, C., Mohan, S., Naim, H. Y., Pinto, B. M., and Rose, D. R. (2010) Structural basis for substrate selectivity in human maltase-glucoamylase and sucrase-isomaltase N-terminal domains. *J. Biol. Chem. 285*, 17763–70.

(18) Quezada-Calvillo, R., Sim, L., Ao, Z., Hamaker, B. R., Quaroni, A., Brayer, G. D., Sterchi, E. E., Robayo-Torres, C. C., Rose, D. R., and Nichols, B. L. (2008) Luminal starch substrate "brake" on maltase-glucoamylase activity is located within the glucoamylase subunit. *J. Nutr. 138*, 685–92.

(19) Li, C., Begum, A., Numao, S., Park, K. H., Withers, S. G., and Brayer, G. D. (2005) Acarbose rearrangement mechanism implied by the kinetic and structural analysis of human pancreatic alpha-amylase in complex with analogues and their elongated counterparts. *Biochemistry 44*, 3347–57.

(20) Trapero, A., and Llebaria, A. (2013) Glucocerebrosidase inhibitors for the treatment of Gaucher disease. *Future Med. Chem. 5*, 573–590.

(21) Winchester, B., and Fleet, G. W. (1992) Amino-sugar glycosidase inhibitors: versatile tools for glycobiologists. *Glycobiology 2*, 199–210.

(22) Rowe, P. M. (1999) Glycoscience moves from the laboratory to the clinic. *Lancet 354*, 402.

(23) Jacob, G. S. (1995) Glycosylation inhibitors in biology and medicine. *Curr. Opin. Struct. Biol. 5*, 605–11.

(24) Lairson, L. L., Henrissat, B., Davies, G. J., and Withers, S. G. (2008) Glycosyltransferases: structures, functions, and mechanisms. *Annu. Rev. Biochem. 77*, 521–55.

(25) Davies, G., and Henrissat, B. (1995, September 15) Structures and mechanisms of glycosyl hydrolases. *Structure*.

(26) Wolfenden, R. (2006) Degrees of difficulty of water-consuming reactions in the absence of enzymes. *Chem. Rev. 106*, 3379–96.

(27) Withers, S. (2001) Mechanisms of glycosyl transferases and hydrolases. *Carbohydr. Polym. 44*, 325–337.

(28) Sinnott, M. (1990) Catalytic mechanism of enzymic glycosyl transfer. *Chem. Rev. 90*, 1171–1202.

(29) Lee, J. K. (2003) Using NMR spectroscopy to measure natural abundance 13C kinetic isotope effects on the acid catalyzed and enzymatic hydrolysis of methyl glucosides. Thesis (M.Sc.) -- McMaster University, 2004.

(30) Wolfenden, R., Lu, X., and Young, G. (1998) Spontaneous hydrolysis of glycosides. *J. Am. Chem. Soc. 120*, 6814–6815.

(31) Brito-Arias, M. (2007) Synthesis and characterization of glycosides, p 364. Springer US, New York, NY.

(32) Davies, G., and Henrissat, B. (1995) Structures and mechanisms of glycosyl hydrolases. *Structure 3*, 853–859.

(33) McCarter, J. D., and Withers, S. G. (1994) Mechanisms of enzymatic glycoside hydrolysis. *Curr. Opin. Struct. Biol. 4*, 885–92.

(34) Koshland, D. (1953) Stereochemistry and the mechanism of enzymatic reactions. *Biol. Rev.* 416–436.

(35) Yip, V. L. Y., and Withers, S. G. (2004) Nature's many mechanisms for the degradation of oligosaccharides. *Org. Biomol. Chem. 2*, 2707–13.

(36) Lee, S. S., Yu, S., and Withers, S. G. (2002, May 8) alpha-1,4-Glucan lyase performs a trans-elimination via a nucleophilic displacement followed by a syn-elimination. *J. Am. Chem. Soc.*

(37) Lee, S., Yu, S., and Withers, S. (2003) Detailed dissection of a new mechanism for glycoside cleavage: α-1, 4-glucan lyase. *Biochemistry*.

(38) Davies, G. J., Planas, A., and Rovira, C. (2012) Conformational analyses of the reaction coordinate of glycosidases. *Acc. Chem. Res. 45*, 308–16.

(39) Vasella, A., Davies, G. J., and Böhm, M. (2002) Glycosidase mechanisms. *Curr. Opin. Chem. Biol. 6*, 619–29.

(40) Biarnés, X., Ardèvol, A., Planas, A., Rovira, C., Laio, A., and Parrinello, M. (2007) The conformational free energy landscape of beta-D-glucopyranose. Implications for substrate preactivation in beta-glucoside hydrolases. *J. Am. Chem. Soc. 129*, 10686–93.

(41) Vocadlo, D. J., and Davies, G. J. (2008) Mechanistic insights into glycosidase chemistry. *Curr. Opin. Chem. Biol. 12*, 539–555.

(42) Lovering, A. L., Lee, S. S., Kim, Y.-W., Withers, S. G., and Strynadka, N. C. J. (2005) Mechanistic and structural analysis of a family 31 alpha-glycosidase and its glycosyl-enzyme intermediate. *J. Biol. Chem. 280*, 2105–15.

(43) Lee, J. K., Bain, A. D., and Berti, P. J. (2004) Probing the transition states of four glucoside hydrolyses with 13C kinetic isotope effects measured at natural abundance by NMR spectroscopy. *J. Am. Chem. Soc. 126*, 3769–76.

(44) Breitmeier, D., Günther, S., and Heymann, H. (1997) Acarbose and 1-deoxynojirimycin inhibit maltose and maltooligosaccharide hydrolysis of human small intestinal glucoamylase-maltase in two different substrate-induced modes. *Arch. Biochem. Biophys. 346*, 7–14.

(45) Sim, L., Jayakanthan, K., Mohan, S., Nasi, R., Johnston, B. D., Pinto, B. M., and Rose, D. R. (2010) New glucosidase inhibitors from an ayurvedic herbal treatment for type 2 diabetes: structures and inhibition of human intestinal maltase-glucoamylase with compounds from Salacia reticulata. *Biochemistry 49*, 443–51.

(46) Fersht, A. (1985) Enzyme-Substrate Complementarity and the Use of Binding Energy in Catalysis, in *Enzyme Structure and Mechanism* (Fersht, A., Ed.) Second., pp 311–346. W. H. Freeman and Company, New York, NY.

(47) Berti, P. J., and McCann, J. A. B. (2006) Toward a detailed understanding of base excision repair enzymes: transition state and mechanistic analyses of N-glycoside hydrolysis and N-glycoside transfer. *Chem. Rev. 106*, 506–55.

(48) Berti, P., and Tanaka, K. (2002) Transition state analysis using multiple kinetic isotope effects: mechanisms of enzymatic and non-enzymatic glycoside hydrolysis and transfer. *Adv. Phys. Org. Chem. 37*, 239–314.

(49) Schramm, V. L. (1998) Enzymatic transition states and transition state analog design. *Annu. Rev. Biochem. 67*, 693–720.

(50) Berti, P., and Schramm, V. (1997) Transition state structure of the solvolytic hydrolysis of NAD+. *J. Am. Chem. Soc. 7863*, 12069–12078.

(51) Berti, P. J., Blanke, S. R., and Schramm, V. L. (1997) Transition State Structure for the Hydrolysis of NAD Catalyzed by Diphtheria Toxin. *J. Am. Chem. Soc. 119*, 12079–12088.

(52) Oppenheimer, N. J. (1994) NAD hydrolysis: chemical and enzymatic mechanisms. *Mol. Cell. Biochem. 138*, 245–51.

(53) Warshel, A. (1978) Energetics of enzyme catalysis. *Proc. Natl. Acad. Sci. 75*, 5250–5254.

(54) Berti, P. J. (1999) Determining transition states from kinetic isotope effects. *Methods Enzymol. 308*, 355–97.

(55) Huskey, P. W. (1991) Origins and Interpretations of Heavy-atom Isotope Effect, in *Enzyme Mechanism from Isotope Effects* (Cook, P., Ed.), pp 37–72. CRC Press, Boca Raton.

(56) Sühnel, J., and Schowen, R. L. (1991) Theoretical Basis for Primry and Secondary Hydrogen Isotope Effects, in *Enzyme Mechanism from Isotope Effects* (Cook, P. F., Ed.), pp 3–36. CRC Press, Boca Raton.

(57) Kurita, E., Matsuura, H., and Ohno, K. (2004) Relationship between force constants and bond lengths for CX (X = C, Si, Ge, N, P, As, O, S, Se, F, Cl and Br) single and multiple bonds: formulation of Badger's rule for universal use. *Spectrochim. Acta. A. Mol. Biomol. Spectrosc. 60*, 3013–23.

(58) Guthrie, R. D., and Jencks, W. P. (1989) IUPAC recommendations for the representation of reaction mechanisms. *Acc. Chem. Res. 22*, 343–349.

(59) Chen, X.-Y., Berti, P. J., and Schramm, V. L. (2000) Transition-State Analysis for Depurination of DNA by Ricin A-Chain. *J. Am. Chem. Soc. 122*, 6527–6534.

(60) McCann, J. a B., and Berti, P. J. (2007) Transition state analysis of acid-catalyzed dAMP hydrolysis. *J. Am. Chem. Soc. 129*, 7055–64.

(61) Parkin, D. W. (1991) Methods for the Determination of Competitive and Noncompetitive Kinetic Isotope Effects, in *Enzyme Mechanism from Isotope Effects* (Cook, P. F., Ed.), pp 269–290. CRC Press, Boca Raton.

(62) Northrop, D. B. (1991) Intrinsic Isotope Effects in Enzyme-Catalyzed Reactions, in *Enzyme Mechanism from Isotope Effects* (Cook, P., Ed.), pp 181–196. CRC Press, Boca Raton.

(63) Bigeleisen, J and wolfsberg, M. (1958) Theoritical and Experimental Aspects of Isotope Effects in Chemical Kinetics. *Adv. Phys. Chem. Chem. 1*, 15–76.

(64) Zhang, Y., Bommuswamy, J., and Sinnott, M. L. (1994) Kinetic Isotope Effect Study of Transition States for the Hydrolyses of .alpha.- and .beta.-Glucopyranosyl Fluorides. *J. Am. Chem. Soc. 116*, 7557–7563.

(65) Huang, X., Tanaka, K. S. E., and Bennet, A. J. (1997) Glucosidase-Catalyzed Hydrolysis of a- D -Glucopyranosyl Pyridinium Salts : Kinetic Evidence for Nucleophilic Involvement at the Glucosidation Transition State. *J. Am. Chem. Soc. 7863*, 11147–11154.

(66) Bennet, A. J., and Sinnott, M. L. (1986) Complete Kinetic Isotope Effect Description of Transition States for Acid-Catalyzed Hydrolyses of Methyl a-and b-glucopyranosides. *J. Am. Chem. Soc. 108*, 7287–7294.

(67) Tanakas, Y., Taoo, W., Blanchards, J. S., and Hehren, E. J. (1994) Transition State Structures for the Hydrolysis of a-D-Glucopyranosyl of Glycosylases * Fluoride by Retaining and Inverting Reactions. *J. Biol. Chem. 269*, 32306–32312.

(68) Indurugalla, D., and Bennet, A. J. (2001) A Kinetic Isotope Effect Study on the Hydrolysis Reactions of Methyl Xylopyranosides and Methyl 5-Thioxylopyranosides: Oxygen versus Sulfur Stabilization of Carbenium Ions. *J. Am. Chem. Soc. 123*, 10889–10898.

(69) Duggleby, R. G., and NORTHROP, B. D. (1990) Calculations of Intrinsic Isotope Effects and the Detection of Tunneling in Enzyme-Catalyzed Reactions *439*, 435–439.

(70) Cogoli, A., and Semenza, G. (1975) A probable oxocarbonium ion in the reaction mechanism of small intestinal sucrase and isomaltase. *J. Biol. Chem. 250*, 7802–7809.

(71) Horrocks, D. (1974) Scintillator Solutions, in *Applications of Liquid Scintillation Counting* (Horrocks, D., Ed.), pp 35–68. Academic Press, INC., New York, NY.

(72) Horrocks, D. (1974) Prepration of Counting Samples, in *Applications of Liquid Scintillation Counting* (Horrocks, D., Ed.), pp 145–174. Academic Press, INC., New York, NY.

(73) Leo, W. (1988) Techniques for Nuclear and Particle Physics Experiments. *Nucl. Instruments Methods Phys. Res.*

(74) Horrocks, D. (1974) Background, in *Application of Liquid Scintillation Counting*, pp 198–207. Academic Press, INC., New York, NY.

(75) Horrocks, D. (1974) Cerenkov Counting, in *Applications of Liquid Scintillation Counting*, pp 263–275. Academic Press, INC., New York, NY.

(76) Laurier Research Instrumentation. (2010) User Guidline & Standard Operating Procedure for the Beckman Coulter LS6500 Multipurpose Scintillation Counter, pp 1–26.

(77) Horrocks, D. (1974) Basic Processes, in *Application of LIquid Scintillation Counting*, pp 12–34. Academic Press, INC., New York, NY.

(78) Glad, S., and Jensen, F. (1996) Basis set and correlation effects on transition state geometries and kinetic isotope effects. *J. Phys. Chem. 100*, 16892–16898.

(79) Scott, A., and Radom, L. (1996) Harmonic vibrational frequencies: an evaluation of Hartree-Fock, Møller-Plesset, quadratic configuration interaction, density functional theory, and semiempirical scale. *J. Phys. Chem. 100*, 16502–16513.

(80) Bigeleisen, J., and Mayer, M. G. (1947) Calculation of Equilibrium Constants for Isotopic Exchange Reactions. *J. Chem. Phys. 15*, 261.

(81) Saunders, M., Laidig, K. E., and Wolfsberg, M. (1989) Theoretical calculation of equilibrium isotope effects using ab initio force constants: application to NMR isotope perturbation studies. *J. Am. Chem. Soc. 111*, 8989–8994.

(82) Foresman, J. (1996) Frisch Æ (1996) Exploring chemistry with electronic structure methods. *Gaussian Inc., Pittsburgh, PA.*

(83) Wong, M. (1996) Vibrational frequency prediction using density functional theory. *Chem. Phys. Lett. 256*, 391–399.

(84) Frisch, M. J., Trucks, G. W., Schlegel, H. B., Scuseria, G. E., Robb, M. A., Cheeseman, J. R. Scalmani, G., Barone, V., Mennucci, B., Petersson, G. A., Nakatsuji, H., Caricato, M., Li, X., Hratchian, H. P., Izmaylov, A. F., Bloino, J., Zheng, G., Sonnenberg, J. L., Hada, M., Ehara, M., Toyota, K., Fukuda, R., Hasegawa, J., Ishida, M., Nakajima, T., Honda, Y., Kitao, O., Nakai, H., Vreven, T., Montgomery, J. A., Jr. Peralta, J. E., Ogliaro, F., Bearpark, M., Heyd, J. J.,

Brothers, E., Kudin, K. N., Staroverov, V. N. Kobayashi, R., Normand, J. Raghavachari, K., Rendell, A., Burant, J. C., Iyengar, S. S., Tomasi, J., Cossi, M., Rega, N., Millam, N. J., Klene, M., Knox, J. E., Cross, J. B., Bakken, V., Adamo, C., Jaramillo, J., Gomperts, R., Stratmann, R. E., Yazyev, O., Austin, A. J., Cammi, R., Pomelli, C., Ochterski, J. W., Martin, R. L., Morokuma, K., Zakrzewski, V. G., Voth, G. A., Salvador, P., Dannenberg, J. J. Dapprich, S., Daniels, A. D., Farkas, Ö., Foresman, J. B., Ortiz, J. V., Cioslowski, J., and Fox, D. J. Gaussian, Inc., Wallingford CT, 2009. Gaussian 09.

(85) Lanzetta, P. a, Alvarez, L. J., Reinach, P. S., and Candia, O. a. (1979) An improved assay for nanomole amounts of inorganic phosphate. *Anal. Biochem. 100*, 95–7.

(86) Schlegel, H. B. (1994) Some thoughts on reaction-path following. *J. Chem. Soc. Faraday Trans. 90*, 1569–1574.

(87) Buszewski, B., and Noga, S. (2012) Hydrophilic interaction liquid chromatography (HILIC)--a powerful separation technique. *Anal. Bioanal. Chem. 402*, 231–47.

(88) Robards, K., and Whitelaw, M. (1986) Chromatography of monosaccharides and disaccharides. *J. Chromatogr. A 373*, 81–110.

(89) Hvizd, M., Bailey, B., Crafts, C., Plante, M., and Acworth, I. Simple Separation and Detection Techniques for the Analysis of Carbohydrates. *dionex.com* 1–8.

(90) Zhu, C., Goodall, D., and Wren, S. (2005) Elevated temperature HPLC: principles and applications to small molecules and biomolecules. *LC GC North Am. 8*.

(91) Verhaar, L., Kuster, B., and Claessens, H. (1984) Retention behaviour of carbohydrate oligomers in reversed-phase chromatography. *J. Chromatogr. A 284*, 1–11.

(92) Corradini, C., Cavazza, A., and Bignardi, C. (2012) High-Performance Anion-Exchange Chromatography Coupled with Pulsed Electrochemical Detection as a Powerful Tool to Evaluate Carbohydrates of Food Interest: Principles and Applications. *Int. J. Carbohydr. Chem. 2012*, 1–13.

(93) Lewis, B. E., and Schramm, V. L. (2003) Isotope effect-mapping of the ionization of glucose demonstrates unusual charge sharing. *J. Am. Chem. Soc. 125*, 7872–7.

(94) Fleming, I. D., and Pegler, H. F. (1963) The determination of glucose in the presence of maltose and isomaltose by a stable, specific enzymic reagent. *Analyst 88*, 967.

(95) Dahlqvist, a. (1961) Determination of maltase and isomaltase activities with a glucose-oxidase reagent. *Biochem. J. 80*, 547–51.

(96) Ferri, S., Kojima, K., and Sode, K. (2011) Review of Glucose Oxidases and Glucose Dehydrogenases : *5*, 1068–1076.

(97) Basner, A., and Antranikian, G. (2014) Isolation and biochemical characterization of a glucose dehydrogenase from a hay infusion metagenome. *PLoS One 9*, e85844.

(98) Lamari, F. N., Kuhn, R., and Karamanos, N. K. (2003) Derivatization of carbohydrates for chromatographic, electrophoretic and mass spectrometric structure analysis. *J. Chromatogr. B. Analyt. Technol. Biomed. Life Sci. 793*, 15–36.

Appendix

Coordinates for optimized structures. All structures were optimized at the RB3PW91/6-31+G** level of theory.

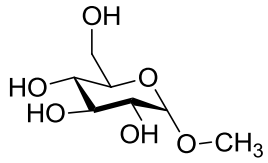

Compound 1

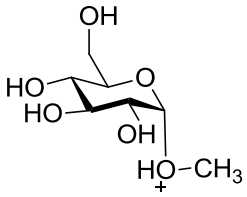

Compound 2

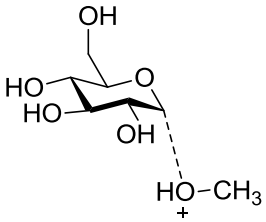

Compound 3‡

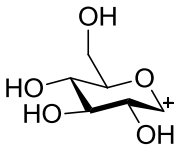

Compound 4

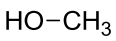

Compound 5

Compound 1

```
# rb3pw91/6-31+g**
Reactant

0 1
C       0.88147    -1.02182    -0.77698
C       1.25598     0.45996    -0.87106
O      -0.32131    -1.37014    -0.38508
O       1.88194    -1.66668     0.12057
H       1.20133    -1.63720    -1.61830
C       0.54994     1.29640     0.18986
C      -1.18441    -0.51293     0.44060
C       1.64754    -1.69658     1.50305
O       2.66654     0.58630    -0.70765
H       0.93829     0.81075    -1.86091
C      -0.94091     0.97356     0.18626
C      -2.60381    -0.94314     0.12893
O       0.67544     2.66907    -0.08989
H       0.96116     1.05948     1.18418
H      -0.96444    -0.73766     1.49050
H       0.69226    -2.17787     1.75667
H       2.45099    -2.30053     1.93529
H       1.68685    -0.70372     1.97957
H       3.11113     0.77284    -1.54435
O      -1.60397     1.63514     1.23424
O      -2.86997    -0.60378    -1.21415
H      -1.36379     1.24530    -0.79145
H      -3.26100    -0.41552     0.83269
```

H	-2.69385	-2.02418	0.30368
H	1.52641	2.99991	0.22170
H	-1.56300	2.58681	1.07064
H	-3.78661	-0.81020	-1.42821

Compound 2

Protonated alpha-methyl glucopyranoside

1 1

C	0.95356	-0.88251	-0.91965
C	1.24175	0.61398	-0.77078
O	-0.23136	-1.35536	-0.61311
O	2.13220	-1.56930	0.07277
H	1.31897	-1.33766	-1.84061
C	0.47527	1.23056	0.39370
C	-1.15301	-0.68974	0.31909
C	1.78981	-2.28085	1.29327
O	2.64042	0.79147	-0.55972
H	0.91595	1.09916	-1.69933
C	-0.99395	0.82952	0.30773
C	-2.54094	-1.14371	-0.08647
O	0.52352	2.63507	0.33680
H	0.88772	0.86214	1.34663
H	-0.93286	-1.06566	1.32477
H	0.95937	-2.93884	1.04360
H	2.66428	-2.87204	1.56628
H	1.52052	-1.58264	2.08784
H	3.08333	1.13304	-1.34692
O	-1.70712	1.27819	1.43275
O	-2.81041	-0.61083	-1.36446
H	-1.42027	1.22897	-0.62354
H	-3.23628	-0.77211	0.67771
H	-2.56961	-2.24210	-0.08645
H	1.34985	2.95931	0.71460
H	-1.72001	2.24454	1.42229
H	-3.71076	-0.83159	-1.62773
H	2.79452	-0.84416	0.17838

Compound 3

Transition State Structure

1 1

C	0.50234	-1.15390	-1.22920
C	0.22902	-1.50542	0.17086
O	0.94306	-0.03196	-1.58259
O	-3.23535	0.01160	-0.60167
H	0.25985	-1.83449	-2.04989
C	-0.38808	-0.22698	0.81650
C	1.35522	1.01788	-0.59306
C	-4.04226	1.16432	-0.85823
O	-0.59101	-2.63051	0.18679
H	1.21268	-1.67924	0.64871
C	0.68672	0.85973	0.78653

C	2.86805	0.96282	-0.57694
O	-0.72033	-0.49495	2.15226
H	-1.27428	0.07151	0.24218
H	0.99858	1.93612	-1.06342
H	-3.43133	2.03732	-0.62168
H	-4.34172	1.21819	-1.91085
H	-4.93564	1.17881	-0.22403
H	-0.59636	-3.00616	1.07634
O	0.16388	2.13266	1.08106
O	3.21961	-0.30698	-0.06397
H	1.45602	0.57063	1.51676
H	3.20931	1.78786	0.06421
H	3.26178	1.11919	-1.58920
H	-1.68063	-0.53434	2.24039
H	-0.06575	2.16589	2.01919
H	4.17882	-0.40352	-0.03147
H	-3.75621	-0.77728	-0.79088

Compound 4

Oxacarbenium Ion

1 1

C	-0.27664	-1.51582	-0.80057
C	-1.18122	-0.87569	0.17926
O	0.78614	-0.98945	-1.21260
H	-0.55426	-2.44697	-1.30316
C	-1.14814	0.65195	-0.12722
C	1.35088	0.25468	-0.59554
O	-2.45987	-1.41513	0.03311
H	-0.74358	-1.01838	1.18143
C	0.28516	1.15428	0.05927
C	2.42694	-0.24213	0.34801
O	-1.94847	1.35667	0.77210
H	-1.46726	0.81454	-1.16648
H	1.78388	0.77102	-1.45414
H	-2.80263	-1.73025	0.87794
O	0.47588	2.42065	-0.51735
O	1.76761	-1.00044	1.34331
H	0.46731	1.17661	1.14327
H	2.92774	0.64701	0.75602
H	3.16467	-0.84032	-0.20118
H	-2.86703	1.35822	0.47396
H	-0.02573	3.07633	-0.01384
H	2.40460	-1.34973	1.97828

Compound 5

Methanol

0 1

H	-1.14856	-0.75242	-0.00007
O	-0.74627	0.12219	0.00002
C	0.66324	-0.02060	0.00001
H	1.08132	0.98843	-0.00103

H	1.02890	-0.54578	-0.89355
H	1.02905	-0.54416	0.89446